Spring 2018

AN IMPROVED INFILTRATION MODEL AND DESIGN SIZING APPROACH FOR STORMWATER BIORETENTION FILTERS INCLUDING ANISOTROPY AND INFILTRATION INTO NATIVE SOILS

Daniel Macadam
University of New Hampshire

AN IMPROVED INFILTRATION MODEL AND DESIGN SIZING APPROACH FOR STORMWATER BIORETENTION FILTERS INCLUDING ANISOTROPY AND INFILTRATION INTO NATIVE SOILS

BY

DANIEL MACADAM
BA Fine Arts, Gordon College, 2010

THESIS

Submitted to the University of New Hampshire
in Partial Fulfillment of
the Requirements for the Degree of

Master of Science
in
Civil Engineering

May, 2018

ProQuest LLC.
789 East Eisenhower Parkway
P.O. Box 1346
Ann Arbor, MI 48106 – 1346

This thesis has been examined and approved in partial fulfillment of the requirements for the degree of Master of Science in Civil Engineering by:

Thesis Director, Dr. Thomas P. Ballestero
Associate Professor
Civil and Environmental Engineering
University of New Hampshire

Dr. James Houle
Research Assistant Professor
Environmental Research Group
University of New Hampshire

Dr. Alison Watts
Research Assistant Professor
Civil and Environmental Engineering
University of New Hampshire

On April 11, 2018

Original approval signatures are on file with the University of New Hampshire Graduate School.

ACKNOWLEDGEMENTS

The Horne St. bioretention site in this study was originally funded and constructed under the cooperation of the EPA Region 1 office and the UNH Stormwater Center under the EPA Regional Applied Research Effort (RARE) grant and continued for the current study under the EPA Science To Achieve Results (STAR) project *Taking it to the Streets: Green Infrastructure for Sustainable Philadelphia Communities*.

Thank you to my thesis advisor, Dr. Ballestero, and committee members Dr. Houle and Dr. Watts for their vast knowledge in the field, patience, helpful criticism, and abundantly cheerful and pleasant attitudes that have pushed my research forward, challenged me greatly, and made it a joy all the while.

Much appreciation also goes to UNHSC staff Tim Puls for teaching me many field methods, for many hours of guidance, and being a great sounding board for ideas as my knowledge of stormwater has developed.

Thank you to many fellow graduate students, especially Ethan Ely and David Tarushka, for their wonderful company and encouragement during many devoted hours of field and laboratory work.

I am incredibly grateful for the loving support of my immediate and church families. Their patience and encouragement has spurred me ever onward and fueled my hopes of making this world a more wonderful place to live.

TABLE OF CONTENTS

LIST OF TABLES

LIST OF FIGURES

LIST OF SYMBOLS

Symbol	Units	Description
a	ft.	GP: Radius of the borehole
A_f	ft.^{2}	BS: Filter surface area
A_w	ft.^{2}	Total treatment watershed area draining to the filter
CN	–	USDA NRCS dimensionless curve number
d_f	ft.	BS: filter planting soil bed depth
ET	ft.	Rate of evapotranspiration as the mean daily rate
f	ft./hr.	Infiltration rate
F	ft.	Cumulative infiltration
FS	–	Factor of Safety
h	ft.	Depth of water from a datum relative to the contextual use
h_f	ft.	BS: Average depth of ponded water on the bioretention surface
h_{max}	ft.	BS: Maximum ponding depth
H	ft.	GP: Depth of head in the borehole
h_{pipe}	ft.	BS: Elevation of the underdrain (to the invert)
I	–	Percent impervious cover draining to the structure (in decimal form)
K	ft./hr.	Hydraulic conductivity
K_s	ft./hr.	Saturated hydraulic conductivity
K_{fs}	ft./hr.	Field saturated hydraulic conductivity
l	ft.	BS: Length of filter
P	ft.	Design precipitation (90% annual rainfall)
q	ft.^{3}/s.	Discharge (used in various locations throughout)
Rv	–	Unitless runoff coefficient as a function of impervious cover
t	hr.	Time
T_c	hr.	Time of concentration
t_f	hr.	BS: Drain time required for the WQV to filter through the planting soil bed
WQV	ft.^{3}	Water Quality Treatment Volume

ΔS	ft.^{3}	Difference between water stored from the final to the initial condition
$\Delta\theta$	ft.^{3}/ ft.^{3}	Difference between field saturated and ambient volumetric water content of soil
η	ft.^{3}/ ft.^{3}	Porosity
Ψ	ft.	Soil water tension (positive)
θ_i	ft.^{3}/ ft.^{3}	Ambient volumetric water content in the soil
θ_s	ft.^{3}/ ft.^{3}	Saturated volumetric water content in the soil

Note: GP indicates symbols specific to the Guelph Permeameter

BS indicates symbols specific to a Bioretention System

ABSTRACT

AN IMPROVED INFILTRATION MODEL AND DESIGN SIZING APPROACH FOR STORMWATER BIORETENTION FILTERS INCLUDING ANISOTROPY AND INFILTRATION INTO NATIVE SOILS

by

Daniel Macadam

University of New Hampshire, May 2018

Bioretention filters are a common Best Management Practice used to treat pollutants and water volumes of stormwater runoff from urbanized watersheds. The current static sizing criterium for new design applies Darcy's law to the Water Quality Volume (WQV) as it filters through the bioretention soil media. In retrofit applications, the WQV is instantaneously stored in the system pore space, including the ponded surface. While these designs are simple to implement, the systems areas are oversized because no infiltration or other outflow is considered in the design.

The retrofit bioretention study site for this research located in Dover, NH (HSBS) treats a 21.9 ac. suburban watershed with 38% impervious cover. The static design treatment rainfall for the HSBS was 0.16 inches. Monitored data yielded a mean peak discharge reduction and mean volume reduction of 62% and 35% with standard deviations of 25% and 37%, respectively. Of 45 observed storms with one-minute logging intervals, 67% of the events were fully treated and ponding did not exceed the designed

elevation; 95% of these events were less than 1.27 inches. The static design rainfall was in the 5.4th percentile, almost 800% less than the largest observed treated storm with no bypass. The volume balance model developed in this study used a Green and Ampt approach for the vertical bottom and lateral sidewall infiltrations integrated over the duration of the event. The model requires basic watershed and climatic properties, design dimensions, and anisotropic native soil characteristics. Comparing estimates of bottom-only infiltration and the developed model to observed infiltrated volumes yielded mean errors of -79% and -8%, with RMSE of 3210 cu. ft. and 2650 cu. ft., respectively. On average, 39% of the total infiltrated volume occurred through the sidewalls. The retrofit treatment rainfall for the model was 0.52 inches. This was 225% larger than the current static design rainfall and was in the 49th percentile of the observed, treated events for HSBS, which was an improvement of 44% over the current static design.

CHAPTER 1. INTRODUCTION

1.1 Stormwater Background

Stormwater runoff is the water associated with a rain or snowmelt that has been conveyed and may be measured in a downstream river, stream, ditch, gutter, or pipe shortly after precipitation. Historically, runoff was managed by conveyance through engineered systems such as gutters or pipes through cities with one goal in mind: remove the water from roads and walkways as rapidly and efficiently as possible (National Research Council, 2008). Some arid areas collected stormwater for irrigation or drinking and others treated it as wastewater if convenient. This treatment in a combined sewer system eliminated the cost of separate pipe systems but commonly resulted in sewage overflows during rainstorms (National Research Council, 2008).

Stormwater can pollute receiving streams, rivers, lakes, ponds, groundwater, and bays through excess volume of runoff and/or by excess nutrient loads or pollutants. The increasing amount of impervious cover (paving and buildings) due to watershed urbanization changes the flow regime and causes stormwater to runoff more quickly than in natural watersheds. This causes the runoff to arrive at the receiving water body over a shorter amount of time leading to increased peak flows and total runoff volumes. Even if the runoff was pure water, the increased runoff volumes may result in geomorphic instabilities of streams. The increased volumes of runoff alone often cause instability in streams resulting in bank and bed erosion. However, stormwater often carries nonpoint source pollution from the watershed.

Urbanization and the increased amount of impervious cover change the flow regime and decrease the nutrient absorption in the watershed. A natural watershed may infiltrate rainfall, store water in the soil, and release the water through the process of evapotranspiration. These functions are decreased or lost as a watershed is paved or developed. Instead, rainfall will wet the surfaces and runoff to the outlet, collecting trash and pollution as it goes. The effects of urbanization on watershed hydrology are shown in Figure 1.

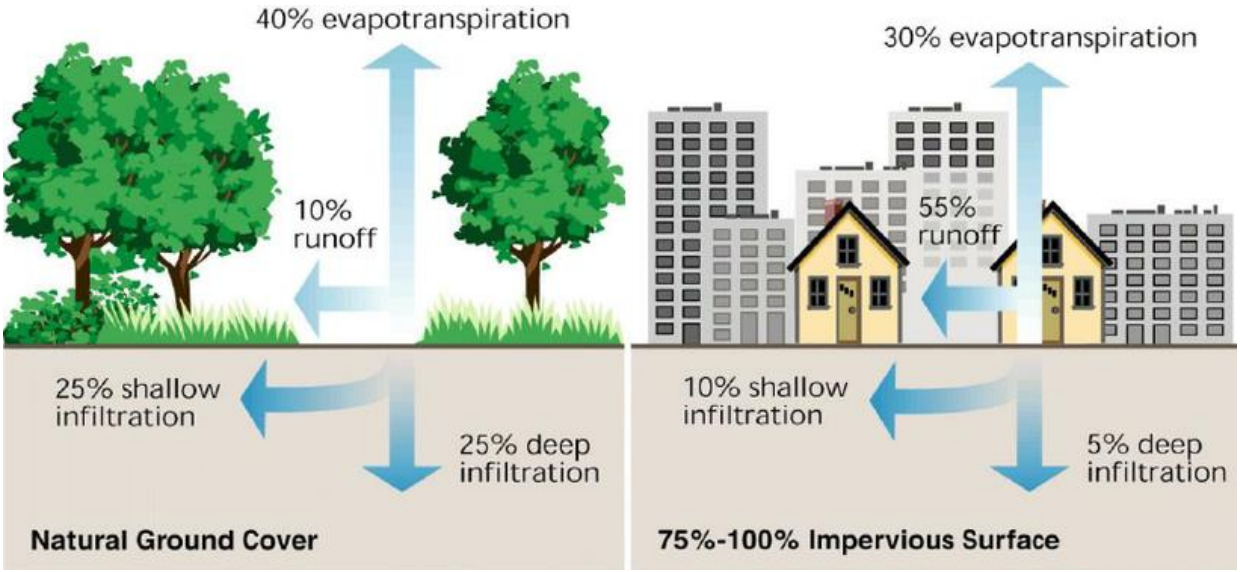

Figure 1: Effects of urbanization on watershed water balance.
Source: https://www.researchgate.net/Change-in-watershed-characteristics-after-urbanization_fig4_272751593 (*modified*)

Stormwater may be difficult to treat because it is everywhere in the landscape. Its production and conveyance are not constant, fluctuating with rainfall or snowfall and dry periods, and it is difficult to attenuate these fluctuations.

The US EPA estimated the number of regulated municipal separate storm sewer systems (MS4s) was about 7,000, including 1,000 Phase I municipalities and 6,000 in Phase II. The number of industrial permittees is thought to be around 100,000. The total

number of permittees under the stormwater program at any time numbers greater than half a million (National Research Council, 2008).

1.2 Current Issues

Many old cities such as Boston or Philadelphia, for example, have old and partially outdated infrastructure such as combined storm and sewer systems. As mentioned previously, old systems were developed to efficiently remove stormwater from roads and walkways. It was costly and labor-intensive to design and build separate storm sewer systems for the occasional rainfall so rainfall was diverted into sewer lines instead, often separating stormwater from wastewater by an interior knee wall. At low flows, wastewater would be directed to the wastewater treatment plant while stormwater was directed directly into rivers or other receiving bodies. At times of high flow and large rainfall events, these systems may reach capacity and overflow the knee wall thereby mixing waters. The mixed flows then deliver raw, untreated sewage to receiving waters. While many combined storm and sewer systems have been replaced with separate networks, reducing peak flows and total volumes of stormwater runoff through treatment via green stormwater infrastructure (GI) is vital and a cost-effective way to reduce system loads. GI refers primarily to the use of small, engineered, on-site stormwater practices designed to treat the quality and quantity of runoff at its source (National Research Council, 2008). Figure 2 is a diagram depicting the differences in MS4 and CSS systems.

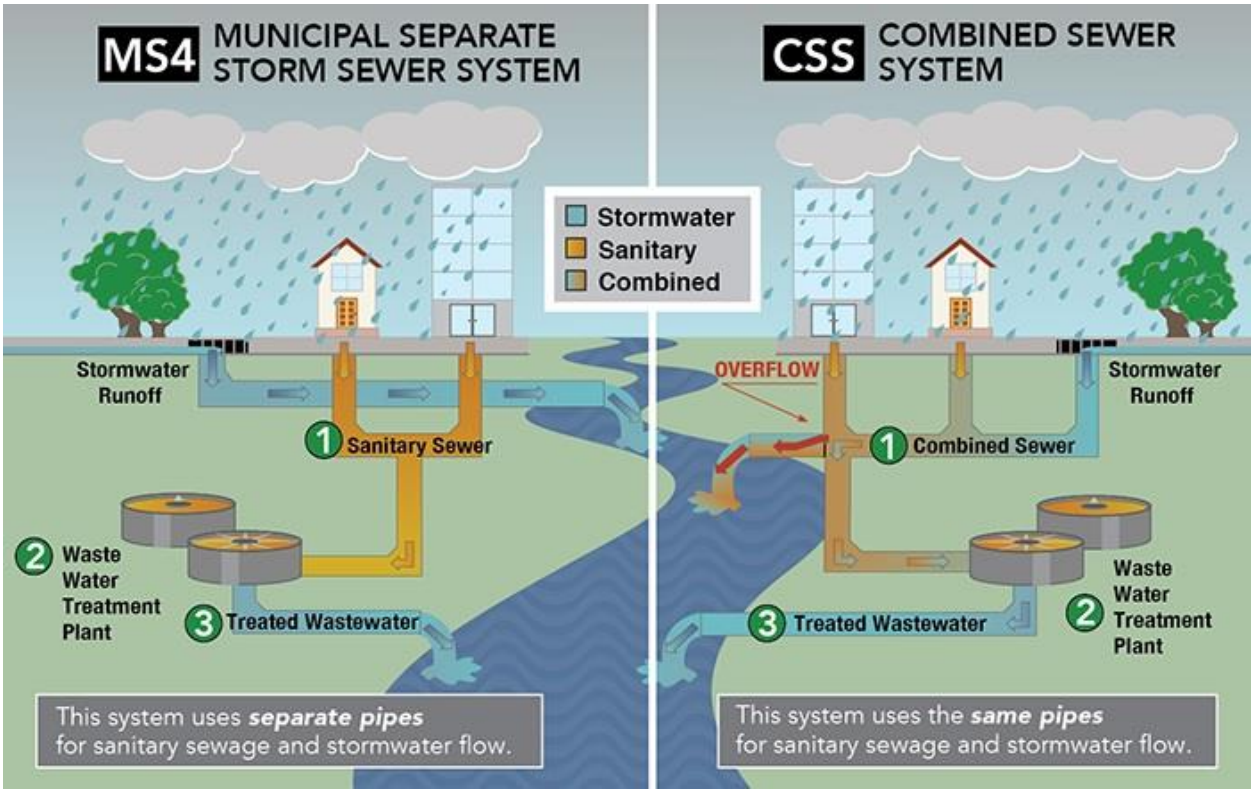

Figure 2: Comparison of MS4 and CSS systems.
Source: D.C. Department of Energy and Environment (2016)

Increased, focused urbanization increases the impervious cover and replaces pervious cover. While there is a current trend to “green” cities and small spaces within them, the rate of urbanization is much greater than the rate of natural landscaping. This may be seen all over the country as suburbs become urban areas and rural farmland and forest are paved with new suburban subdivisions or shopping malls with parking lots.

Increased population density and urbanization is causing increased nutrient and pollution loads from watersheds. While the total pollution loads are increasing, it has been proven that the majority of pollutants conveyed by stormwater runoff occur in the “first flush” of a rainfall event. Early studies in Florida indicated that the first flush carries 90% of the pollution from a storm (Hydrologic Aspects of Nonpoint Pollution, 1995). To treat

this first flush, the policy of treating the first half inch of runoff was adopted in most the U.S. as the Water Quality Volume (WQV). However, recent research has shown that pollutant removal from this first half inch drops off considerably as site imperviousness increases; since then, the 90% rule has been used to capture and treat 90% of annual runoff and therefore 90% of the pollutant load (Comprehensive Environmental Inc. & NH DES, 2008). In New Hampshire, this is roughly equivalent to treating the runoff from the first 1 inch of precipitation for each rainfall event. This will be referred to as the “design” event generally in this study.

1.3 Bioretention Filters

Bioretention filters are a best management practice (BMP) developed in the early 1990’s by the Prince George’s County, MD, Department of Environmental Resources (PGDER) (1993). They were designed to treat stormwater runoff from impervious surfaces at commercial, residential, and industrial areas. Bioretention filters are a layered system of gravel or pea stone and an engineered soil mixture often planted with native vegetation or grasses. The vegetation reduces the potential for erosion and assists in removing pollutants from the captured runoff.

Runoff first passes through the vegetated area, trapping gross particulates and debris. It may pond on the surface if the influent discharge is higher than the rate of filtration, allowing for some evaporation. It then filtrates through the bioretention soil media (BSM), further filtering finer particulates and treating chemical pollutants through plant root uptake and/or microbial metabolization. The organic layer provides an environment suitable for plant growth as well as microorganisms. Microorganisms degrade petroleum-based

pollutants and assist in plant root uptake. Clay particles in the BSM provide adsorption sites for hydrocarbons, heavy metals, nutrients, and other pollutants (USEPA, 1999). See Figure 3 for a cross-section view a typical bioretention filter as built at the University of New Hampshire Stormwater Center (UNHSC).

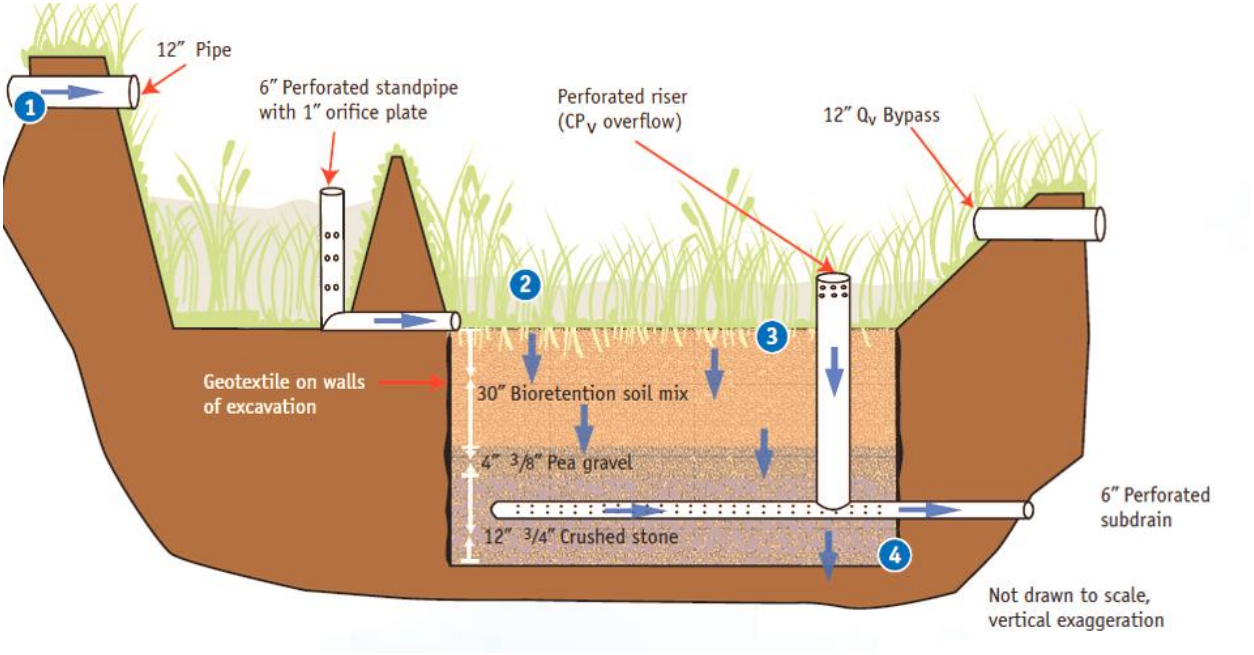

Figure 3: An example of a typical bioretention filter cross-section showing an optional forebay. Diagram courtesy of UNHSC (2009).

Figure 3 shows the (1) inlet to the bioretention system that carries the runoff from the treatment watershed into the forebay. The forebay helps trap gross solids and trash that could quickly clog the bioretention filter surface. After passing through the forebay, the water flows through the vegetated surface where ponding may occur at (2). Section (3) shows the BSM layer and filtration through the root zone into the lower stone layers. Filtered water drains into the bottom layer of gravel or pea stone and may be temporarily stored before infiltrating into the native soils gradually (4). In the case of very low

permeable native soils or high influent flow rates, the filtered runoff may exit the bioretention through an underdrain which connects to the outlet of the system. At the top-right of the diagram, the perforated riser and bypass give a high-flow bypass for events that exceed the design event such that high flows may efficiently be conveyed out of the system while preventing damage to the filter. As with any BMP, a maintenance plan must be developed and followed if the system is to continue functioning as designed. See (UNHSC, 2017b) for details.

Guidelines suggest that contributing watersheds for treatment by one bioretention should be between 0.25 - 1.0 acres, with a maximum area of 5 acres (USEPA, 1999); common ratios for watershed to filter areas are between 10 to 40. The maximum depth of ponding is suggested to be less than 6 inches as ponded water at greater depths may take in excess of four days to drain (USEPA, 1999); the UNHSC recommends less than 18 inches of ponding depth. This may pose a problem to vegetation that is water-sensitive. Additionally, mosquitoes and other insects may start to breed in stagnant water if left standing for more than four days.

For new design, the current design standards for sizing the ponding and treatment area of the bioretention filter are the same as those set in 1993 by PGDER. The design is a static design using a dynamic filtration equation through the BSM. For a system built as a retrofit filter in an as-built situation, the common current design is to size the filter to hold the Water Quality Treatment Volume in the filter. This will be discussed in more detail in Section 2.1.

1.4 Soil Characteristics

This section is a brief introduction to the terms and concepts associated with soil properties that will be used in detail in this study and is not meant to be comprehensive. More detailed descriptions and background may be found in a soil physics or hydrology textbook.

Porosity (η) is the index of pore space in a soil. It is generally in the range of 0.3 to 0.6 (Hillel, 1998). Porosity is defined as the ratio of pores or voids to the total material bulk volume. This index does not say anything about the size or distribution of the pores, however.

Volumetric water content (VWC) is similar to porosity. While porosity is the ratio of total voids to bulk volume, VWC is the ratio of the volume of water to the bulk volume. If a soil is oven dried, it can have a VWC of zero as the volume of water in the sample would be zero. On the other hand, a sample that is completely saturated cannot contain a volume of water greater than the volume of voids. This sets the porosity as the upper limit.

Soil particles are classified by their size. Using the USDA soil classification method, clay particles are defined as being less than 0.002 mm; silt is between 0.002 - 0.05 mm; sand is between 0.05 - 2.0 mm; and gravels are greater than 2.0 mm (USDA SCS, 1987).

Any soil may be tested using a standard sieve and/or hydrometer analysis (ASTM Int'l, 2004) (ASTM Int'l, 2016) to determine the distribution of various soil particles as described above. This is called a Particle Size Distribution (PSD) and is presented as the mass percent finer for various particle sizes. This PSD may be used to classify the soil sample using the USDA soils triangle as shown in Figure 4.The triangle is read as a graph with three axes (clay, silt, and sand). Notice the axes labels are rotated to be parallel to

the direction of its grid. The total percentage of each axis for any point within the triangle will be one (100%). For example, the red dot shown in the “loam” area is comprised of 20% clay, 45% silt, and 35% sand. The total is 100%. It should be noted that soils may be classified by different standards such as the U.S. Department of Agriculture (USDA), International Soil Science Society (ISSS), U.S. Public Roads Administration (USPRA), British Standards Institute (BSI), Massachusetts Institute of Technology (MIT), or German Standards (DIN). See Figure 3.1 from Hillel (1998) for a detailed description. The USDA classification will be used in this study. The PSD is useful to distinguish different textured soils and correlating the soil texture with other soil characteristics such as permeability and hydraulic conductivity.

Hydraulic conductivity (*K*) is an important parameter when discussing flow through porous media. It represents the permeability of flow through the media and has units of length per time. Not only does hydraulic conductivity depend on the porosity of a soil, but also the structure and sizes of the conducting pores (Hillel, 1998). For example, a certain gravel and clay may have similar values of porosity, but the size of the conducting pores in clay will be much smaller than in gravel, thus the hydraulic conductivity in the clay is expected to be smaller than that of the gravel. Hydraulic conductivity may vary with moisture content and will become a constant in a porous medium when saturated as it approaches a steady state. This is referred to as the saturated hydraulic conductivity. The product of hydraulic conductivity and a hydraulic gradient is the flow velocity, or Darcian velocity, as it was first observed and described by Henry Darcy in 1856. Hydraulic conductivity is a property of the soil and the fluid. Characteristics that affect the value of hydraulic conductivity are total porosity, the distribution of pore sizes, tortuosity, the fluid’s

density, and the fluid's viscosity (Hillel, 1998). It is assumed in this study that the water density and viscosity are constant as the range of working temperatures in stormwater systems do not vary significantly.

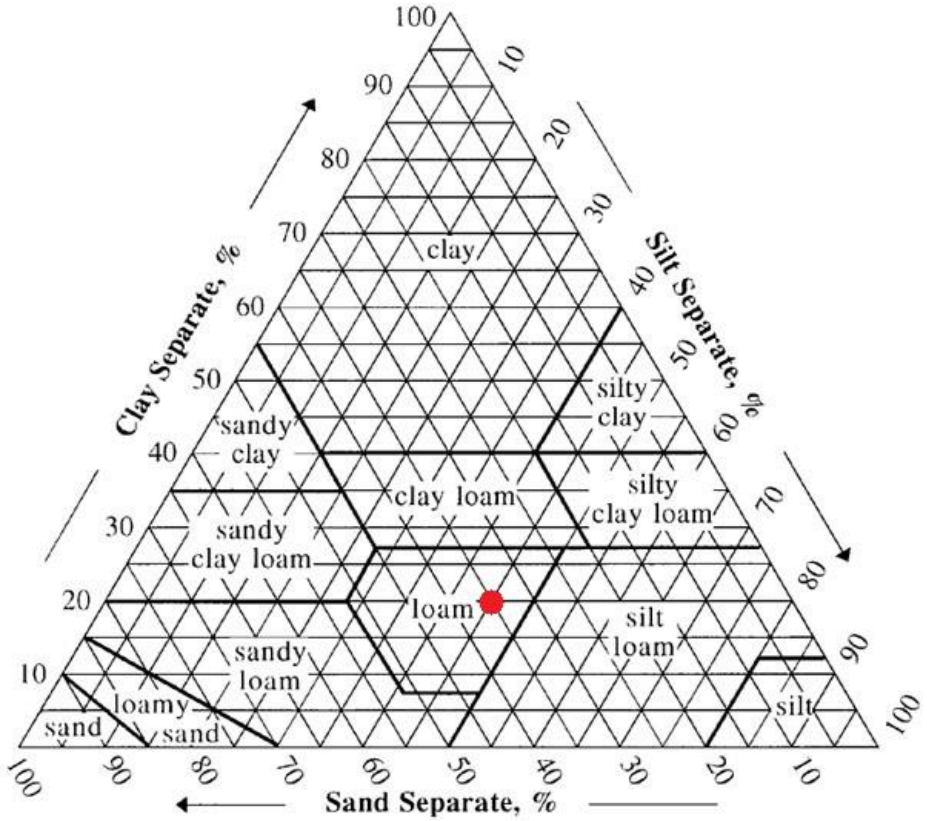

Figure 4: USDA soil textural triangle, showing a loam sample (red point) comprised of 20% clay, 45% silt, and 35% sand.
Source: https://www.nrcs.usda.gov/wps/portal/nrcs/detail/soils/survey/?cid=nrcs142p2_054167

Surface tension is responsible for a suction force between pore water and soil particles. Electrostatic forces between water molecules and particle surfaces draw a film of water around particles in unsaturated conditions, leaving a pocket of air in the void spaces (Todd & Mays, 2005). This suction head (ψ) (also known as matric potential, or

matric tension) is the energy due to soil suction forces. It may be expressed in units of pressure, but units of length will be used in this study to represent head.

Anisotropy describes the directional properties of hydraulic conductivity. In alluvial conditions, this may occur because deposited particles are seldom spherical and can rest with their flat sides down or due to a deposition of layers of different materials that have varying values of hydraulic conductivity. The layers of varied conductivity tend to retard vertical flow in preference to horizontal flow parallel to the layers' interface. Under these conditions, horizontal hydraulic conductivity will be a greater value than in the vertical direction (Todd & Mays, 2005).

1.5 Methods for Estimating Hydraulic Conductivity

The estimation of hydraulic conductivity is very important for the infiltration models to be discussed. This section will give a brief overview of several methods that were used for estimating *K* in this study. The methods discussed will be particle size distribution, double ring infiltrometer, and the Guelph permeameter.

The first method discussed will be the particle size distribution. This test method separates particles of a soil into size ranges to analyze the structure of the soil. For large particles, square open sieves are used to separate and determine the gradation of particles between 3 inches (75 mm) and the No. 200 (75 μm) sieves. Such a test is described by ASTM Test Method D6913-04 (ASTM Int'l, 2004). This test method is not applicable for soils containing extraneous matter such as wood fragments. This is relevant to BSM as it often contains organic matter such as wood chips or shredded bark which

must be removed prior to performing this test. For particles larger than 3 inches, Test Method D5519 may be used.

For particles smaller than the No. 200 (75 µm) sieve, ASTM Test Method D7928-16 may be used (ASTM Int'l, 2016). This sedimentation or hydrometer method uses the principle of Stoke's Law as particles fall through stationary liquid. Because the particle terminal settling velocity is proportional to the square of the diameter, the particles are sorted by size in both time and position when settling in a container of liquid. This method assumes that particles are spherical and smooth, there is no interference between particles, there is no difference between the settling particles in the middle and the sides of the container, flow is laminar, and all particles have the same density (ASTM Int'l, 2016). This method may be used to evaluate the fine-grained fraction of a soil and be combined with a dry or wet sieve analysis, resulting in the complete gradation curve. If the soil sample contains almost no clay or silt, this method is unnecessary as the sieve method alone will properly evaluate the gradation.

Estimation of hydraulic conductivity from a PSD is generally based on the use of the Kozeny-Carmen Equation or variations of it which involve a relationship between saturated conductivity (K_s), porosity, and some represented particle diameter. While actual measurements are preferred, the Kozeny-Carmen Equation provides a crude estimate of the order of magnitude for saturated hydraulic conductivity. Mishra, et al. developed a methodology to not only estimate K_s but also the uncertainty for it and other parameters (1989). However, they note that while estimating conductivity from PSD data is convenient, soil parameter estimates, especially K_s, may be associated with large uncertainty.

The next method for estimating *K* involves the use of a double ring infiltrometer (DRI). This method is particularly applicable to uniform fine-grained soils that do not contain high amounts of plastic clays and gravel-sized particles. Soils should be regarded as naturally occurring fine or coarse grain soils or processed materials (ASTM Int'l, 2009). This method is conducted at the ground surface with vegetation in place. Therefore, it is especially useful on built bioretention systems and surface soils. A quick and convenient tool for a similar estimation is a Turf-Tec infiltrometer. Its small size makes it convenient for travel to sites and uses very little water as the rings' volumes are small. The UNHSC has found generally that estimates of K_s from the Turf-Tec infiltrometer are about four times greater than a standard DRI (unpublished). The limitation of this method was mentioned: it is performed on the soil surface. Therefore, a DRI test may only be performed in the soil profile if a borehole is dug large enough to accommodate the infiltrometer and leave room for the observer to record measurements. This is often impractical in the field.

A convenient and easy to operate infiltrometer that deals with those issues is the Guelph Permeameter (GP). The GP tests are in situ and require very little equipment, water, and training to operate. It involves measuring the steady state liquid recharge necessary to maintain a constant depth of water in an uncased, cylindrical well above the water table (Reynolds & Elrick, 1986). The permeameter is based on the Mariotte principle used to maintain a constant head within the water reservoir. The borehole may be dug manually with an auger. If testing in soils with a high clay content, it is recommended to grind off the bottom to give a flat bottom well, which is assumed in the analysis. Additionally, both the auger and probe tend to smear the walls of the well as it

is dug and is often visible as a polished surface when seen with a flashlight. Smearing may lead to unrepresentative low recharge rates. However, the smear layer may be removed with a small spite wheel or stiff brush to break up and pluck the walls (Reynolds & Elrick, 1986). The hole depth is usually up to about three feet, but can theoretically be extended to about 26 feet with easy modifications to the apparatus. To minimize the error of negative values of the field saturated hydraulic conductivity (K_{fs}) caused by macropores or layer boundaries between two head measurements, it is recommended to test by ponding three or more head levels instead of just two and use the least squares approach. This tends to average the variation between the heads by producing a weighted mean (Reynolds & Elrick, 1986). If only a rough estimate of K_{fs} is needed, a single or double head test may be run using the Laplace approach or a double-head test using Richard's analysis. While this method can be accurate, it has been found to produce a high percentage of invalid (negative) values of K_{fs} and ψ because it is sensitive to the ratio of recharge rates from the two heads. For more accurate estimations, multiple head tests are run and the data analyzed using the least squares approach presented by the authors. These methods have been successful in uniform, structureless materials. In other conditions, a single head test with an assumption about the alpha parameter may be used, which has given good estimates without invalid results (Elrick, Reynolds, & Tan, 1989).

The GP measures field saturated hydraulic conductivity in porous media containing entrapped air. Depending on the amount of entrapped air, K_{fs} can be as much as 50% lower than the truly saturated hydraulic conductivity (Reynolds & Elrick, 1986). Their work indicates that in granular material, primarily horizontal K is measured while an average of

vertical and horizontal K is measured in a structured medium (Bouwer & Jackson, 1974). The GP is a cost-effective method for measuring field saturated hydraulic conductivity and sorptivity. The downside to this method as indicated by the authors is that it only provides a “point” measurement and therefore requires replication. However, this can also be said of the other tests mention here.

The DRI and GP methods discussed here are both useful and applicable in different situations. Lee, et al. statistically compared 20 measurements at four sites using these methods and found universally that the highest number of failures were for clay sites under wet conditions due to smearing of the well surface by the auger. The average time for a measurement was often the lowest for the GP. Macropores played a smaller role in the GP as the vertical, small-diameter auger hole is expected to intersect and hydraulically activate fewer macropores in loam soil, but perhaps the same number in a clay soil. The GP was suggested where K_s is suspected to be neither dominated by macropores or by the soil matrix but a mixture (1985). Another study by Ebrahimi and Moradi compared the DRI and GP and found that the while the GP had higher mean values of K_s, the two methods yielded a non-significant difference in means (2015). Mohanty, et al. compared the GP to a velocity permeameter, a disk permeameter, and a double tube method in glacial till. The authors found that the GP yielded lower values than the other methods (1994). Gupta, et al. compared the GP, a DRI, and a rain simulator in a sandy-loam and found the estimated means were statistically the same for the GP and DRI methods (1993).

1.6 Infiltration and Infiltration Models

Water in the form of precipitation or irrigation applied to the soil surface enters the soil through infiltration. Infiltration occurs over space and time and may transport fluids as well as soluble contaminants into the vadose zone. In a bioretention system used to treat stormwater, the initial water content and saturated hydraulic conductivity in the BSM are the primary factors affecting the soil-water filtration process (Williams, Ouyang, Chen, & Ravi, 1998). Ponded water that is not infiltrated or runs off the surface may return to the atmosphere through evapotranspiration. Water that is infiltrated is distributed through the soil profile through matric potential, head differentials, and gravity. Soil profiles that are deposited into distinct layers, as is often the case in naturally formed soils, tend to disrupt the vertical infiltration by anisotropy as described previously (Williams, Ouyang, Chen, & Ravi, 1998).

Water in the vadose zone is generally conceptualized as three stages: infiltration, redistribution, and drainage (Ravi & Williams, 1998). Briefly, infiltration describes the movement of water on the soil surface into the soil by gravity. Redistribution describes the movement of the soil moisture through the profile. This may include movement due to gravity, suction gradients, surface exfiltration (ET), recharge from the unsaturated zone to the saturated zone, and interflow moving downslope. Drainage may refer to the removal of groundwater through either artificial means such as ditches or pipe or natural means such as mole holes. Groundwater is drained into the channels due to hydraulic gradients in the soil and are often conveyed to the drainage outlet via gravity (Hillel, 1998). In this study and the following infiltration models, however, all three stages will be grouped into the term “infiltration”.

The first group of infiltration models is based on empirical data. These are often in the form of a simple equation and parameters are found by curve fitting the model to measured infiltration data. Examples of such empirical models include Kostiakov's (1932), Horton's (1940), Mezencev's, USDA SCS (1957), Holtan's (1961), and Boughton's (1966) Equations. However, for this study intending to give guidance on a model for general system performance and design work, empirical models are inappropriate to use as they are based on measured infiltration and do not have a general physical basis.

Another type of infiltration model is based on unsaturated flow conditions. Richards equation is a well-known and powerful equation to use in unsaturated and saturated conditions with homogeneous or nonhomogeneous and isotropic or anisotropic soil conditions. However, due to its nonlinearity and complexity of measurements for soil parameter inputs, it is impractical and inefficient to use in the present study.

Green and Ampt derived the first physically based equation describing soil-water infiltration (1911). It has gained wide acceptance in soil physics and hydrology because of its simplicity and satisfactory performance (Ravi & Williams, 1998). The model assumes a constant water content profile and a well-defined piston type wetting front. The soil is saturated down to the wetting front, where the soil moisture content on the other side of the wetting front is at some initial water content and assumed to be uniform throughout the soil profile (homogeneous). The soil-water pressure head on the unsaturated side of the wetting front is assumed to be the matric potential (Green & Ampt, 1911). The matric potential aligns with the soil's initial water content as described by the soil moisture characteristic curve. Bouwer demonstrated that the hydraulic conductivity K_s presented by Green and Ampt is not equal to the actual saturated hydraulic

conductivity but may be approximated as one-half the saturated hydraulic conductivity (1966).

As the equation for the cumulative infiltration using the approach from Green and Ampt yields an implicit solution, an explicit solution was developed by Salvucci and Entekhabi (1994) which was more straightforward than the implicit solution. They reported an error of less than 2% at all times when compared to the exact values of the implicit Green and Ampt model. While the implicit model must be calculated iteratively or with a numerical solver, the derived explicit model does not. The same assumptions of the explicit model are: homogenous soil conditions and properties; constant, non-zero surface ponding depth; and the surface is not at a constant water content.

The parameters in the Green and Ampt equation may be estimated from tables for a given soil texture such as Tables 7, 8, and 11 from (Williams, Ouyang, Chen, & Ravi, 1998). While these parameters may be obtained from a table, in situ physical measurements are preferred.

Additional work was done by Philip for falling and variable head infiltration using a modified Green and Ampt approach. Under falling head ponding conditions, the maximum time of infiltration can be estimated (1992). This may be useful in design as an approximation for the time it takes for ponded water to infiltrate. His study on variable head ponded infiltrated concluded that the dynamic depth of ponding had little effect on the infiltration process because “the contribution of water depth to the potential difference between the soil surface and the wetting front is small compared with that due to capillarity” (matric potential) (1993).

CHAPTER 2. CURRENT DESIGN

2.1 Current Static Sizing

First, a distinction must be made between the terms “new” and “retrofit” as they are used in this study. The simplest distinction between the two may be made by comparing the surrounding site conditions before and after construction of GI. If the surrounding site is being fully developed as in a new subdivision or other construction, the design is “new”. If the surrounding site remains unchanged before and after the installation of GI, the design is “retrofit”. The Horne St. site study discussed in Chapter 3 is an example of a retrofit system installed in an existing subdivision. The design criteria will be distinguished here.

For new design, Prince George’s County Department of Environmental Resources set the design standard for the sizing in 1993. The design used a static approach to temporarily hold and treat the WQV. The WQV in New Hampshire and other regions is based on capturing the runoff from the first one inch of rainfall, which represents treating the 90th percentile of yearly rainfall, and therefore the pollutants (Comprehensive Environmental Inc. & NH DES, 2008). The WQV is a function of a “design” precipitation (*P*), the contributing watershed area (A_w), and a unitless runoff coefficient (*Rv*) that is a function of the percentage of impervious cover (*I*) in that watershed.

$$\mathrm{WQV} = \mathrm{P}\ \mathrm{Rv}\ \mathrm{A_w} \tag{1}$$

Where the unitless runoff coefficient is given by:

$$\mathrm{Rv} = 0.05 + 0.9\,\mathrm{I} \quad (2)$$

The percent impervious cover is given in decimal form.

The current design standard for newly constructed filters was developed by PGDER calculates the required ponding area (and bioretention filter area). It was developed by a modification of Darcy's Law and is a function of the hydraulic conductivity of the filter media, bed depth, hydraulic head, and sediment loading (Claytor & Schueler).

$$A_f = \frac{WQV\ d_f}{K\left(h_f + d_f\right)t_f} \quad (3)$$

Where:
- A_f = Surface area of the bioretention planting bed (ft.^{2})
- WQV = Water Quality Treatment Volume (ft.^{3})
- d_f = Planting soil bed depth (ft.)
- K = Hydraulic conductivity of the planting soil bed (ft./d)
- h_f = Average height of water above the bioretention bed (ft.); $h_f = \frac{1}{2}\,h_{max}$
- t_f = Time required for the WQV to infiltrate into the planting soil bed (d). Recommended 1 - 2 days.

Note that the design equation derived by PGDER shown in Equation (3) does not show a Factor of Safety (*FS*) used in current engineering practice. This Factor of Safety (typically 2-3) is used as the divisor under the hydraulic conductivity.

As shown by Equation (3), the goal of the design was to filter the WQV (instantaneously placed into the system) through the filter media. The design approach did not consider the fate of the WQV as it may be put into storage in the filter media or underlying stone, infiltrated into native soils, or released as effluent through the underdrain. The only consideration was filtering the WQV through the filter media in a specific drain-down time. Note that this sizing approach assumes the BSM is the hydraulic

throttle. In some designs, a restrictive orifice in the underdrain may be designed as the hydraulic throttle.

While the current design approach does indicate how quickly the WQV should filter through the media and thus not leave exposed surface ponding for extended periods of time, it fails to indicate how much volume is expected to be stored in the system and lost due to ET and infiltration into native soils horizontally through the sidewalls and vertically into the bottom of the filter.

For retrofit systems, the existing site conditions often constrain the allowable filter surface area. With a constrained area, the full treatment rainfall of one inch often cannot be treated, and the treatment rainfall must be calculated for the allowable site system are and volume. This may be accomplished by using Equation (3) for the given location and other parameters; however, for many states including New Hampshire, the filter may be sized using a static volumetric calculation. The full WQV must be instantaneously stored in the system. This is calculated by the total available pore space in the stone layer, bioretention soil media, and surface ponding. The bulk volume of each layer multiplied by its respective porosity will give the available storage space, with the porosity of the surface ponding being one.

2.2 Other Modeling Methods

While the method derived by PGDER and the volumetric calculation are the current design standard, other models have been developed in the attempts to improve the design by using dynamic models. Some dynamic models that model the filter in different states, unlike the SCS 24 hr. rainfall distribution will be presented here.

Akan (2013) developed a simple to use and physically based mathematical model for preliminary design of a filter size. All parameters were physically based; therefore, calibration of the model was unnecessary. The input parameters must be measured in situ or obtained from tables of soil characteristics. The solution output was a series of dimensionless solution graphs to check if the given system would drain in the desired time. Using the Dimensionless SCS Unit Hydrograph, the model required only the peak discharge of the runoff rather than a complete hydrograph, with the assumption that the complete hydrograph takes the same shape as the Unit Hydrograph.

Using a similar assumption to the approach by PGDER, only vertical infiltration through the BSM was considered. However, unlike PGDER, the Akan model was dynamic in the way the influent discharge reached the filter. Unlike the PGDER approach, which assumed the WQV arrived instantaneously, Akan's model allowed for a unit hydrograph to dictate the influent discharge rate which varied over time. In the bioretention system, the model employed a Green and Ampt approach for a sharp wetting front infiltrating vertically through the BSM. There were four phases of an event considered by the model. Briefly, the phases describe a 1) ponded condition where the wetting front is connected to the ponded surface and moving downward, 2) a ponded surface when the entire BSM is saturated, 3) no surface ponding or influent discharge as the "piston" of water travels downward as both the wetting front and trailing "surface" of the piston travel together, and 4) the lower edge of saturation remains at the bottom of the filter and the upper edge moves downward as the BSM drains. See Figure 1 of the paper for a schematic of these phases (Akan, 2013).

Palhegyi (2010) developed another model similar to that of Akan except evapotranspiration (ET) was considered over time. It was a computational model to simulate the water balance for vertical distribution in the soil layers applicable to bioretention filters. The model consisted of a surface reservoir, soil layers, and outlet controls. The modeled soil moisture was divided into two parts: retained and drainable fractions. The retained fraction of soil moisture represented the field capacity and could only be depleted by ET. The drainable fraction would eventually percolate into the native soils. During a simulated event, ET was assumed to be zero. Otherwise, average monthly ET rates were used as input.

The model was compared to several bioretention sites at Villanova University, Pennsylvania. The author claimed that the model both over- and under-predicted different storm events, but it performed satisfactorily overall.

The model results indicated that ET was two orders of magnitude smaller than deep percolation over a period of several days. Generally, the soil moisture was fully drained between storm events during the rainy season, and deep percolation only occurred after field capacity had been satisfied.

The author's conclusion was that bioretention filters treating watersheds with 100% impervious cover should be sized to treat a runoff volume from 2 to 4 inches of precipitation; if the impervious cover is around 20% to 30%, the standard treatment from 1 inch of precipitation is adequate. The author notes, however, that the results were specific to the areas where the study was conducted.

While there are some models that consider the dynamic behavior of rainfall and its effect on runoff using a Green and Ampt approach ((Philip, 1993), (Chu, 1978),

(Rossman, 2017)) or Richards equation (Dussailant & Wu, 2004), such models only consider one-dimensional (vertical) infiltration into native soils or the bottom of an LID system in the case of EPA SWMM, assuming that horizontal flow in soils is negligible relative to vertical seepage.

Lateral infiltration is often assumed to be negligible in modeling and design, yet the models do not accurately account for the total infiltrated volume observed in the field. The horizontal infiltration may play a large role in infiltration and may improve modeling and design methods if included. While infiltration wetting fronts in vertical and horizontal orientation have been of interest to soil physicists since the Green and Ampt model in 1911, simple saturated horizontal models are not common. Many employ Richards equation and are solved numerically due to the nonlinear nature. An analytical solution was developed by Huang and Wu (2012) for 1-D horizontal and vertical water infiltration for time-varying rainfall. As an analytical solution to Richards equation, the model had assumptions about the initial and boundary conditions, and applied the Fourier integral transformation to solve the one-dimensional nonlinear differential equation of flow in unsaturated soils. They used exponential water content and hydraulic conductivity relationships to linearize the Richards equation (Huang & Wu, 2012). In the 1-D horizontal infiltration, the bottom and soil-side boundary were assumed to have a pressure head of zero, and the surface and water-side boundary could have either water infiltration fluxes or constant pressure heads due to the water level. The analytical solution for steady, unsaturated horizontal infiltration required the infiltration rate, saturated hydraulic conductivity, a pore-size distribution parameter, the horizontal distance between the boundaries, and water head. Starting from an assumed initial pressure head distribution

of zero, the model was run until steady-state conditions and produced a time-varying solution of pressure head profiles and wetting front length. While the analytical solution is convenient for checking numerical methods, the same issues of impracticality in the application in this study remain.

CHAPTER 3. SITE STUDY

3.1 Location and Climate

The Horne St. bioretention system (HSBS) is located on Horne St. just south of Glencrest Ave. in Dover, NH – in EPA region one.

The climate in Dover, NH is considered coastal, cool, and temperate. The average annual precipitation (including snow-water) is 48 inches, nearly uniformly distributed throughout the year with monthly averages of 4.1 inches. The mean annual temperature is 48° F, with an average low of 15.8° F in January and an average high of 82° F in July (UNHSC, 2005).

3.3 Watershed

The HSBS was built in a typical suburban neighborhood adjacent to an elementary school playground. The watershed is shown in Figures 5 through 8. The watershed was analyzed using ArcMap GIS software with LIDAR elevations and impervious cover from the NH GRANIT clearinghouse. The LIDAR elevation maps had a resolution of 2 m. and an accuracy of 15 cm vertically. The impervious cover layer had a resolution of 1 ft. The soils information was extracted from the USDA Web Soil Survey. The analyses were verified by in-field surveys.

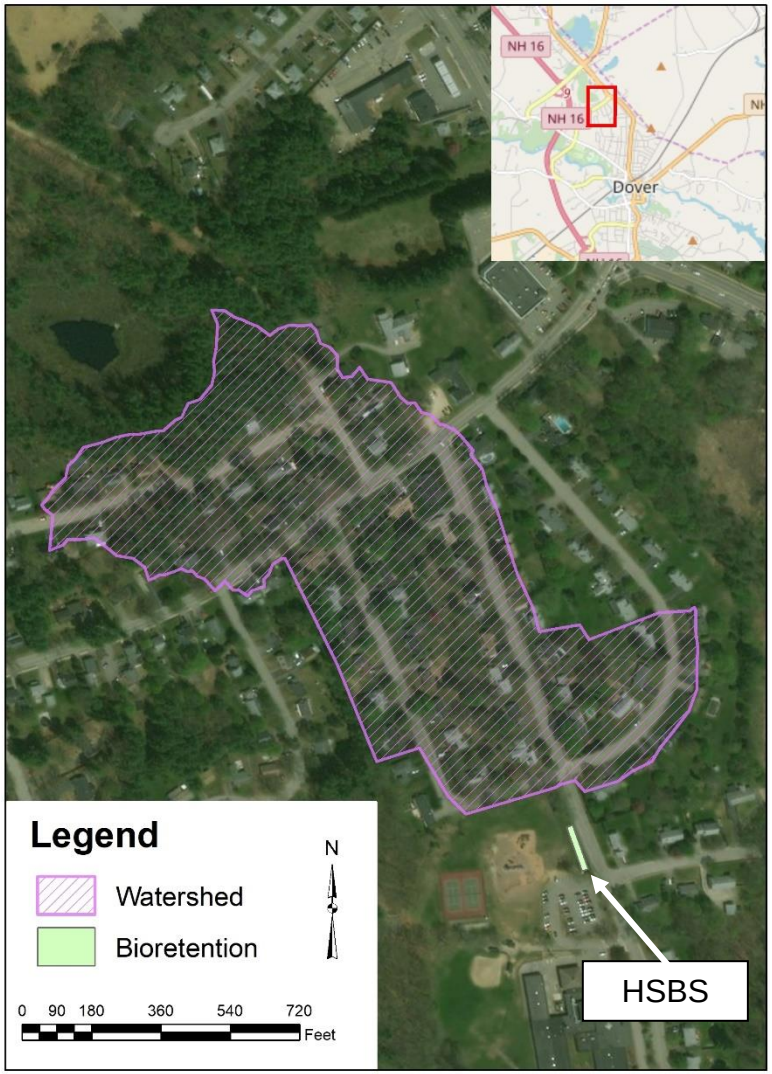

Figure 5: Contributing watershed for the Horne St. bioretention: contributing watershed area and bioretention area

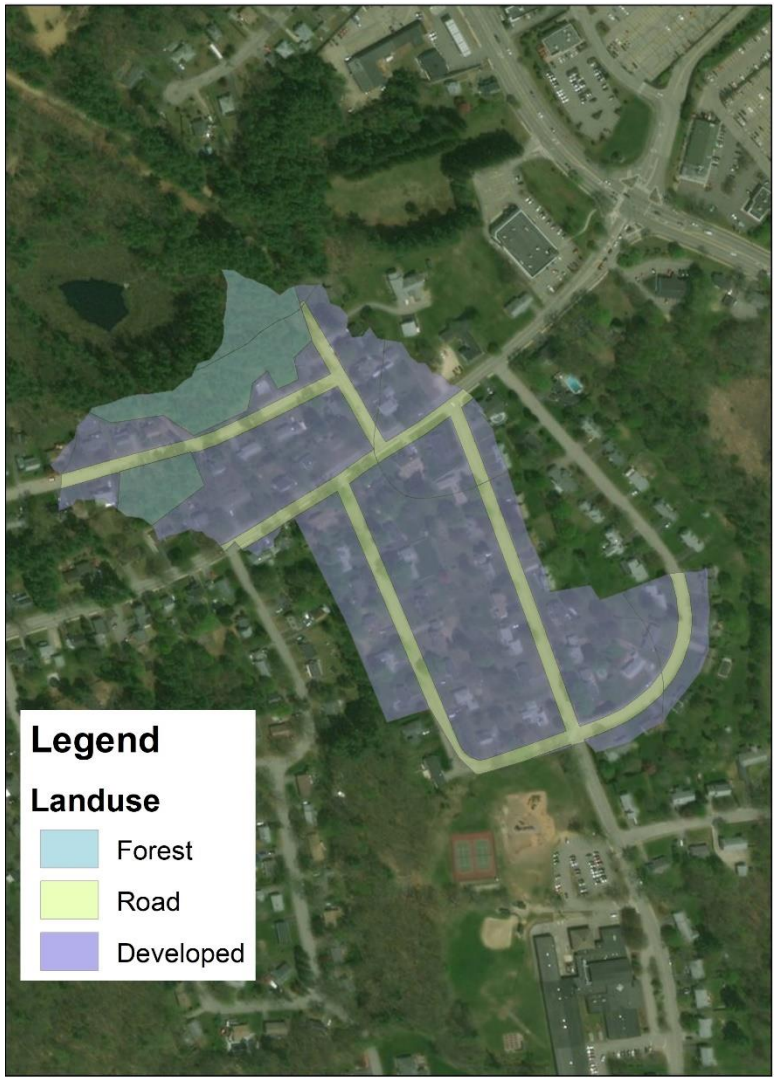

Figure 6: Contributing watershed for the Horne St. bioretention: land use with forested, paved, and 1/3 acre residential lots

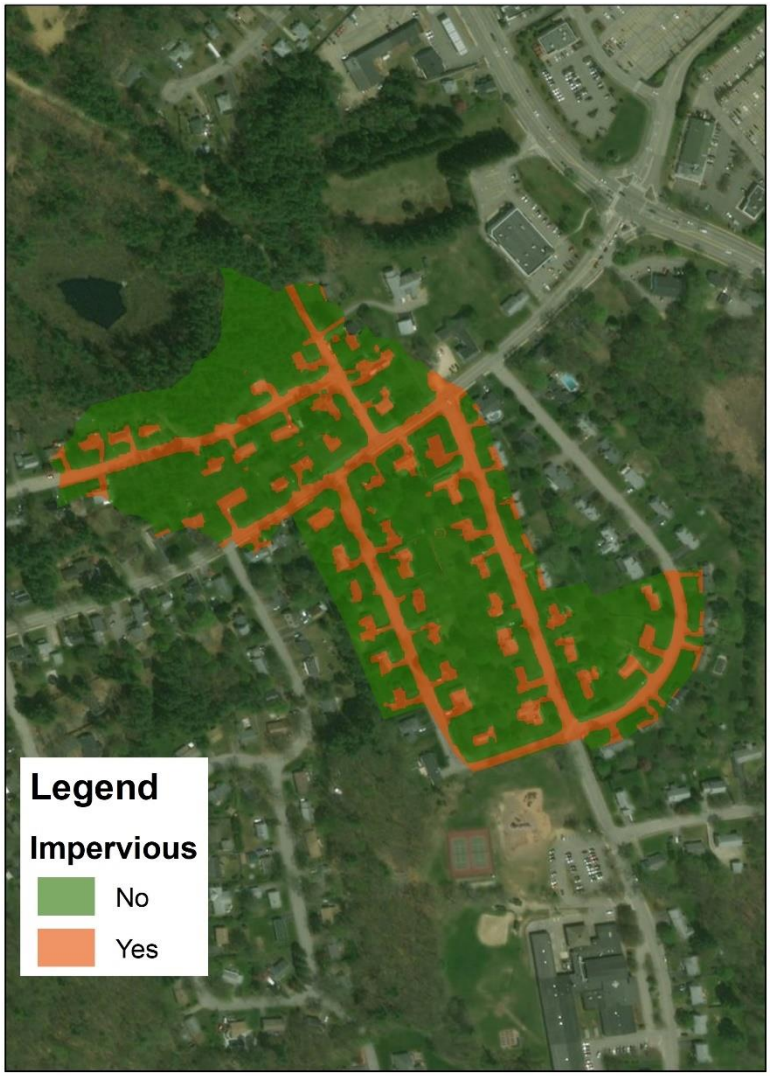

Figure 7: Contributing watershed for the Horne St. bioretention: pervious and impervious cover

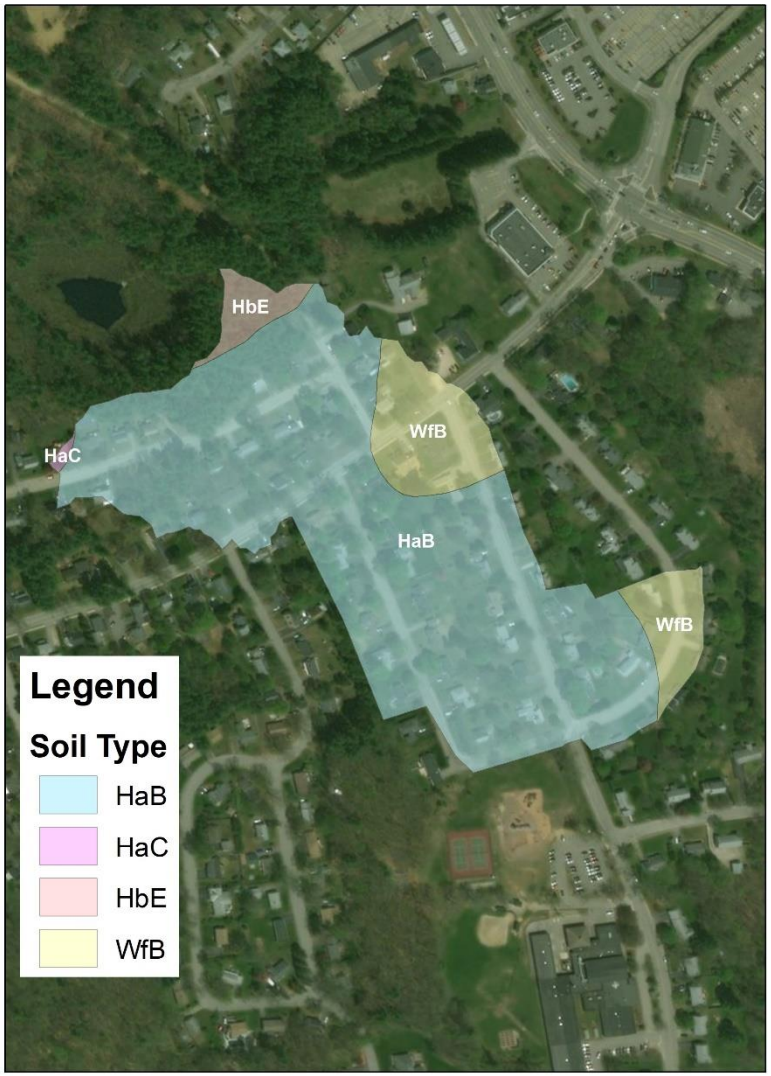

Figure 8: Contributing watershed for the Horne St. bioretention: soil types from Web Soil Survey

As shown in Figure 5, the contributing watershed has an area of 21.9 acres (38% impervious) and the bioretention has a media area of 2,100 sq. ft. (0.048 acres). The ratio of watershed to filter areas is 455:1. The impervious area in the watershed to filter ratio is about 173:1. This is well above the recommended maximum watershed area of about 5 acres (USEPA, 1999) (Comprehensive Environmental Inc. & NH DES, 2008), above conventional watershed to filter ratios of 10 to 40, and above the directly disconnected impervious area to filter area ratio of about 16:1 (Philadelphia Water Department, 2015). However, because the system was built as a retrofit installation to treat a suburban watershed, the existing site location constrained the maximum filter area.

Figure 6 shows the land use within the watershed. This analysis was used to determine the watershed average NRCS Curve Number (CN). Most of the watershed is 1/3 residential lots with paved roads, and there is a section in the northern end that is forested and in good condition.

Figure 7 shows the pervious and impervious cover (IC). While the data from Figure 6 was used for estimating the CN, this data gave a more precise estimation of impervious cover. The watershed is 38% impervious cover.

Figure 8 shows the soil types from Web Soil Survey. While the watershed has varying types of soil, all of them are in the Hydrologic Soil Group (HSG) A. This was also used in estimating the CN. HSG A soils have a saturated hydraulic conductivity of the least transmissive layer of at least 1.42 in./hr. (USDA NRCS, 2007).

The CN was estimated using the data from Figure 6 and 8. The summary data for estimating the weighted CN is given in Table 1. The CN data were obtained from Table 2-2 from TR-55 (USDA NRCS, 1986). The watershed has a weighted CN of 60.

Table 1: Watershed characteristics for estimating the weighted NRCS Curve Number.

Land Cover	HSG	IC	Area (ac)	IC (ac)	CN
Woods, Good	A	0%	2.69	0.00	30
Paved Road	A	100%	3.58	3.58	98
Residential: 1/3 ac	A	30%	15.68	4.70	57
		Total	**21.95**	**8.28**	

The contributing watershed had a path length of 1854 feet from the hydraulically farthest point to the watershed outlet (bioretention inlet). The time of concentration (T_c) is the time required to travel from the hydraulically farthest point to the outlet. The average slope for the watershed was about 0.8%. Using the velocity method for mostly shallow concentrated flow along paved and grass gutters, the estimated velocity was about 1.8 fps. The path length divided by the velocity gave a time of concentration of about 17 minutes. On a hydrograph, this is the time from the end of excess rainfall to the point of inflection on the receding limb (McCuen, 1941). Analysis of hydrograph data for the HSBS recorded at 1-minute logging intervals yields the median observed T_c of about 16.5 minutes. This was consistent with the estimated time. See Appendix A.1 for more details.

The lag time describes the delay from when excess rainfall begins until runoff reaches its maximum peak at the outlet (USDA NRCS, 2010). The HSBS hyetographs and hydrographs give the estimated observed median lag of about 9 minutes. See Appendix A.1 for more details.

3.4 System Design

The HSBS was a retrofit filter for the subdivision just South of Glencrest Ave. and Horne St. in Dover, NH. Using the conventional sizing given by Equation (3) and a design precipitation of 1 in. would result in a filter surface area of about 12,000 sq. ft. However, as a retrofit design, the site restrictions limited the shape and area of the filter. The built system surface area was 140 ft. x 15 ft., or 2,100 sq. ft. (UNHSC, 2012b), (UNHSC, 2016b). As such, the retrofit design event using Equation (3) was about 0.16 inches over the watershed described in Section 3.3; using the static volumetric calculation, the treatment storm was about 0.14 in. For consistency in this study, the treatment storm will refer to the 0.16 in. event. The WQV for this event calculated using Equation (1) is 4966 cu. ft. The ponding area has a maximum depth of four inches and a surface incline of 1%; the maximum volume of water held on the ponded surface before bypass is 336 cu. ft. The native soils in the bottom of the excavation had measured infiltration rates of 0.20 in./hr., 0.16 in./hr., and 0.11 in./hr. at 14 ft., 73 ft., and 119 ft. from the inlet, respectively. The areally weighted mean infiltration rate was about 0.16 in./hr., which would classify the native soils at the bottom of the excavation in the range of HSG C (USDA NRCS, 2007).

The filter is comprised of two layers. The bottom layer is 2 ft. of 3/8 inch pea stone with a 12-inch perforated underdrain the length of the system located 6 inches above the bottom of the excavation. Above the stone layer is a 2 ft. layer of BSM comprised of 60% sand, 20% woodchips, 10% compost, and 10% topsoil (UNHSC no longer recommends the addition of compost to the BSM (UNHSC, 2017a)). The BSM was prepared and installed by the City of Dover. Due to poorly drained native soils, a 0.25 ft. layer of 1.5-

inch reservoir stone was placed between the pea stone and native soils (UNHSC, 2016b). Note that unlike the diagram in Figure 3, the stone reservoir layer in HSBS was primarily pea gravel rather than ¾-inch crushed stone. See Figures 9 to 11 for the design plans showing the cross-section, plan, and profile views of the built filter.

As the filter was long, narrow, and at a slight incline following the grade of the road and sidewalk (1%), a unique design element was added by dividing the filter into three terraced cells by the addition of 4-inch berms or check dams. This was done to slow the flow of water across the filter surface from the inlet to the outlet to allow more time for infiltration through the BSM and to increase the volume of surface ponding. The completed system with views from the North and South is shown in Figures 12 and 13, respectively.

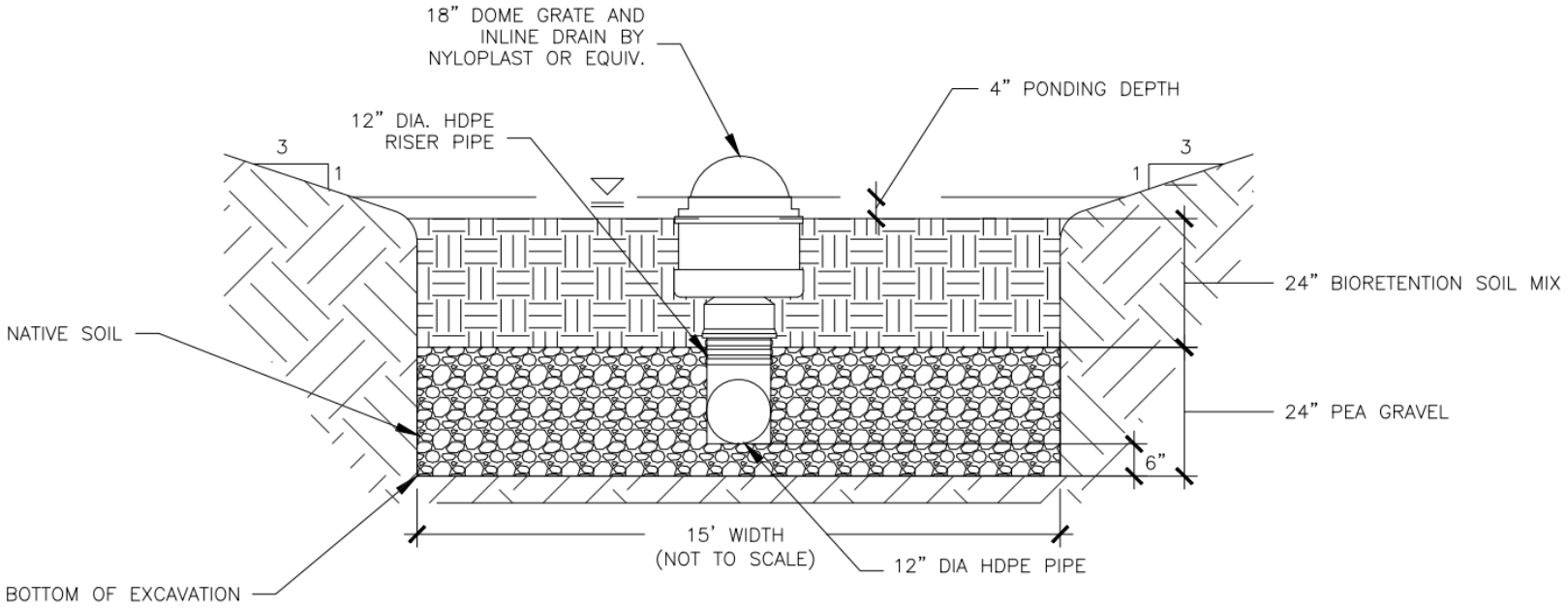

Figure 9: Horne St. bioretention system plans showing the cross-section view with the high-flow bypass and underdrain (UNHSC, 2012b).

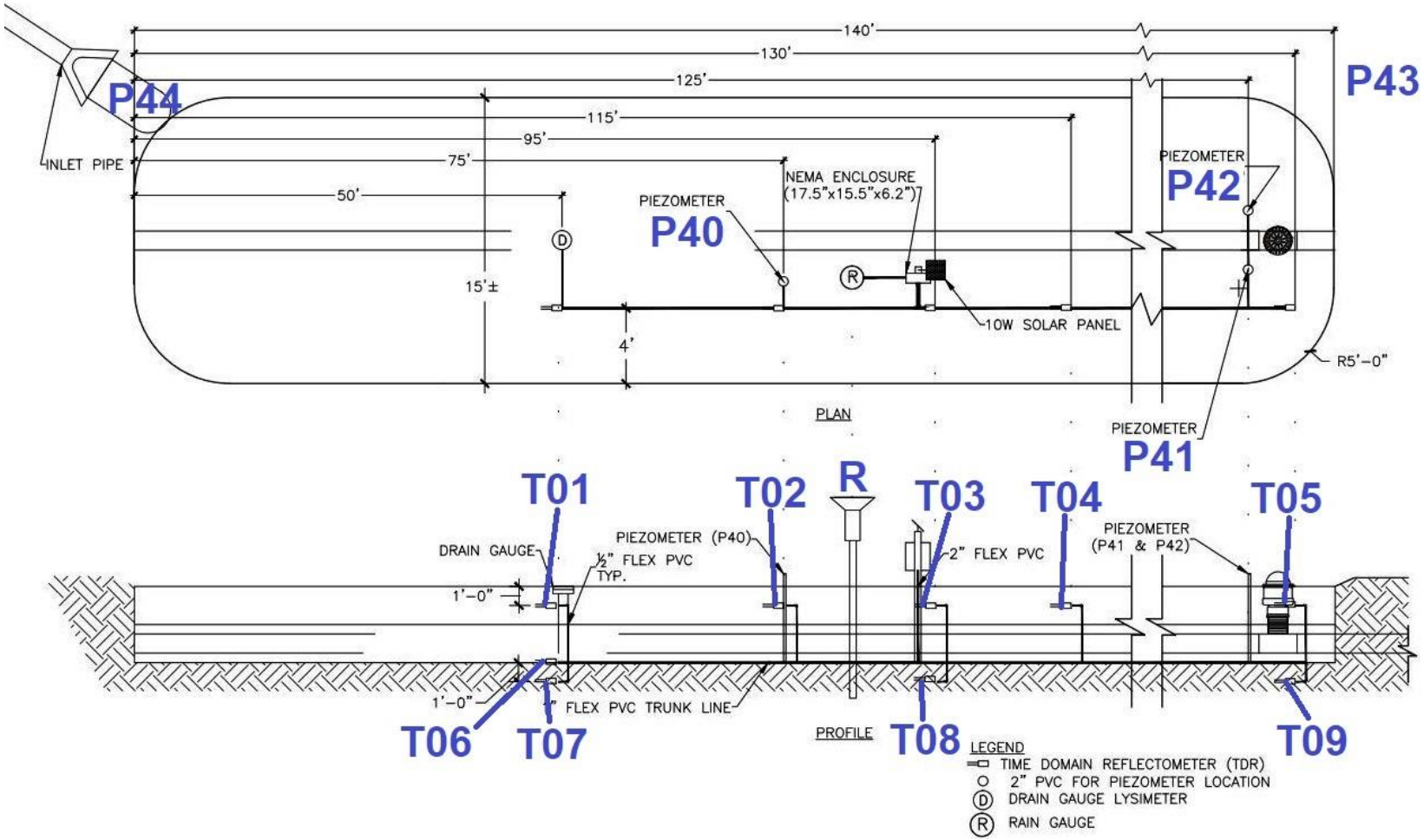

Figure 10: Horne St. bioretention system plans showing the plan and profile view with instrumentation (UNHSC, 2012b).

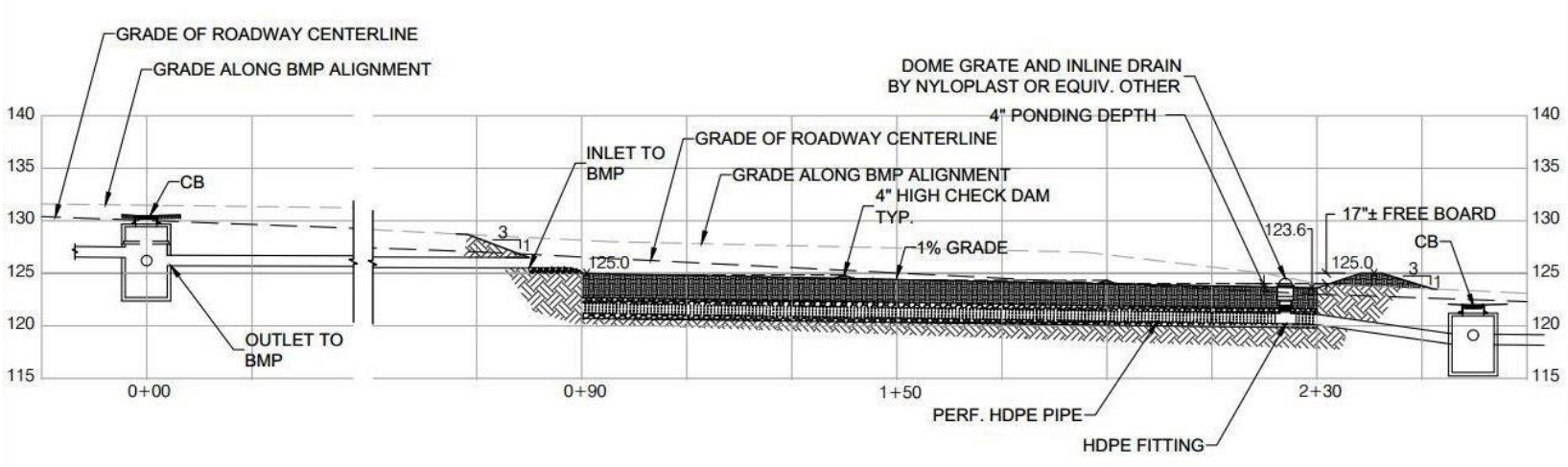

Figure 11: Horne St. bioretention system plans showing the profile view to connecting storm sewer pipes and grade of roadway (UNHSC, 2012b).

Figure 12: Horne St. bioretention system with viewed from the North, showing the inlet.

Figure 13: Horne St. bioretention system viewed from the South showing the high-flow bypass and two wells with P41 and P42 pressure transducers.

3.5 Instrumentation

The instrumentation in the HSBS was developed collaboratively between the EPA and UNHSC since the site was the focus of a previous EPA Regional Applied Research Effort (RARE) study. All instrumentation was installed by UNHSC staff. The system contains nine Time Domain Reflectometers (TDR) measuring Electrical Conductivity (EC), temperature, and VWC; five pressure transducers (PT) measuring water depth and temperature in wells; an unheated rain gage measuring the depth of rainfall; and a drain gauge lysimeter. See Table 2 for detailed instrumentation locations. Figure 10 shows the plan and profile view of instrumentation.

Table 2: Horne St. bioretention instrumentation list, locations, and names

Type of Sensor	Description of the Location	X* (ft.)	Y* (ft.)	Z* (ft.)	Abbreviated Name
TDR	BSM, 1 ft. below surface	50	3.5	1	T01
TDR	BSM, 1 ft. below surface	75	3.5	1	T02
TDR	BSM, 1 ft. below surface	95	3.5	1	T03
TDR	BSM, 1 ft. below surface	115	3.5	1	T04
TDR	BSM, 1 ft. below surface	130	3.5	1	T05
TDR	Bottom of pea stone	50	3.5	4	T06
TDR	Native soil, 1 ft. below excavation	50	3.5	5	T07
TDR	Native soil, 1 ft. below excavation	95	3.5	5	T08
TDR	Native soil, 1 ft. below excavation	130	3.5	5	T09
PT	Bottom of pea stone	75	3.5	4	P40
PT	Bottom of pea stone	125	3.5	4	P41

PT	Surface ponding	125	-3.5	4	P42
PT	Effluent – behind compound weir	180	-20	6	P43
PT	Influent - OCF Cutthroat flume	0	-3	0	P44
Lysimeter	Cell 1, top of DCT is 6” below media surface	50	0	0	L51
Rain Gauge		85	0	-5	R
NEMA Enclosure		95	0	-1	
Enclosure Humidity Sensor	Inside NEMA Enclosure				HB2
Charge Regulator	Inside NEMA Enclosure				CA1
Data Logger	Inside NEMA Enclosure				

*The X, Y, and Z dimensions are defined as follows:
X is the horizontal distance along the centerline of the control from the inlet; positive toward the South.
Y is the horizontal distance perpendicular to the centerline of the system; positive toward the West.
Z is the vertical distance from the surface of the media into the ground; positive into the ground.

The PT are located at the inlet, outlet, and in three wells within the system shown as P40-P44 in Figure 10. P44 at the inlet was installed in the stilling well of an OCF 36-inch L x 8-inch W Cutthroat Flume in July 2016. The flume was installed to facilitate calibration and measurement of the inlet discharge.

P43 is located at the effluent pipe behind a 12 inch, Thel-mar volumetric weir. The weir was installed to more accurately measure effluent discharge at low flows. The compound weir during a medium flow is shown in Figure 15.

Figure 14: Inlet monitoring using an OCF 36x8 inch Cutthroat Flume. The blue line seen at the bottom center of the image is the data line for the pressure transducer located in the stilling well.

Figure 15: Outlet monitoring using a 12 inch, Thel-mar volumetric weir

3.6 Calibration of Equipment

Before installation of the HSBS, all pressure transducers (PT) were calibrated by immersion in a column of water and compared to a measurement using a tape measure to the nearest 1 mm. For more details, see (UNHSC, 2016b). The installed PT have not been calibrated since construction of the system as the system must be substantially disturbed in order to access the instruments.

The TDR's in the native soils and stone layer could not be calibrated a priori because they are soil media specific. However, T01-T05 in the BSM layer were calibrated in the laboratory in the BSM prepared by the City of Dover; the procedure may be found in Appendix A of (UNHSC, 2016b). The calibration curve from raw measured VWC to actual VWC is estimated by Equation (4).

$$VWC_{actual} = 0.038\ (VWC_{raw})^2 + 0.673\ (VWC_{raw}) + 0.086 \qquad (4)$$

The Campbell Scientific CR1000 data logger clock was not adjusted for daylight savings time and is shown in EST in this study. The manufacturer rated the logger clock with an error of ± 3 minutes per year (Campbell Scientific, Inc., 2011).

Both the influent and effluent discharges were calibrated by a simple yet accurate method using a large container of a known volume and a stopwatch. During storm events, the discharges were measured by capturing the water in the container and timing how long it would take to fill. The time of the measurement was recorded to compare to logged data from the respective PT. For example, if the 22-gallon container filled in 7 seconds, the discharge would be:

$$q = \frac{22\ gal}{7\ s} \times 60 \frac{s}{min} = 188.6\ gpm = \ 0.420\ cfs$$

At the time of that measurement, the logged water depth may have recorded 0.195 ft. With many such measurements, rating curves were made for both the inlet flume and the outlet weir and are shown in Figures 16 and 17, respectively.

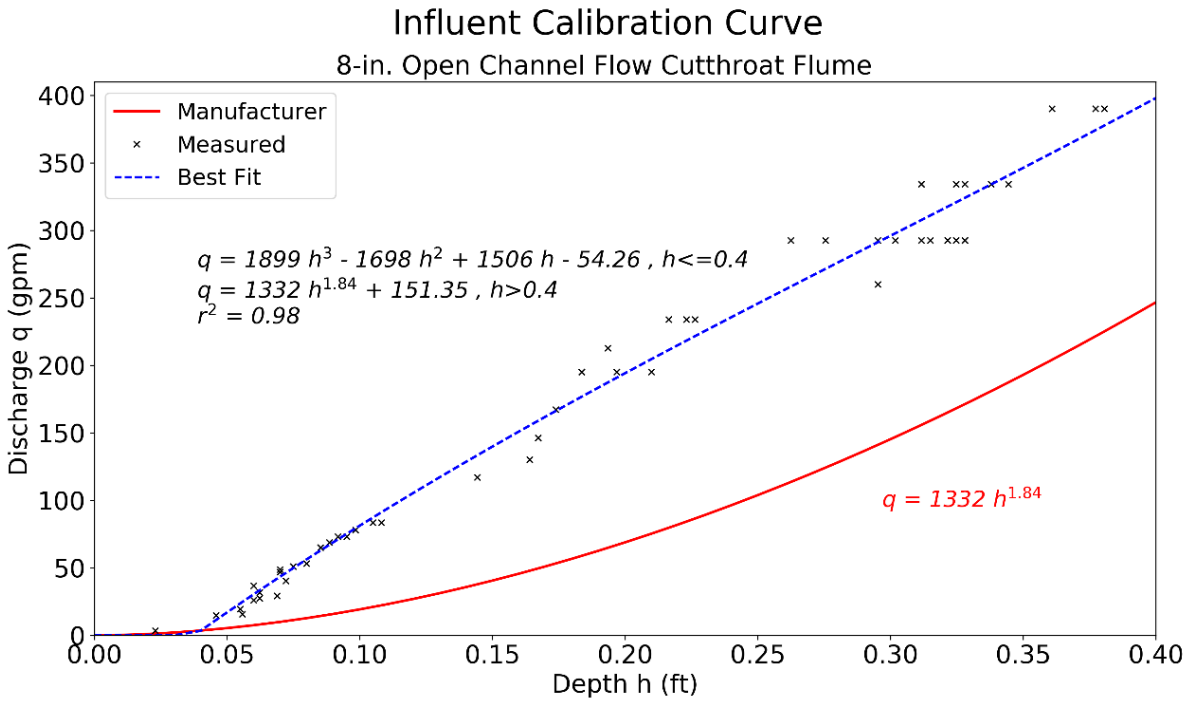

Figure 16: Calibration curve for the inlet – 8-inch OCF Cutthroat Flume.

Because the maximum reasonable depth for measurement for calibration was near 0.4 feet, the curve above this elevation was assumed to follow the slope of the rating curve from the flume manufacturer. Therefore, the r^2 shown in Figure 16 only describes the equation for depths less than or equal to 0.4 feet.

Several data points above 0.35 ft. in Figure 17 create a horizontal pattern. During high flows, the rate of change of flow was often high. The measured discharges were matched to measured water depths at the same time as the start of the measurement. If the flow varied from the start of the measurement to the end, the data may form such a pattern.

Another reason for such a pattern may involve the precision of timing the discharge. Measurements at high discharges were taken to the nearest whole second. This would explain the discontinuity in data points that were within one second of each other.

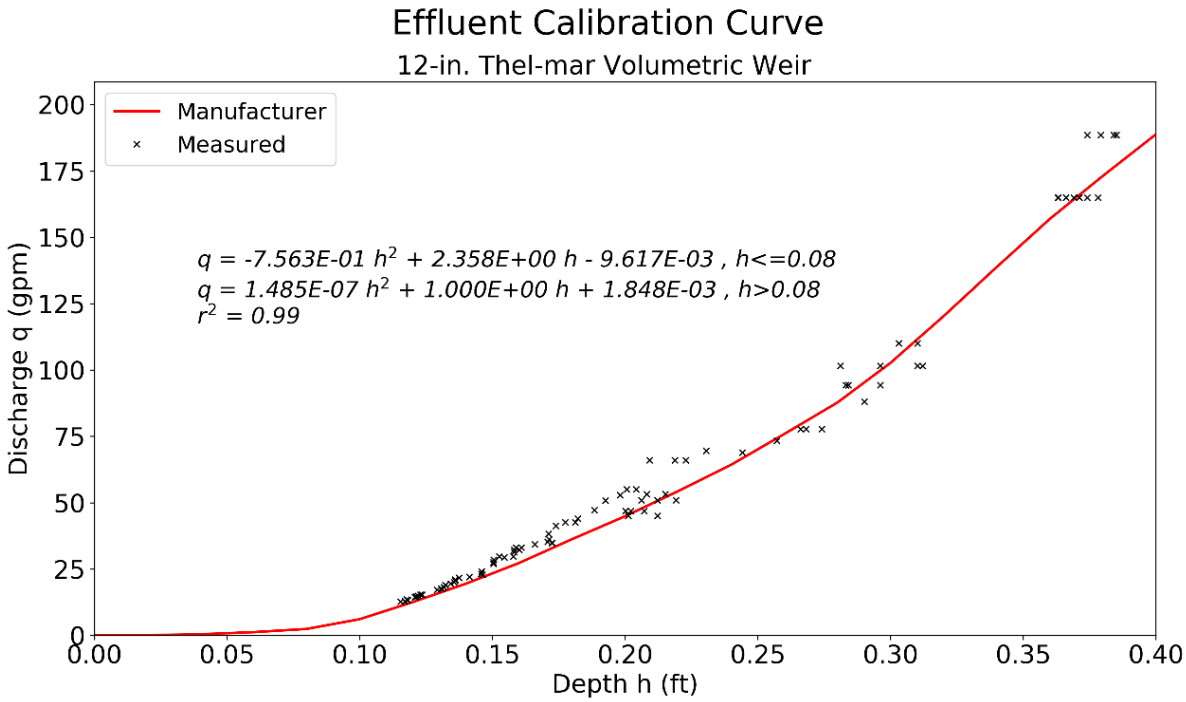

Figure 17: Calibration curve for the outlet – 12" Thel-mar Volumetric Weir.

When the HSBS was first installed, a weir was also placed at the end of the inlet pipe. However, with the high discharge rates, the weir was repeatedly blown out of the pipe. The weir was replaced by an Aqua-Troll AT200 pressure transducer fastened inside the pipe and lying parallel to the direction of flow. While this was replaced by the OCF flume on 7/11/16, another rating curve was created between the AT200 depth and the OCF flume discharge in order to use the older AT200 data. This rating curve is shown in Figure 18.

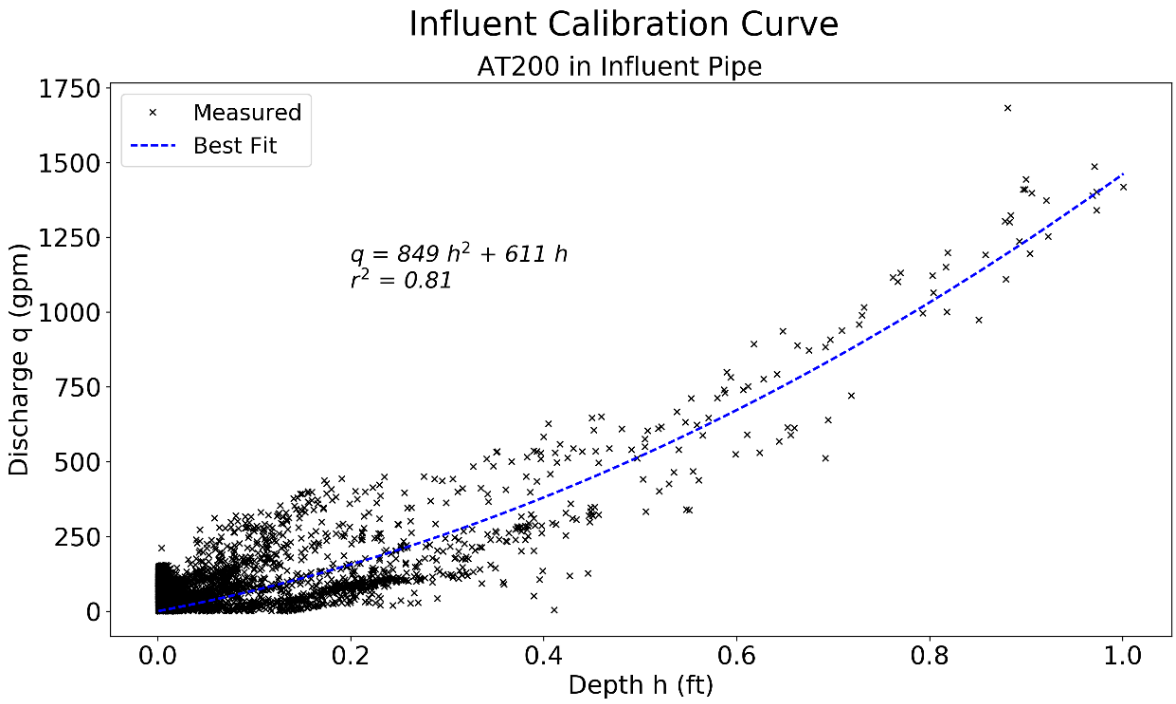

Figure 18: Calibration curve for the AT200 in the inlet pipe.

3.7 Measured Soil Properties

The surface soils surrounding the HSBS are generally well-draining soil in the HSG A category as shown in Figure 8. This applies to the surface layer of the native soils; however, the soil profile is stratified. Underlying the well-draining sandy layer are predominantly silt and clay-rich soils. The soil properties were tested along the center of the BSM at a depth of one foot as well as down the soil profile on the sidewall of the system several feet away from the excavation. The sidewall was tested using the GP and method described in Section 1.5. During the test, when the soil profile was observed to change in texture, a sample was taken to create a PSD using the combined sieve and hydrometer tests. Results of the PSD for the BSM and a representative sample of the

sidewall profile are shown in Figure 19. The PSD for the BSM was developed in 2013 by UNHSC staff. See Appendix A.2 for the collected PSD data.

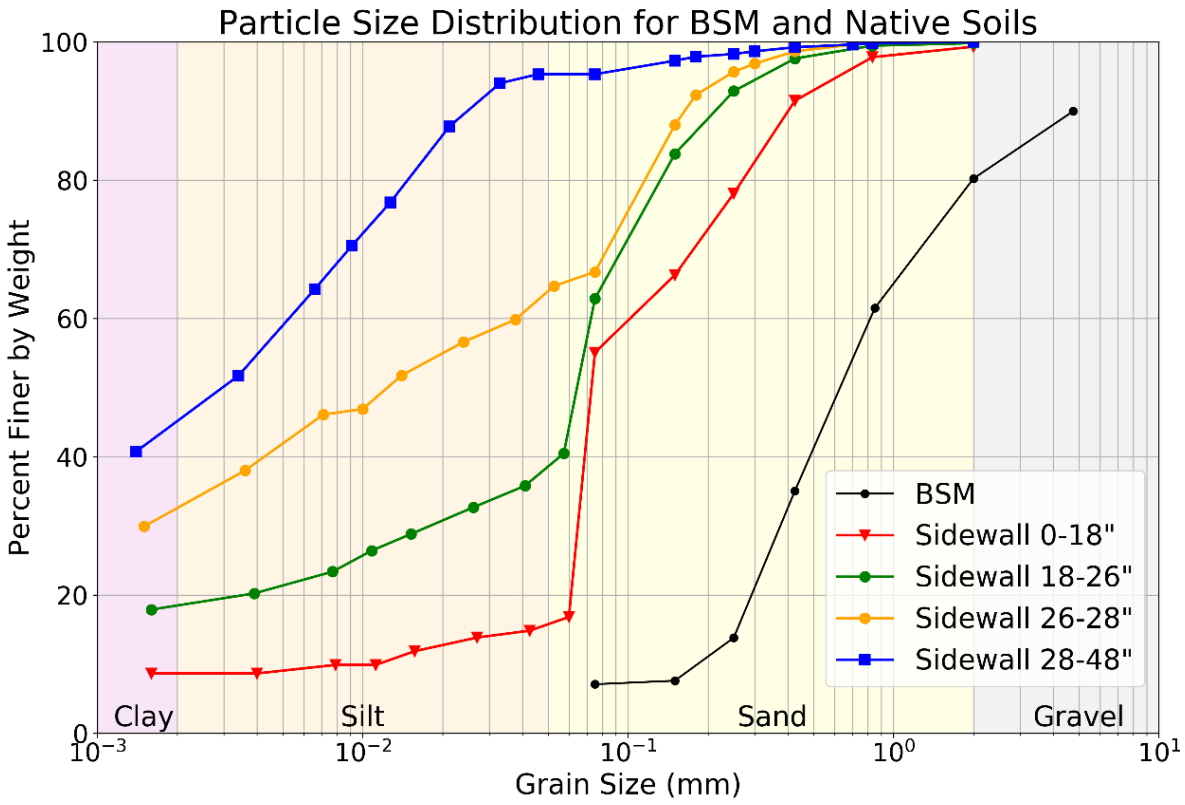

Figure 19: Representative PSD for the BSM and native soil profile.

Figure 19 shows the difference in soil textures between the BSM and sidewall profile. The BSM is almost entirely sand with a fraction of gravel particles. This coarse structure with the majority of fines removed allows for rapid drainage and prevents clogging and hypoxic conditions in the root zone. The upper layer (18 inches) of the native soil sidewalls is considered sandy loam by the USDA soil texture classification shown in. Moving down the native soil profile, there are layers of loam and clay loam that are 8 inches and 2 inches deep, respectively. The next and largest layer measured was from 28-48 inches made of silty clay. This layer was horizontally aligned with the stone layer of the filter as

well as the bottom of the excavation. See Table 3 for a summary of the soil textures and locations.

Table 3: Soil textures of BSM and sidewall profile

Soil	Depth (in.)	USDA Soil Texture
BSM	0-24	Sand
Native sidewall	0-18	Sandy loam
Native sidewall	18-26	Loam
Native sidewall	26-28	Clay loam
Native sidewall	28-48	Silty clay

The same soil information may be shown on the USDA soil texture triangle for visual representation as in Figure 20.

Field saturated hydraulic conductivity was tested using the GP with multiple head test at depths of 1 and 4 feet for three sidewall locations near the center of each bioretention cell. Table 4 shows the geometric means for the Laplace and least squares approaches. These depths were chosen because they were representative of the center of the BSM layer and the bottom of the excavation. While the Laplace approach yielded fairly consistent values, the least squares results were used for this study as they were suggested for improved accuracy and minimizing error due to macropores by Reynolds and Elrick (1986).

Using the GP data at various heads, the horizontal hydraulic conductivity may be estimated. The radius of the borehole was constant for each test, but the depth of head varied. For each test depth, the conductivity vs the ratio of borehole radius (*a*) to head (*H*) was graphed. As suggested by Reeve and Kirkham, extrapolating the line of best fit and finding the y-intercept yields the mathematical horizontal conductivity as the radius of the

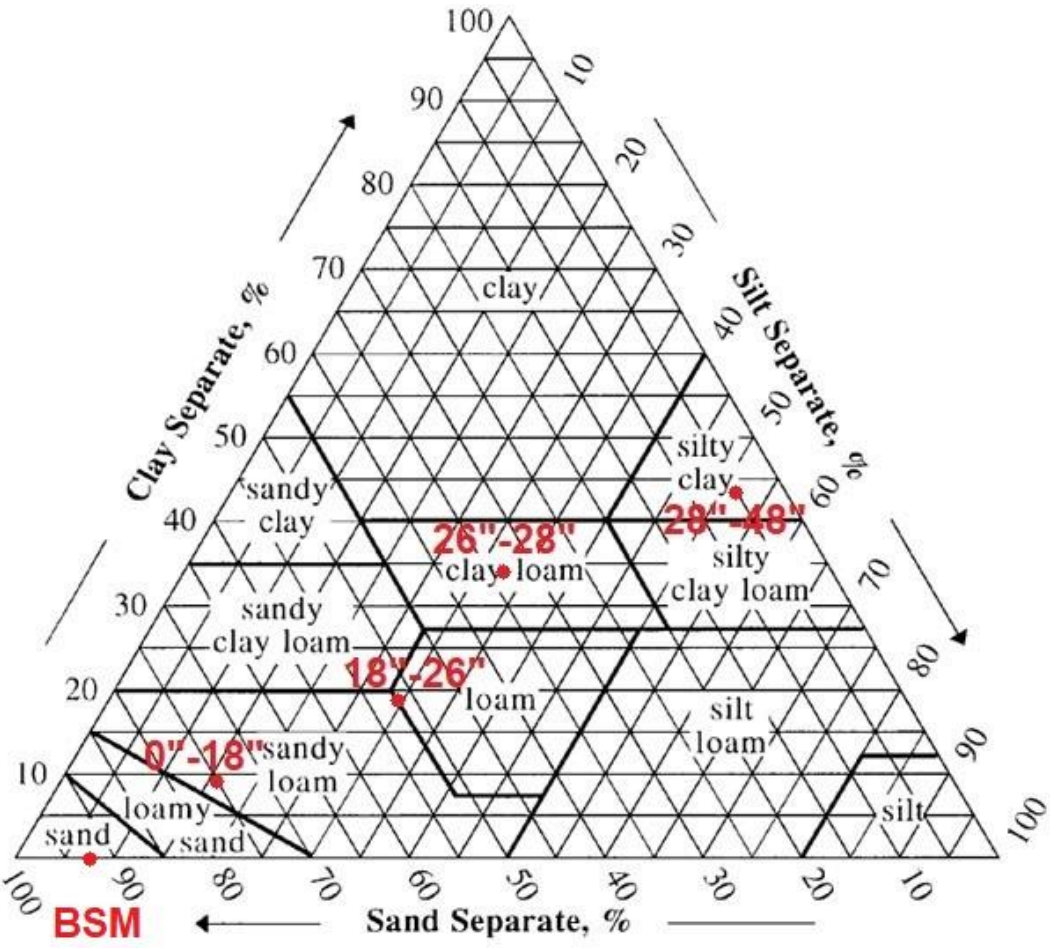

Figure 20: USDA soil textural triangle, showing the BSM and native soils profile.
Source: https://www.nrcs.usda.gov/wps/portal/nrcs/detail/soils/survey/?cid=nrcs142p2_054167

Table 4: Vertical field saturated hydraulic conductivity of BSM and native soils using the GP

Soil	Depth (ft.)	Vertical Field Saturated Hydraulic Conductivity (in./hr.)	
		Laplace	Least Squares
BSM	1	4.45	6.79
Native	1	0.812	0.416
Native	4	0.01574	0.227

borehole approaches zero (1951). Conceptually, this is like a test in a borehole that has a very large radius compared to water depth; this would primarily measure vertical

infiltration. Conversely, a test in a borehole with a very small radius and a large test water depth would primarily measure the lateral infiltration. Mathematically, this relationship is represented by the ratio of borehole radius to borehole depth. As the radius approaches zero, the extrapolated conductivity would be representative of the lateral direction. The authors stress, however, that the vertical component may not be found by extending the best fit line to infinity. An example of this type of extrapolation to estimate horizontal hydraulic conductivity for one GP test at a depth of 1 ft. is shown in Figure 21. Extrapolating to the y-intercept yielded a horizontal conductivity of 1.366 in./hr. for this test. The geometric mean of three tests conducted at a depth of 1 ft. along the HSBS sidewall yielded an extrapolated horizontal conductivity of 1.657 in./hr.; at a depth of 4 ft., the geometric mean was 0.0363 in./hr.

In addition to the GP results just presented, three measurements were taken using a Turf-Tec DRI to estimate the infiltration rates of the native soils during construction (September 2012) as well as the BSM in 2017. During construction, three tests were performed in the native soils at the bottom of the excavation (a depth of 4 ft.). These tests were performed at 14, 73, 119 feet from the inlet; as these were the approximate centers of the three bioretention cells. The infiltration rates at these locations were 0.8, 0.64, and 0.43 in./hr., respectively (UNHSC, 2016b). The areally weighted mean is 0.1559 in./hr. Similarly, the saturated infiltration rate in the BSM was measured, and the areally weighted mean was 5.87 in./hr. This falls within the range of the Laplace and least squares results for the GP seen in Table 4.

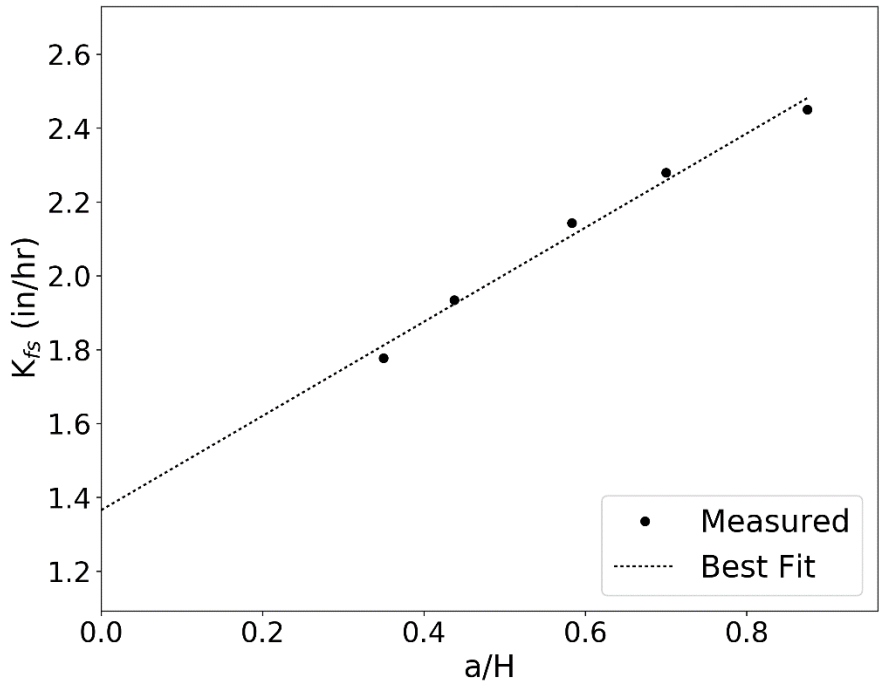

Figure 21: Field saturated hydraulic conductivity vs the ratio of borehole radius to head in the native soil sidewall at a depth of 1 ft. relative to the BSM and 73 ft. from the inlet. The extrapolated horizontal conductivity is 1.366 in./hr.

Combining the Turf-Tec and GP tests for each sample location using the geometric mean of all samples yields the values in Table 5. These calculated values were used in computation in this study.

Table 5: Summary of saturated hydraulic conductivities for the HSBS BSM and native sidewall

Soil	Depth (ft.)	Saturated Hydraulic Conductivity (ft./hr.)	
		Vertical	Horizontal
BSM	1	5.28E-1	
Native	1	3.46E-2	1.38E-1
Native	4	8.74E-2	3.02E-3

3.8 Data Analysis

The HSBS CR1000 data logger has been recording data since late 2012, much of this data was recorded with time intervals less than five minutes. To process such a large dataset, all analyses were performed in Python using Numpy, Scipy, and Pandas packages, which made post-processing large time-series arrays an efficient and powerful process.

The first step in postprocessing the dataset included removing non-real points such as 7999 or infinity. These could occur at periods of measurement that were outside the capabilities of the instrument such as saturation in the TDR or freezing temperatures in the PT. Additionally, the influent PT (P44) was removed during winter months with freezing temperatures as the inlet pipe was exposed to the surface and ice often formed, leading to inconsistent data and possible damage to the instrument.

The next step for the complete data set was to “zero” the data according to system dimensions in order to apply the appropriate calibration curve. For example, the inflow pressure transducer was located in the bottom of the flume well, measuring the depth of water from the bottom of the well instead of the bottom of the flume. To zero the data, the difference in depth from the bottom of the flume to the bottom of the well was subtracted from the raw data. This “zeroing” process was performed for the inlet, outlet, and ponding PT, or P44, P43, and P42, respectively. See Table 6 for their values.

Table 6: Horne St. zero readings for post-processing data

Instrument	Description	"Zero" Reading (ft.)
P44	Inlet OCF Flume	0.1310
P43	Outlet Thel-Mar Weir	0.225
P42	Ground surface from PT	3.73

The complete and zeroed dataset was then ready to apply the appropriate calibration curves. The inlet water depths were converted to discharge according to the calibration curves shown in Figures 16 and 18 depending on the instrument installed. The outlet discharge was calculated using the manufacturer's discharge table as confirmed by Figure 17. Note that the calibration curves are shown in units of gpm, but this was converted to cfs using the conversion 448.8 gpm = 1 cfs. The VWC for T01-T05 was corrected using Equation (4).

Next, the continuous time series data was divided into individual storm events. According to the US EPA, rainfall events are defined by having greater than or equal to 0.10 inches total precipitation and having an antecedent dry period of at least six hours with no measurable rain (UNHSC, 2012b). This was easily processed in Python by comparing time intervals between nonzero rainfall data. If the time between rainfall was greater than six hours, a potential new event would begin. The total rainfall for each potential event was summed and compared to the 0.1-inch criteria. Potential events greater than or equal to this limit were considered rainfall events. Note that events presented in this study show the periods where both inflow and outflow were greater than an arbitrary threshold of 20 gpm (0.045 cfs) for display purposes only; all data analyzed was from the complete event duration.

For individual storm events, a volume balance could be calculated. In general, the total runoff volume minus the sum of the total discharge volume plus the change in storage equals the volume lost due to infiltration; this assumes the precipitation and ET over the bioretention surface area were negligible. The total volumes in and out were

easily calculated as the sum of the products of discharges (in or out) times the recorded time interval.

The change in storage in the BSM and stone layers were calculated as the volume of water at the end of the event minus the volume of water at the beginning of the event. As an example, in either the BSM or stone layer, an initial volume of 100 cu. ft. and a final volume of 670 cu. ft. would yield a change of storage of 570 cu. ft. The change in storage in the BSM was calculated using an aerially weighted average VWC according to the dimensions in Figure 10 for T01 through T05. This weighted average VWC times the volume of the BSM gave the volume of water stored in the soil pores. For example, a change in weighted VWC of 0.2 times the volume of the BSM of 4,200 cu. ft. yields 840 cu. ft. of pore water in storage.

Storage in the stone layer was calculated in a similar way, however, water depths in wells P40 and P41 were used instead of VWC. Generally, the volume of water is equal to the bulk volume multiplied by the porosity. For the bioretention, the pore water was calculated as the depth of water times the length, width, and porosity. The maximum VWC from T06 in the stone layer gave porosity of about 0.52. Because the HSBS was built at 1% grade, some trigonometry was used to find the volumes. It was assumed that the water surface connected linearly between the wells P40 and P41; the water level on the edges outside the two wells was assumed to be level. See Appendix A.3 for a detailed explanation and geometric calculations.

3.9 Results

Following the procedure described in Section 3.8, the following results show the time series data for several representative events. Only events with usable inflow data were analyzed. For example, this excluded winter days when the inlet pressure transducer was removed from the stilling well to avoid freezing. Additionally, as the system has been recording data since 2012, there were periods when the logging interval was increased above five minutes. Forty-five non-winter storms with recording intervals of 1-minute were analyzed in this study to reduce errors due to numerical methods for longer intervals. Figures 22 - 25 show the time-series results for a representative 0.17 in. event that is near the current static design event (0.16 in.), a 0.35 in. event, a 1.2 in. event with considerable ponding and high-flow bypass, and a 1.3 in. event with no ponding or bypass, respectively. All event graphs in Figures 22 - 25 have date and time on the x-axis and have three subplots. The top subplot is a time-series of inflow and outflow discharges on the left y-axis and the hyetograph on the reversed, right y-axis. The middle subplot shows the VWC for all TDR's (T01-T09). VWC that reaches a maximum value and becomes horizontal indicates a saturated condition for that TDR. The bottom subplot shows water levels in wells P40, P41, and P42 relative to elevations of the constructed system as shown by broken lines; these construction lines are for a physical reference and match the dimensions of the HSBS cross-section in Figure 9. The line for P42 is absent from the lower subplot for events with no surface ponding. Note that during events with ponding, the P42 line does not return to the system surface as it drains. This is due to the physical location of the perforated holes in the ponding well. To keep soils and debris out of the well, the lowest perforation is located about 1 inch above the ground

surface. This becomes the lower boundary for representing physically accurate data; therefore, data below that level was not graphed.

The summary statistics for all event parameters, including rainfall, antecedent period, rainfall duration, runoff duration, event duration, volumes of influent and effluent, volumes stored, peak inflow, peak outflow, peak ponding depth, peak rainfall intensity, peak flow reduction, volume reduction, and rainfall for events with and with high-flow bypass are shown in Table 21 in Appendix A.4.

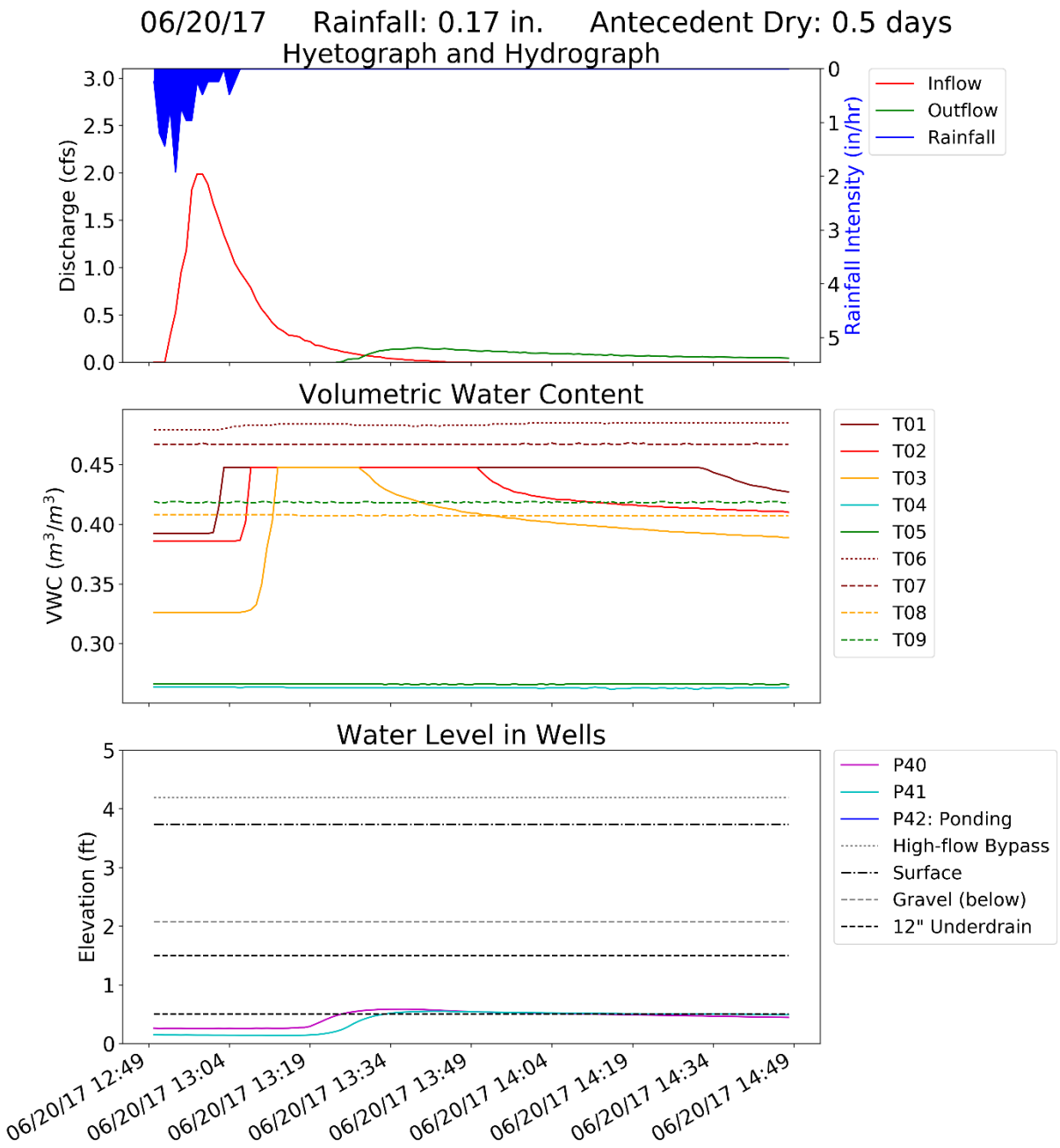

Figure 22: Time series plots for HSBS showing the hyetograph and hydrograph, VWC, and water levels for a 0.17 in. event. The peak flow reduction was 92% and volume reduction was 72%.

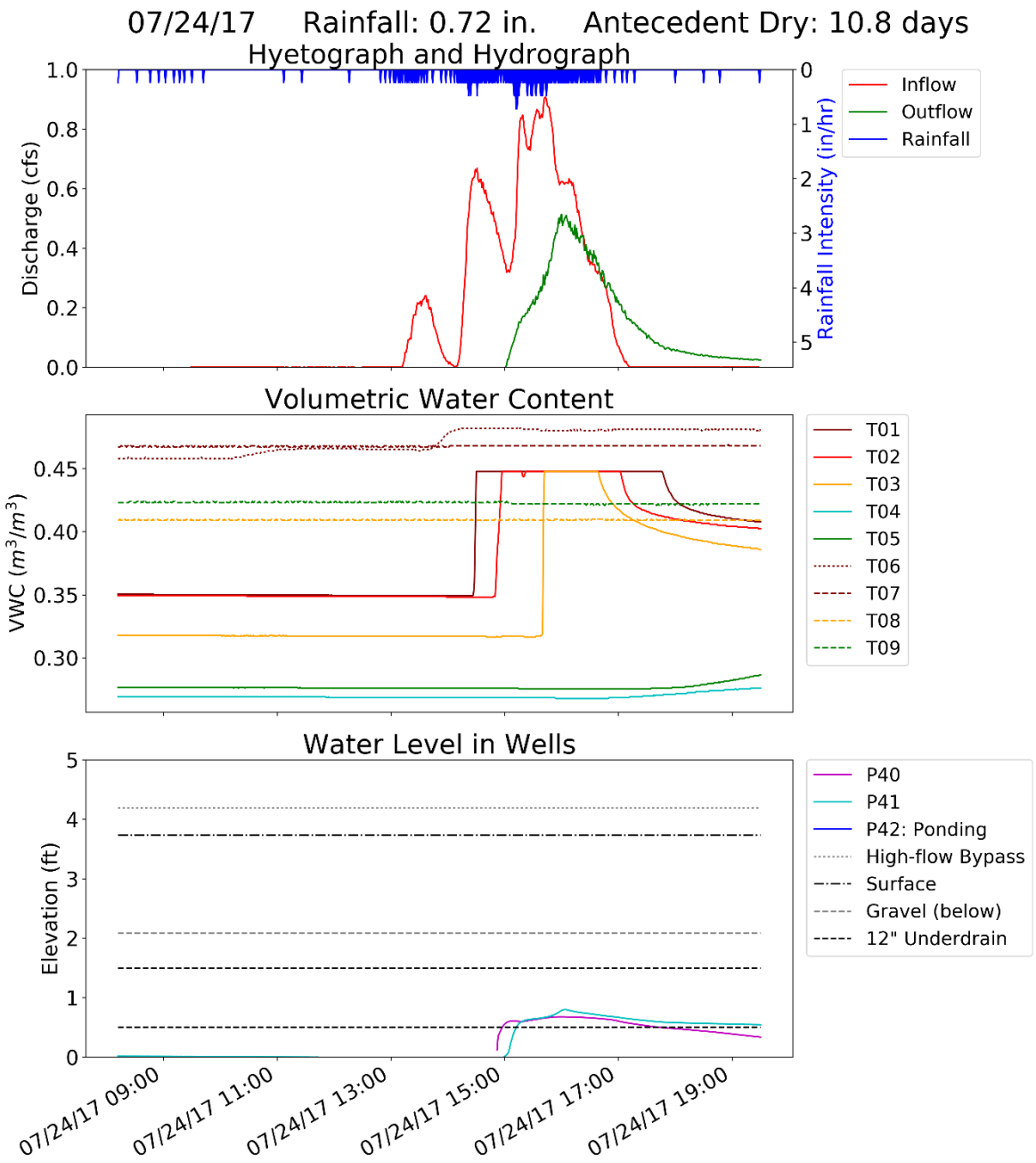

Figure 23: Time series plots for HSBS showing the hyetograph and hydrograph, VWC, and water levels for a 0.72” event. The peak flow reduction was 43% and volume reduction was 51%.

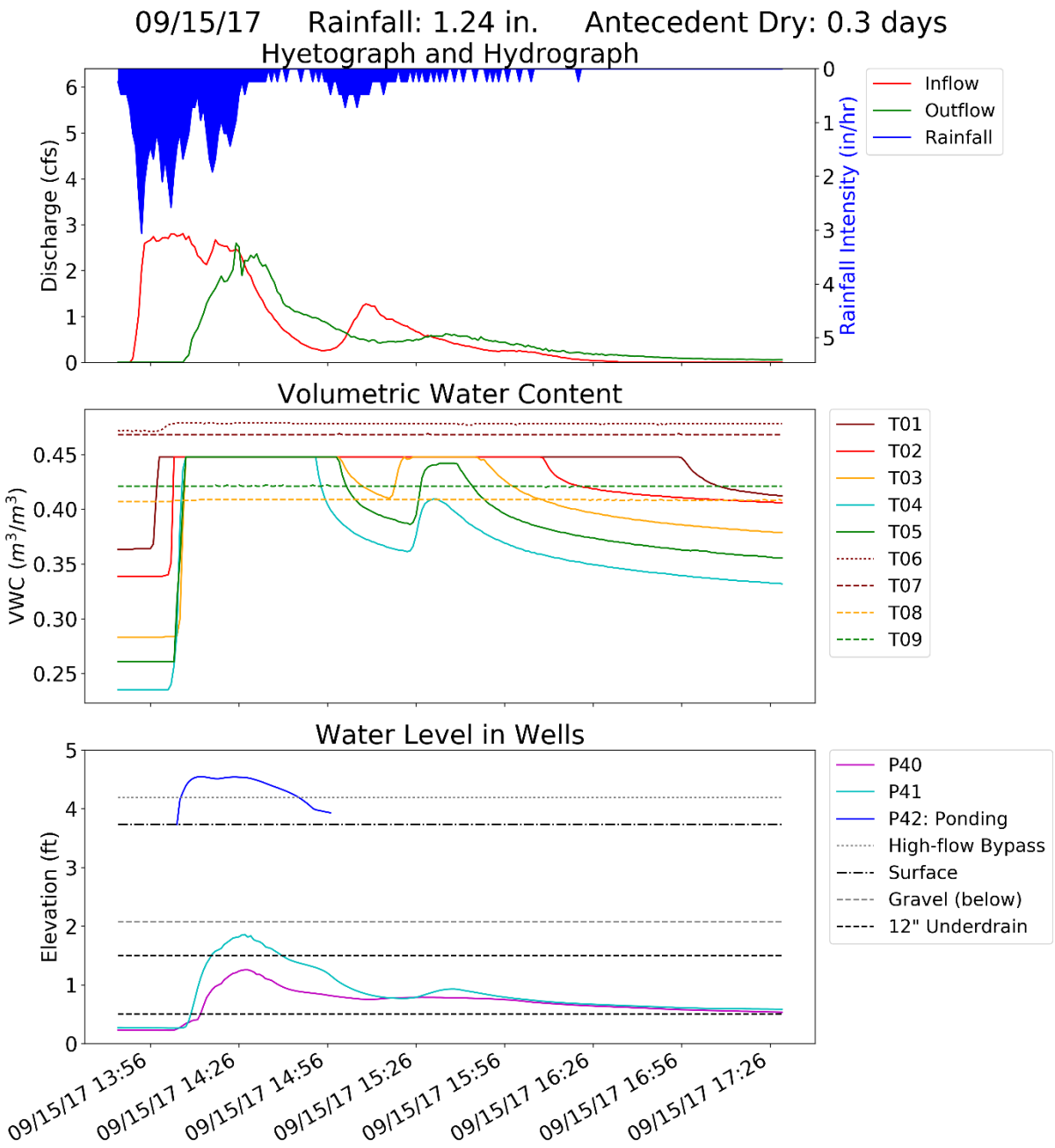

Figure 24: Time series plots for HSBS showing the hyetograph and hydrograph, VWC, and water levels for a 1.24” event with ponding and bypass. The peak flow reduction was 7% and volume reduction was 24%.

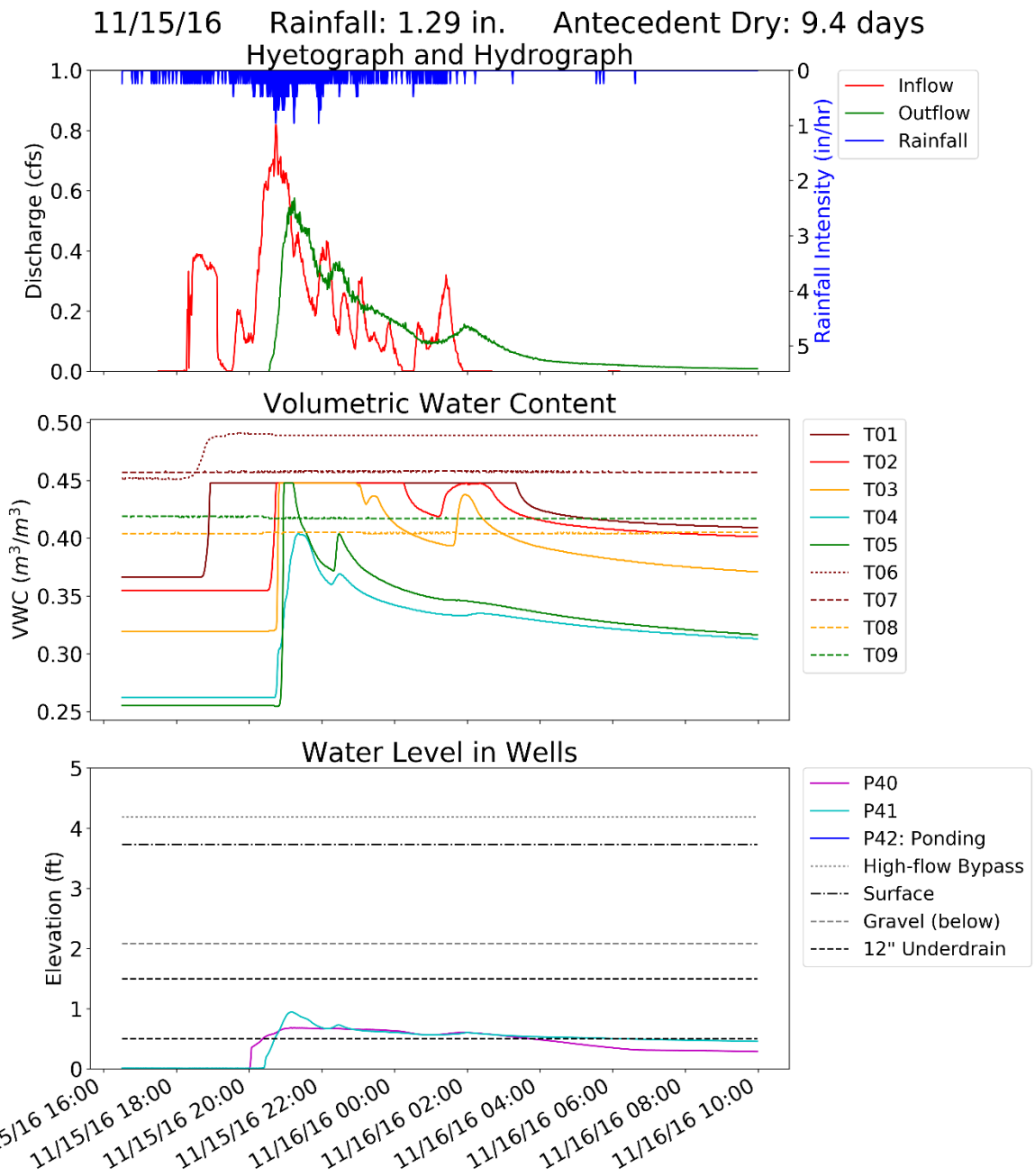

Figure 25: Time series plots for HSBS showing the hyetograph and hydrograph, VWC, and water levels for a 1.29” event without ponding or bypass. The peak flow reduction was 30% and volume reduction was 9%.

The summary of all characteristic and calculated parameters for the storms shown in Figures 22 through 25 is shown in Table 7.

Table 7: Summary of storm parameters for 0.17 in., 0.72 in., 1.24 in., and 1.29 in. events.

	Figure 22	**Figure 23**	**Figure 24**	**Figure 25**
Date	6/20/2017 12:50	7/24/2017 8:12	9/15/2017 13:45	11/15/2016 16:30
Rainfall (in.)	0.172	0.724	1.238	1.292
Effective Rainfall (in.)	0.019	0.072	0.119	0.080
Antecedent Dry Period (day)	0.55	10.76	0.29	9.36
Rainfall Duration (hr.)	0.25	11.28	2.60	14.12
Runoff Duration (hr.)	0.85	3.97	2.82	7.65
Event Duration (hr.)	2.0	11.3	4.2	104.7
Volume In (cu. ft.)	1546	5721	9443	6391
Volume Out (cu. ft.)	433	2795	7164	5786
Storage Media (cu. ft.)	155	256	379	103
Storage Stone (cu. ft.)	219	214	350	17
Volume Infiltrated (cu. ft.)	739	2457	1549	486
Peak Inflow (cfs)	1.99	0.91	2.81	0.82
Peak Outflow (cfs)	0.15	0.51	2.60	0.58
Peak Ponding (ft.)	0	0	0.82	0
Peak Rainfall Intensity (in./hr.)	1.92	0.72	3.06	0.96
Peak Flow Reduction	92%	43%	7%	30%
Volume Reduction	72%	51%	24%	9%

Figure 26 shows box plots for the corrected VWC for all TDR's for all events. Note that T01-T05 are in the BSM (shaded red), T06 is in the stone layer at the bottom of the excavation (shaded grey), and T07-T09 are 1 foot below the bottom of the excavation in the native silty clay (shaded yellow).

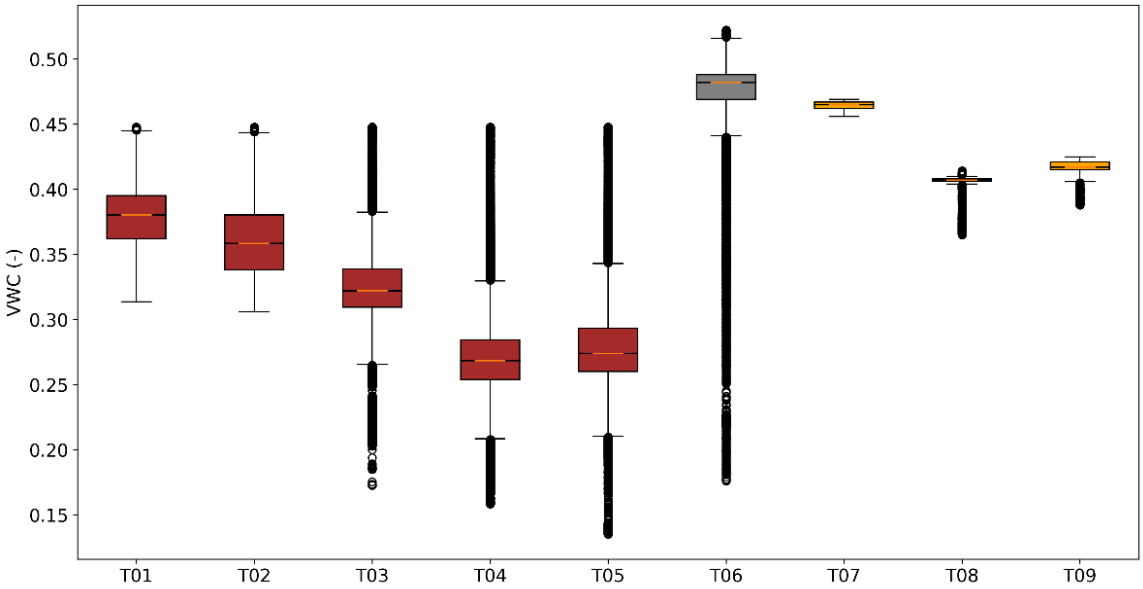

Figure 26: Box plots of TDR VWC data for all events.

Figure 27 shows box plots of several parameters for all storm events. The total storm rainfall, antecedent dry period, peak inflow, peak outflow, and peak ponding depth at P42 were calculated for every event.

Additional box plots of the peak flow reduction and the volume reduction from influent to the effluent are shown in Figure 28. The peak flow reduction is the percentage of reduction from the peak influent discharge to the peak effluent discharge. For example, a reduction of 70% means the peak effluent discharge is 30% that of the peak influent discharge. The peak discharge reduction had a median of 64%, mean of 62%, and standard deviation of 25%. The volume reduction is similar in that it was calculated as the reduction in total influent discharge to total effluent discharge. The volume reduction had a median value of 36%, mean of 35%, and standard deviation of 37%. The actual

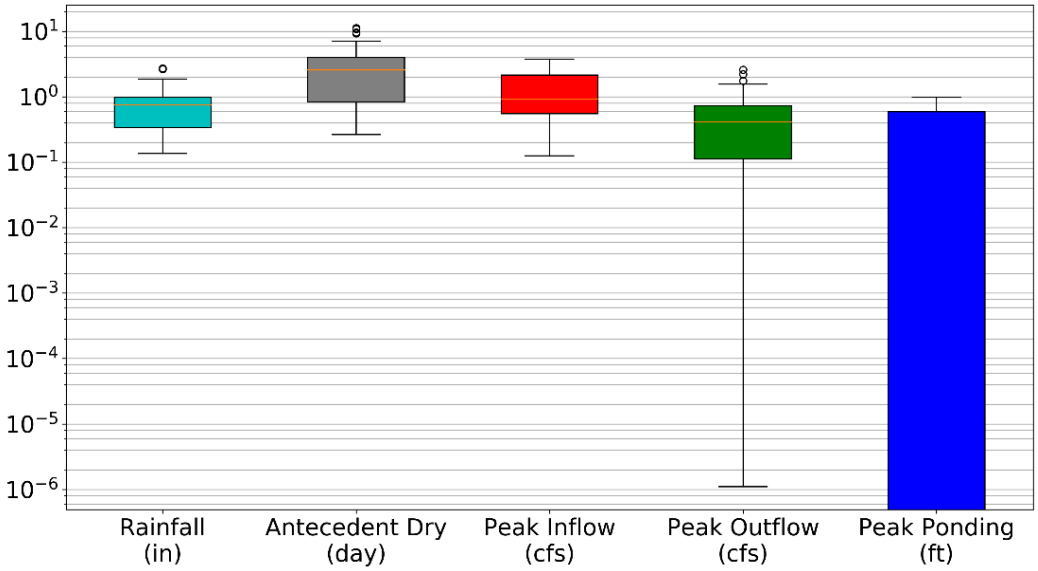

Figure 27: Box plots of total rainfall, antecedent dry days, peak inflow, peak outflow, and peak ponding for all events.

total volume is shown in the right box plot as the total volume of the influent minus the total effluent volume per storm event. The volume reduction per event had a median of 1193 cu. ft., a mean of 1629 cu. ft., and standard deviation of 2620 cu. ft.

Figure 29 shows box plots of the rainfall for storm events. The left box plot describes only events that did not have any high-flow bypass, meaning the surface ponding was below the designed ponding depth (now 4.86 inches). The right box plot describes events where high-flow bypass occurred. The rainfalls for events with no bypass had a median value of 0.55 in., a mean of 0.59 in., and standard deviation of 0.35 in. Events with bypass had median rainfalls of 1.1 in., a mean of 1.3 in., and standard deviation of 0.71 in. In addition to event rainfall in the box plots, the dotted red line indicates the depth of the

design event with the current sizing approach using Equation (3); the design event is about 0.16 in.

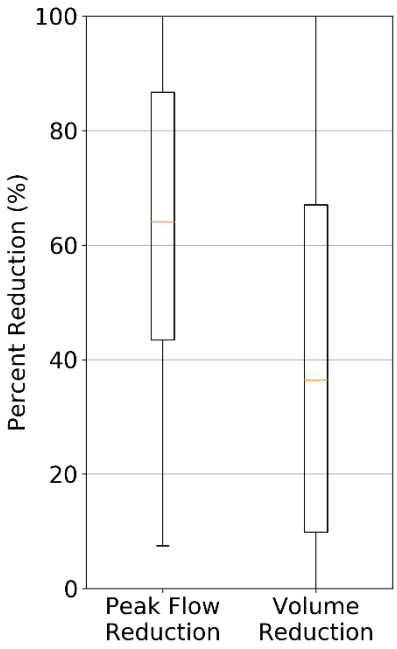

Figure 28: Event summary of peak flow reduction and discharge volume reduction.

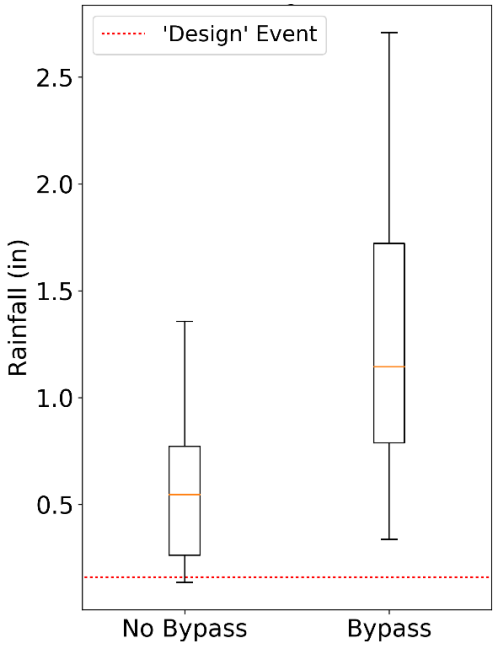

Figure 29: Event summary of event rainfall for events without high-flow bypass and events with bypass.

The volume balance was calculated for each event. The volume infiltrated was calculated as the total influent minus the sum of the total effluent and change in storage in the BSM and stone layers. This assumed the contributing volumes due to precipitation and ET were zero which was reasonable due to the large watershed to filter ratio. Some models and simple estimates of infiltration assume that infiltration only occurs in the bottom of the system as the horizontal components along the system sidewalls are negligible ((Akan, 2013), (Palhegyi, 2010)). Using this bottom infiltration estimate for the individual storms, Figure 30 shows the estimated infiltration vs the calculated observed total infiltration along with a 1:1 reference line.

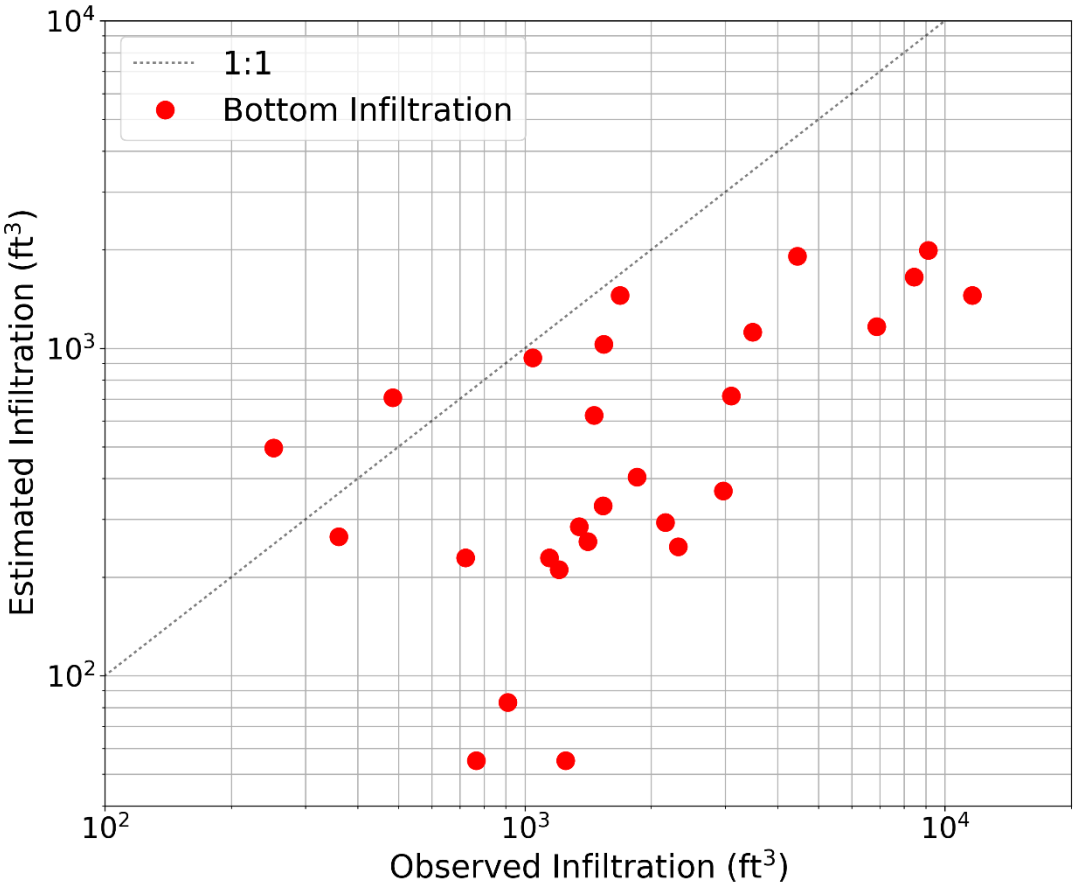

Figure 30: Total observed infiltration and the estimated infiltration using only the vertical component in the bottom of the filter.

See Appendix A.4 for additional results and statistical summaries of the HSBS events.

3.10 Discussion

The HSBS was designed as a retrofit system to treat the runoff from a 21.9-acre suburban watershed. As a retrofit system, the static design event was only 0.16 inches. This design event is barely over the 0.1-inch minimum criteria for an EPA rainfall event. Theoretically, rainfall amounts that exceed the design event should bypass the filter. The

results in Section 3.9 indicate that the HSBS performs much better at processing larger events than the design event.

Figure 22 shows the data for a typical 0.17-inch event, very similar to the design event of 0.16 inches. The effective precipitation (runoff volume divided by watershed area) was 0.02 inches (11% of storm rainfall). The antecedent dry period was 0.5 days, which was well below the median of about 2.6 days. A short antecedent period would likely lead to less storage in the media and possibly less infiltration as the soils would have a higher residual moisture content than normal due to the short draining and redistribution time since the previous rainfall. This could likely decrease system performance. The duration of rainfall and runoff were also significantly shorter than their respective median values for all storms. The durations of rainfall and runoff were 0.3 and 0.9 hours, respectively; and the median values for all events were 9.5 and 6.8 hours, respectively. As the durations of rainfall and runoff were short, the system may be expected to not perform well as the high intensity of runoff due to the short duration of delivery would cause high peak flows and deliver runoff at rates higher than the possible filtration rate leading to surface ponding and possible high-flow bypass.

Although the peak inflow was more than double the median of all events, the system performed very well. The peak flow reduction was about 92%. T01-T03 became saturated and remained so for most of the event with the exception of T03, which started to drain soon after reaching saturation. T04 and T05 indicate that the third cell did not change soil moisture during the event. This indicates that the first and second cell were able to treat all the runoff without any runoff passing the second berm into the third cell. Additionally, P42 (or lack of) indicates that there was no surface ponding in the third cell above the

measurement threshold. With the high intensity of rainfall above the design event and short duration of runoff, it would be expected that the surface ponding should nearly reach the bypass and saturate all treatment cells, yet this is far from the actual performance. The water level in the stone layer was slow to drain after reaching the invert of the underdrain as was expected as the surrounding native soils at that elevation are silty soil with a low hydraulic conductivity. Despite the low conductivity of the bottom native soils, the event had a volume reduction of 72%. This indicates that the 0.17-inch event near the “design” storm either temporarily stored or infiltrated 72% of the inflow runoff, assuming ET was negligible. This performance was much greater than expected for the design storm.

Figure 23 shows a storm of 0.72 in., which was more than four times larger than the design storm. The effective precipitation was 0.07 inches (10% of storm rainfall). The antecedent dry period was 10.8 days. The duration of runoff was almost 4 hours and less than the median of 6.8 hours. The peak flow reduction was 43%. Similar performance was observed for this event to the 0.17 in. event. The first two cells treated most the runoff with only a slight increase in soil moisture seen in the third cell near the end of the storm. Again, no ponding occurred. Water levels in the stone layer reached the invert of the underdrain soon after the peak inflow then drained for the duration of the event. The volume reduction was 51%, which would be high for a storm over four times larger than the design event.

Unlike the previous two events, Figure 24 confirms how the system could not fully treat a large storm. The effective precipitation was 0.12 inches (10% of storm rainfall). The 1.24 in. event occurred after a short antecedent period of 0.3 days. The peak rainfall

intensity was about 3 in./hr. and the duration of rainfall was 2.6 hours. The peak flow reduction was 7%. As expected from an event with high rainfall volume and high intensity, all three BSM cells became saturated and remained at or near saturation for the duration of the event and significant ponding occurred (measured by P42), and high-flow bypass occurred during the peak inflow with a peak ponding level about 0.4 ft. above the bypass. The P40 and P42 wells indicated that the stone layer filled about three-quarters full and fully submerged the underdrain in the system during the peak inflow. The volume reduction was 24%.

In contrast to the previous 1.24 in. event, Figure 25 shows excellent performance during a larger 1.29 in. event with 9.4 days of antecedent dry period. The effective precipitation was 0.08 inches (6% of storm rainfall). The durations of rainfall and runoff were about 14 and 8 hours, respectively. The peak rainfall intensity was much lower at nearly 1 in./hr. The overall performance resembled that of the 0.35 in. event, however, the peak flow reduction and volume reduction were lower at 30% and 9%, respectively. The BSM in the third cell briefly reached saturation then drained to about half the soil moisture content. The stone water levels briefly reached the underdrain during the peak inflow then drained slowly. While the rainfall event was eight times larger than the design event, the system performed well and treated all the runoff with no surface ponding and reduced the peak flow by 30%.

While the two events from Figure 24 and Figure 25 were similar in depth, a contrast in performance was observed. The major differing factors between the events were the antecedent dry period, the peak rainfall intensity and distribution, duration of the rainfall, and duration of the event. The 1.29 in. event did not have ponding and normally would be

expected to exhibit bypass, and only 12% of the runoff should have been treated according to static design. The low rainfall intensity over a longer duration along with a long antecedent dry period developed conditions where the system could perform well and treat the entire event. These factors are ignored in the current static design process and the system is then limited to only theoretically perform for much smaller events.

The box plots of VWC data for all storm events in Figure 26 yield porosity (and saturation) values of 0.45 in the BSM (T01-T05), 0.52 in the stone (T06), and 0.47, 0.41, and 0.43 in the native soil 1 ft. below the system excavation (T07-T09, respectively). The BSM had a weighted areal median saturation of 46%, while the stone had a value of 88%, and the native soils had values between 69-86%. The VWC data in the native soils had a small range but did not indicate if the minimum VWC represented the field capacity in the silty clay between events or if the soils did not drain and never reached field capacity.

Figure 27 summarizes various event parameters for the 45 storms with 1-minutes logging intervals. The event rainfalls ranged from 0.14 to 2.71 in. with a median rainfall of 0.75 in. for all storms. The antecedent dry period ranged from 0.3 to 11.2 days with a median of 2.6 days. The median peak inflow and outflow were 0.9 cfs and 0.4 cfs, respectively. The peak ponding level ranged from 0 to 0.98 ft. above the BSM surface. The maximum peak ponding of 0.98 ft. was 0.58 ft. above the high-flow bypass.

Figures 28 and 29 most clearly describe the overall performance of the HSBS. The peak flow reduction had a median of 64%, mean of 62%, and standard deviation of 25%. The total volume reduction from influent to effluent had median, mean, and standard deviation values of 36%, 35%, and 37%, respectively. The actual volume reduction had a median of 1193 cu. ft. with a standard deviation of 2620 cu. ft., which are equivalent to

0.00125 in. and 0.00274 in. effective precipitation, respectively. While the system was designed for a 0.16-inch storm, the peak flow reduction and volume reductions for such an event were about 100% and 95%, respectively. For 1 inch storm, they were about 50% and 30%, respectively.

Figure 29 summarizes all rainfall events into two categories: those without high-flow bypass and those with it. As expected, events with bypass tend to be larger. The non-bypass events range from 0.14 to 1.36 in., with a median of 0.55 in. The median had a non-exceedance probability of about 57% from a cumulative probability distribution of 195 rainfall events. Events with bypass ranged from 0.34 to 2.71 in., with a median of 1.14 in. The median rainfall with high-flow bypass had a non-exceedance probability of about 87%. See Figure 56 in Appendix A.4 for details. The overlap in the high tail of the non-bypass events and the low tail of the bypass events is likely due to the non-uniform duration and intensity of rainfall as illustrated with the difference between the storms in Figures 24 and 25. The variation in antecedent dry days and watershed initial moisture content may also play a role. The box plots show the observed physical performance of the HSBS. In addition to the observed events, the dotted red line shows the 0.16 in. design event for reference using the current approach described in Chapter 2. The current design event poorly describes the observed data as only a few non-bypass events fall below the design rainfall, but none of the large events with bypass are included as expected. The cumulative probability function from the same data was analyzed using a Weibull plotting position. The non-exceedance probability for the current design rainfall in the non-bypass events was 5% and less than 3% in the bypass events. Ideally, the non-exceedance

probability for the design rainfall in non-bypass events should be 100% and 0% for bypass events.

The observed volume of water infiltrated was graphed against the estimated vertical infiltration through the bottom of the system. Figure 30 shows the 1:1 line is above the estimated bottom infiltration for all but two events. The estimated infiltration had a mean error of -79% compared to the observed infiltration, with a root-mean-square error (RMSE) of 3210 cu. ft. This indicates that in the case of the HSBS, estimating infiltration by only using the bottom vertical infiltration and neglecting the horizontal sidewall component resulted in an underestimation of total infiltration by 79% on average.

CHAPTER 4. PROPOSED MODEL AND DESIGN APPLICATION

4.1 Model Necessity and Goals

It has been shown that while the current design method is easy to apply, it greatly underestimates the observed hydraulic performance of bioretention systems. While an oversized system should exceed the expected “design” treatment and reduce peak volumes, they require more square footage and are more expensive to construct and maintain. A different model is needed to more accurately represent the observed hydraulic performance, correctly size the bioretention area, and estimate the volume of infiltration.

In addition, the model should be easily applied to the design process as is the current standard. The current static design process for new systems only requires five variables to calculate the necessary square footage of the bioretention, three of which are design parameters chosen by the engineer. For a standard BSM used in construction, the hydraulic conductivity does not vary significantly between sites and therefore does not need to be measured for each design. This leaves only the WQV based on the contributing watershed to the site. With only two remaining measured parameters, a few design variables, and Equation (3), the bioretention area may be easily obtained. The design of retrofit systems is equally simple to calculate using the WQV and the porosity of the stone and BSM layers. The filter volume and, therefore, surface area are easily calculated.

The WQV is commonly used as a standard of volume of runoff that should be treated as it represents the pollutant load from 90% of the average annual runoff. Additionally, as it is currently a commonly used standard, it is well understood and easily applied in practice. Therefore, the WQV was used as the load in the application of the developed model for design. Like the current design standard described in Section 2.1, this model considers the WQV as the total influent load to be treated in the system.

As the filter should be sized to treat the WQV, events with a larger WQV (a function of rainfall), should over-flow through the high-flow bypass. This sets a constraint on the maximum allowable depth of ponding.

Similar to the current design, surface ponded water should filter through the BSM within a designated time period to eliminate mosquito breeding and other water quality issues. Often, this period is 24 hours but may be up to four days as discussed in Section 1.3.

The final goal for the new model was to estimate the volume infiltrated into native soils. This was accomplished by the inclusion of anisotropy and the simplified estimation of lateral infiltration in the system sidewalls in addition to the infiltration in the bottom. The measurement or estimation of the soil parameters must be easily measured and reasonably accurate to reduce personnel time and improve model accuracy.

4.2 Model Basis and Definitions

This model resembled the Green and Ampt approach and similar assumptions were made, including a sharp, piston type wetting front and a low groundwater table with insignificant mounding.

The general system sketch in Figure 31 defines the general state for the development of the model in Section 4.4. A state of ponding height (h) is shown infiltrating vertically as a “piston” wetting front of length L_V. The wetting front horizontally has length L_H at a height of zero and where L_H is zero at height h. This conceptual model assumes that the infiltration occurs as a saturated wetting front shown as the shaded area, and the native soils outside the saturated wetting front are at an initial uniform soil moisture before becoming saturated. The native soils are also assumed to have a uniform matric tension (ψ). Note that the sketch in Figure 31 does not represent the movement of infiltrated water over time in the native soil; it is intended as a definition sketch to derive infiltration rates.

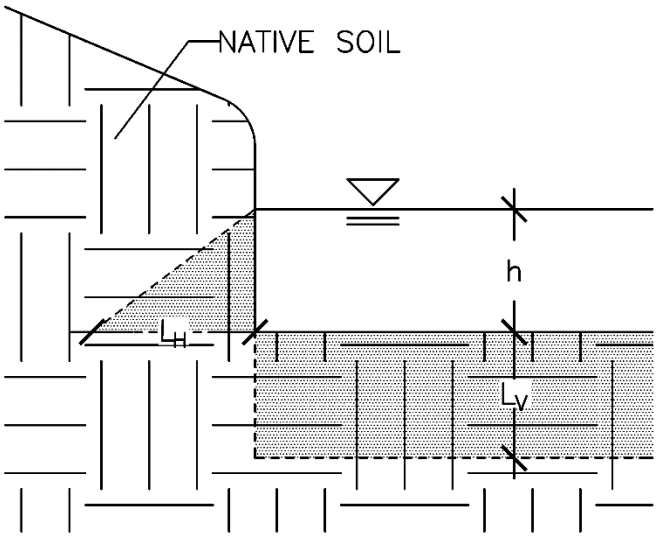

Figure 31: Cross section sketch for model development.

Figure 32 shows the same cross-section for the HSBS as Figure 9, however, this design is not specific to the HSBS and could be used generally for other bioretention with an underdrain. The figure shows the influent discharge from the watershed runoff (q_{in}) entering the system. The only other input to the system is direct precipitation (P). This

may or not be negligible in the total volume of input depending on the design event, bioretention surface area, and volume of runoff from the contributing watershed. The fluxes out of the system include evapotranspiration from the surface (*ET*), infiltration from layers 1 and 2 horizontally into the native soils (f_{1H} and f_{2H}), vertical infiltration from the bottom of the system (f_{2V}), and the overflow discharge from the high-flow bypass (q_{bypass}). Note that q_{bypass} in this sketch includes both high-flow bypass and water collected in the underdrain of the stone layer.

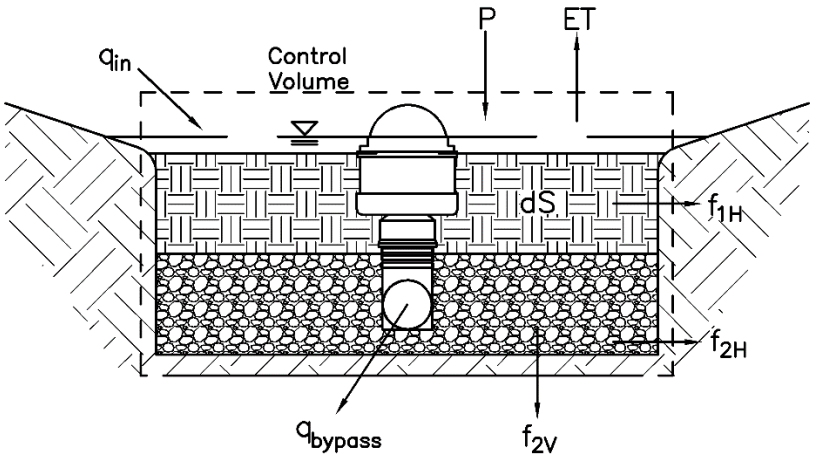

Figure 32: Cross section system fluxes and control volume for model development.

4.3 Assumptions and Initial Conditions

This model assumed saturated soils during the storm events. While the BSM and native soils may initially be unsaturated, the results from the HSBS showed that the BSM had a long-term median saturation of 46%; the stone layer was higher at 90%, and the native soils below the system were near 71%. The median values included periods of drying between events. The median saturation during storms was higher at 76% for the BSM, 95% for the stone, and 80% in the native soils. See Appendix A.4 for details.

Therefore, it was assumed that BSM and soils were saturated during runoff events and reasonably approximated by saturated infiltration in development of this model. Because the infiltration assumes saturated conditions, the lateral infiltration into the sidewalls is divided into f1 and f2 because the stone layer above the underdrain generally not saturated.

It was assumed that native soils were homogeneous and the same depth as the adjacent layers in the bioretention. For example, for a 2 ft. BSM layer, the native soils adjacent to the BSM would be 2 ft. of homogeneous soil. This also applied to the bottom of the stone layer. If the native soils' sidewalls were a composite column or *K* was nonhomogeneous, a representative equivalent homogeneous value should be used as shown by Equation (5). Where the thickness (*z*) and horizontal hydraulic conductivity (K_H) are known for each composite layer (*i*) (Todd & Mays, 2005).

$$Equivalent\ K_H = \frac{\sum_{i=1}^{n} K_{Hi}\ z_i}{\sum_{i=1}^{n} z_i} \quad (5)$$

Additionally, the native soils were assumed to be uniform. The flow was assumed to be controlled by the soil matrix and not macropores.

The model assumed a rectangular system for calculating the perimeter and area of the filter. This could be changed in the model with modifications to the equation by making these parameters custom functions rather than being solved geometrically as was done here.

To use the model as a design tool, it was assumed that the system reset to the same initial conditions for the start of each event. The system was assumed to begin empty (no ponding) and with the BSM and surrounding native soils at field capacity.

4.4 Model Development

The model including vertical and lateral infiltration and was developed in a similar process as the original Green and Ampt model (1911). Throughout the model, subscripts 1 or 2 indicate the constructed layer number aligned with the BSM or stone, respectively.

Using Figure 32 to set up the model, the first step was to develop a complete water balance for a control volume around the boundaries of the system. Generally, the total flux (flow rates) in equals the total flux out plus the rate of change of storage. The governing flux balance is given in Equation (6). Every term has units of discharge (cfs). The areas over which the respective infiltration rates act are described by A_{1H}, A_{2H}, and A_{2V} for each respective layer and direction. The areas are assumed to remain constant because the model assumes saturated conditions for each layer for the event or runoff duration.

$$q_{in} + \frac{dP}{dt} A_f = \frac{dET}{dt} A_f + q_{bypass} + f_{1H} A_{1H} + f_{2H} A_{2H} + f_{2V} A_{2V} + \frac{dS}{dt} \qquad (6)$$

The integration with respect to time represents the summation over the storm event. Integrating Equation (6) with respect to time (*t*) and some algebra to group the precipitation and ET terms, the governing equation with units of volume (cu. ft.) becomes:

$$V_{in} + A_f(P - ET) = V_{bypass} + F_{1H}(t)\, A_{1H} + F_{2H}(t)\, A_{2H} + F_{2V}(t) A_{2V} + \mathrm{d}S \qquad (7)$$

Where the *V* terms are the total volumes (in and bypass) over the time. The second term gives the relatively smaller volumes from the total precipitation *P* and ET multiplied by the filter area. The infiltration rates integrate to cumulative infiltration functions *F(t)* for each respective layer and direction; these are similar in form to the cumulative infiltration

functions in the Green and Ampt model. The change in storage (*dS*) is the total change in water volume in storage in the system from the initial condition to the final condition.

The cumulative infiltration functions *F(t)* were developed in a similar procedure as the Green and Ampt model. Figure 31 gives the definition sketch to derive the cumulative infiltration functions from infiltration rates.

The horizontal infiltration was estimated as a triangular head gradient from the ponding surface to the bottom. The wetting front term in the divisor was estimated as 1/2 the longest distance to the wetting front. As time approaches infinity, the shape may be expected to change from a triangle to a trapezoid as the initial infiltrated triangle travels outward. In such a case, the length to the wetting front would approach L_H rather than $L_H/2$. If the length to the wetting front was estimated by a factor of 1 L_H rather than 1/2 L_H, the retrofit rainfall solution for HSBS would decrease by about 2%. The solution is not sensitive to the exact fraction used for estimation, therefore, ½ was used to more appropriately model short duration events. The matric tension is positive here. The subscripts *H* indicate the horizontal direction. The horizontal rate is given by:

$$f_H = K_H\left(\frac{h+\Psi}{L_H/2}\right) \tag{8}$$

The vertical component followed the same derivation as Green and Ampt; however, the ponding height was assumed to be a positive constant value instead of zero. The vertical infiltration rate resembles Equation (8), however, the extra *L* term in the numerator is included due to gravity. The subscripts *V* indicate the vertical direction.

$$f_V = K_V\left(\frac{h+L_V+\Psi}{L_V}\right) \tag{9}$$

With the infiltration rates defined in Equations (8) and (9), a few more relationships are needed for the integration. The relationship of cumulative infiltration (*F*), distance to the wetting front (*L*), and the change in soil moisture from the initial state to final or saturated state ($\Delta\theta$) is given by:

$$F = L\,\Delta\theta \tag{10}$$

Where *F* and *L* are either vertical or horizontal. However, *L* is L_V in the vertical direction and $L_H/2$ in the horizontal direction.

Generally, the infiltration rate equals the rate of change of cumulative infiltration.

$$f_i = \frac{dF_i}{dt} \tag{11}$$

Replacing the *L* terms in Equations (8) and (9) with the relationship in Equation (10) puts the infiltration rates in terms of cumulative infiltration (*F*). Setting these equal to Equation (11), they are integrated with respect to time using separation of variables with limits of integration from *0* to $F_i(t)$. The evaluated integrations yield the cumulative infiltration functions given by Equations (12) and (13). See Appendix A.5 for the full derivation.

$$F_H(t) = [4(h+\Psi)\Delta\theta\, K_H t]^{1/2} \tag{12}$$

Note that the negative solution to Equation (12) will be invalid as negative cumulative infiltration cannot occur in this model. Only the positive solution is valid.

$$F_V(t) = (h+\Psi)\Delta\theta\, \ln\left(\left|1 + \frac{F_V(t)}{(h+\Psi)\Delta\theta}\right|\right) + K_V\, t \tag{13}$$

Equation (13) is an implicit solution for the vertical cumulative infiltration. While there are explicit approximations for the Green and Ampt equation, the implicit equation was

used in the model as it is easily solved by iteration or solvers with today's computing power.

These cumulative infiltration functions have units of length and are multiplied by the effective area over which they occur to yield units of volume. The cumulative volume infiltration equations become:

$$F_{1H}(t_Q) = 2\left(l + \frac{A_f}{l}\right)(h_1 + d_f)\left[4(h_1 + \Psi_1)\Delta\theta_1\, K_{1H}\, t_Q\right]^{1/2} \quad (14)$$

$$F_{2H}(t_E) = 2\left(l + \frac{A_f}{l}\right)(h_2)\left[4(h_2 + \Psi_2)\Delta\theta_2\, K_{2H}\, t_E\right]^{1/2} \quad (15)$$

$$F_{2V}(t_E) = A_f\left\{(h_2 + \Psi_2)\Delta\theta_2\, \ln\left(\left|1 + \frac{F_{2V}(t_E)}{(h_2 + \Psi_2)\Delta\theta_2}\right|\right) + K_{2V}\, t_E\right\} \quad (16)$$

Where the $2\left(l + \frac{A_f}{l}\right)$ term is the filter perimeter, and *l* is the length of the filter. This representation of the perimeter assumes a rectangular design and eliminates the width variable in deference to the BSM surface area (A_f). The infiltration through the stone layer (layer 2) occurs over the duration of the event (t_E) while the lateral infiltration from layer 1 may only occur while the BSM remains near saturated levels and is therefore shortened and estimated by the duration of the runoff (t_Q).

The final term in the governing equation is the change in storage (*dS*) and is the sum of the change in volumes in the BSM and the stone layers. The volume of water in the BSM equals the bulk volume of the BSM times the change in VWC. The volume of water in the stone layer equals the area of the filter times the porosity and change in water depth. This assumes that there is negligible volume of water stored through capillary action in the upper portion of the stone above the underdrain. The total volume of storage is given as:

$$\Delta S = A_f\left[d_f\left(VWC_f - VWC_i\right) + \eta_{gravel}\left(h_{2f} - h_{2i}\right)\right] \quad (17)$$

Where η is porosity, and h_2 indicates the water depth in layer 2 (stone). The *i* and *f* subscripts for the VWC and h_2 represent the initial and final conditions.

Substituting the cumulative infiltration functions from Equations (14) to (16) and the change in storage from Equation (17) into the Equation (7) give the complete governing equation for the model.

4.5 Input and Output

The model's input parameters may be divided into four general categories: watershed properties, climatic properties, soil characteristics, and design variables. The variables will be discussed generally here, and an example of the model application for the site study is given in Section 4.6.

The first term in the governing equation is the volume in. This is a function of the precipitation and watershed characteristics such as contributing area, impervious cover, and other land use characteristics. For new design, the WQV may be used in place of the V_{in} as it represents the total treatment volume over the duration of the storm. The WQV is a function of precipitation, watershed area, and percent impervious cover as shown in Equations (1) and (2).

The second terms on the left-hand side of the governing equation fall into the climatic category and are the volumes in from precipitation and out from ET. These terms may be negligible compared to the runoff volume depending on the watershed to filter ratio and watershed characteristics. The decision to ignore these terms is a judgment of the

designer based on each system and its watershed. Their inclusion for modeling the HSBS will be discussed in Section 4.6.

The cumulative infiltration functions are largely comprised of variables based on physical characteristics in the native soils. The matric potential (ψ), change in soil moisture ($\Delta\theta$), horizontal saturated hydraulic conductivity (K_H), and vertical saturated hydraulic conductivity (K_V) are all properties of the native soils that ideally are directly measured in situ, but they may be estimated using soil texture from a PSD (Williams, Ouyang, Chen, & Ravi, 1998).

The last category of inputs is design variables. These are chosen at the discretion of the designer; however, they should be within the common values used in the industry and within given guidelines. Such variables are the maximum depth of ponding, elevation of the invert of the underdrain, and depth of the BSM layer. They may vary if the system is new or retrofit as design guidelines vary for each.

The final input variable is time. All three cumulative infiltration terms are functions of time. They represent the cumulative infiltration over the entirety of the storm event; however, the times for each infiltration term are not required to be equal. They may be adjusted to describe the physical conditions of the storm event. For example, Figure 22 shows a brief rainfall then runoff that has a duration of about 40 minutes. The BSM quickly saturates and lateral infiltration into the native soils can occur ($F_{1H}\ (t)$). Over time, the lateral infiltration would decrease and water would filtrate down the BSM layer into the stone layer below. Therefore, the duration of runoff gives an estimation of the duration of lateral infiltration from the BSM. The time for the two cumulative infiltration functions in the stone layer will be extended to the end of the event.

Note that this model does not directly incorporate the use of the 24 hour drain period of surface ponding to avoid mosquito breeding. Because the model was derived from the control volume around the whole bioretention, the drain time of ponded water should be calculated separately to ensure the BSM meets the drain time guidelines. To avoid stagnant surface water, the maximum depth of ponding should drain in the desired drain time (24 hours here). The longest possible drain time where ponded water could be stagnant might occur when rainfall and runoff cease and the ponded water is at a maximum depth, assuming the BSM is the hydraulic throttle. Assuming the top of the stone layer is at atmospheric pressure, Darcy's Law may be used to estimate the drain time. Because the change in head is zero, the head gradient is zero and the Darcian velocity reduces to the hydraulic conductivity of the BSM. The maximum ponding depth divided by the hydraulic conductivity yields the time for ponded water to drain down below the BSM surface. Note that this differs from the current new design approach as it considers the entire WQV percolating through the depth of the BSM; however, if the goal is not to have ponded water on the surface, only the maximum ponded water height must drain to the ground surface and not through the entire depth of the BSM. For example, with HSBS, a maximum ponding depth of 4.86 inches divided by the BSM vertical K_s of 6.33 in./hr. yields a drain-down time of about 0.8 hours. This may be compared to the HSBS inflow and outflow hydrographs. The lag between peak inflow to outflow gives an estimate of the routing time through the BSM. The hydrographs in Figures 22 to 25 had peak discharge lags of about 0.67 hr., 0.52 hr., 0.46 hr., and 0.47 hr., respectively. These are about 30% lower than the estimated maximum drain-down period of 0.8 hours, but they are within the expected ranges for events without maximum ponding. The more

physically accurate drain time of 0.8 hours differs drastically from the assumed drain time used by the current design on the order of days. This would imply the current design method of filtering the WQV through the BSM over a day or so would yield a filter surface area that is oversized and very conservative. The method described here assumes the BSM is the hydraulic control and the stone at the bottom of the BSM layer remains at atmospheric pressure as it does in the HSBS.

The model output depends on the application. Comparing the model to a built system such as the HSBS where all design parameters, climatic, watershed, and soil characteristics are known and measured leaves no unknown variables. As such, the calculated infiltration may be graphed or tabulated as convenient for comparison. In Section 4.6, the model is applied to the HSBS.

For use in design applications, two approaches may be used. The model may be applied to new design or a retrofit design. The reason the two approaches differ is that the constraints for each vary and some constraints need to be applied to the model to reduce the number of unknown variables. Generally, to design a bioretention using this model, the climatic, watershed, in situ native soil characteristics, and design variables must first be measured and/or estimated. The remaining unknown variables are precipitation (P), BSM filter area (A_f), and filter length (l). The filter width is also unknown but is not needed to run the model assuming a rectangular shape.

For use in new design, the precipitation is a constant according to the regulation for the given location. The design precipitation in New Hampshire is 1 inch. The solution would then be a curve of filter areas with their associated widths and lengths where the governing equation is balanced for the 1-inch event. An example general solution for a

new design is shown in Figure 33. As there is no singular solution, the designer may choose the optimal single size based on site and budget constraints. The cheapest option for construction, cost of materials, and maintenance will be the filter with the smallest surface area.

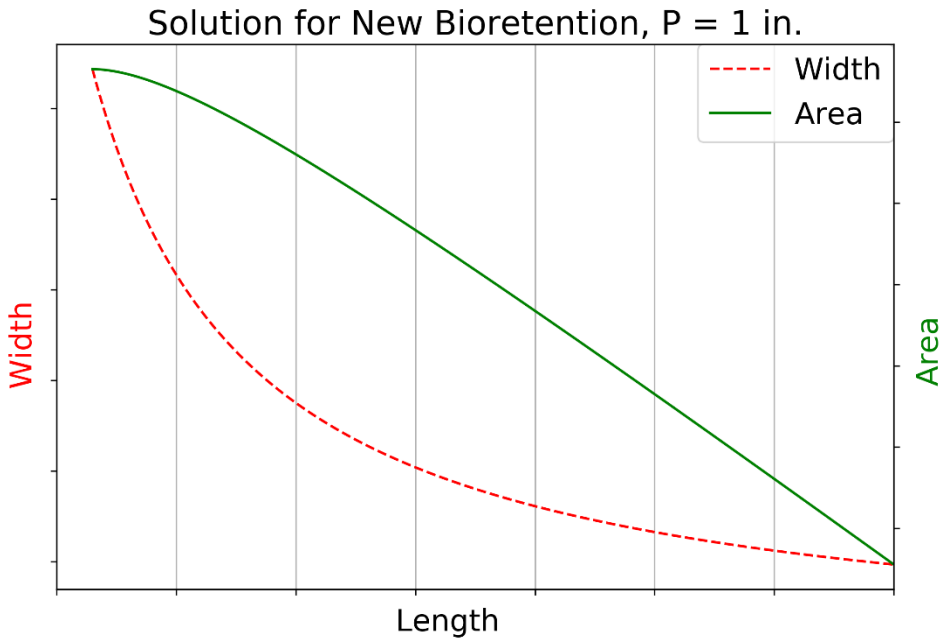

Figure 33: Example general solution to the model for a new design approach. The precipitation is constrained at 1 inch.

In retrofit design, the size constraint for the maximum bioretention area drives the model. Instead of having a set precipitation like the new design approach, the area is set and the precipitation and length are the unknown variables. The solution then takes the form of a curve of precipitation depths with their associated filter lengths and widths that balance the governing equation. Figure 34 shows an example solution for retrofit designs.

The curves in Figure 34 indicate that for any filter area, as the length increases and approaches infinity, the width approaches zero. While there is an infinite number of

mathematical solutions, of course, a bioretention will have a finite and reasonable length and width in practice. The left end of the x-axis (length) represents a square filter, and the

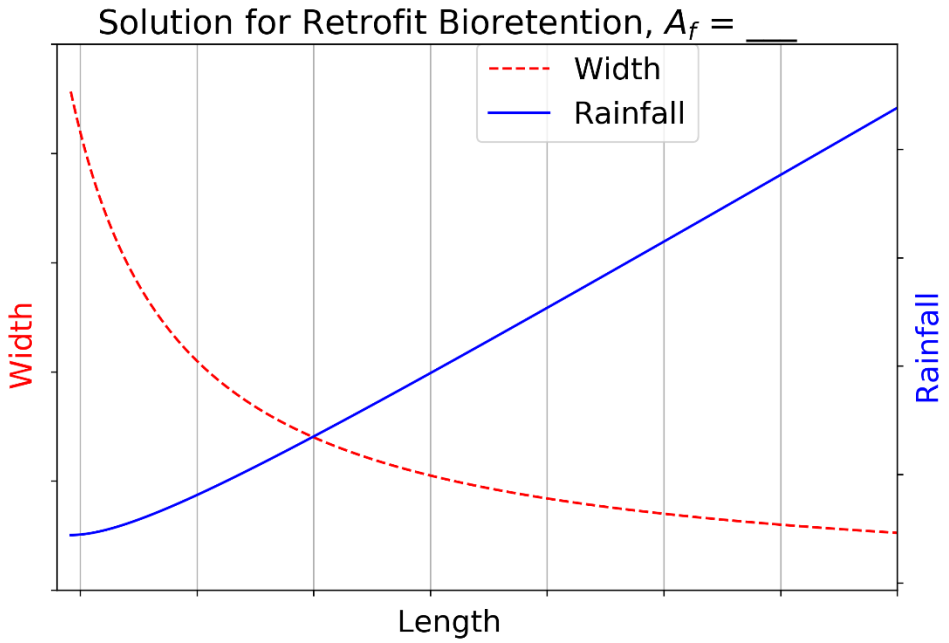

Figure 34: Example solution to the model for a retrofit design approach. The filter area is constrained based on site conditions.

right end represents an extended rectangular shape with a large length to width ratio. As the length increases, the design rainfall increases. This indicates the effectiveness of lateral infiltration due to the increased surface area of the sidewalls as the filter's perimeter increases. This may be contrasted with a model where only bottom infiltration is considered. In such a case, infiltration would only be a function of the bottom area; therefore, changing the length and width would have no impact on the infiltration capacity and the design precipitation would be constant.

4.6 Application on Study Site

First, the model will be applied to the HSBS study site using the complete governing equation given by Equation (7) to compare to observed data for individual storms using the calculated inflow and outflow volumes, rainfall, BSM soil moisture, and water elevations in the stone. Next, the design process will be demonstrated for the HSBS as if designing an unbuilt retrofit bioretention system.

The model will be applied to the data from the 0.17-inch storm event shown in Figure 22 to show the application using real data. Then the results from all storm events will be shown for comparison.

The total volume in was calculated using the “Inflow” hydrograph in red. The discharge multiplied by the time interval of the logger gave the volume for that time interval. The summation of all discrete inflows gave the total volume in (runoff) in cubic feet. The inflow volume was 1546 cu. ft. This can quickly be estimated for verification using the area of a triangle for the inflow; a quick estimation yields (1/2)(1560 s.)(2 cfs) = 1560 cu.ft. Using the same method, the “Outflow” yields a total volume of 792 cu.ft. The calculated total precipitation was 0.17 inches using the same procedure.

ET was not measured for the HSBS, but it was assumed to be negligible for this analysis. NOAA estimates the mean seasonal (May-October) pan evaporation to be about 24.43 inches at Masabesic Lake, about 30 miles from HSBS (NOAA). Assuming it is equally distributed, the mean daily ET would be about 0.160 inches. Assuming ET during the rainfall was zero and could act for the duration of the event after rainfall, ET would remove about 1.3 cu. ft. This was about 0.2% of the effluent volume and was therefore ignored. The direct precipitation on the filter surface was about 30 cu. ft., which was about

1.9% of the inflow volume and was also ignored. For systems where the watershed to filter ratio is much lower or in hot and dry climates where ET is more influential, the *P* and *ET* terms should not be ignored.

The change in storage was calculated using Equation (17) for the areally weighted VWC in the BSM and the depths of water in the stone layer. While the areally weighted VWC is not shown in Figure 22, an example calculation will be shown for T01. The initial VWC of T01 was 0.39, and the final VWC was 0.43. The change in VWC multiplied by the volume of BSM where T01 applies yields the volume of water in storage observed by T01. The change in storage for this example would be (0.43-0.39)(2 ft. height)(15 ft. width)(55 ft. length) = 66 cu. ft. This procedure was repeated for each TDR and well in the stone layer for the storm event. This event had a change in storage of -120 cu.ft. in the BSM layer and -37 cu.ft. in the stone layer. Note that the entire duration of the event was not shown in Figure 22 and the TDR data ends the event lower than the initial values. The negative volumes in storage mean there were greater volumes of stored water in the system before the event than at the end. This may occur with events with a short antecedent period after a large event and when the BSM and stone layers are allowed to drain excess stored water during the event. Generally, the events show positive stored volumes.

The remaining terms in the governing equation describe the cumulative infiltration functions given by Equations (14) to (16). Because the infiltration was not directly measured in the HSBS, the total infiltrated volume may be estimated as the difference between the influent volume and the sum of the effluent volume and change in storage.

For the example here, the observed volume infiltrated was 1546 cu.ft. – [792 cu.ft. + (-120 cu.ft.) + (-37 cu.ft.)] = 911 cu.ft.

The cumulative infiltration functions require several design, storm, and soil characteristic parameters. The design parameters for the system geometry for HSBS were given as the system has been built. The area (A_f) and length (l) are 2100 sq. ft. and 140 ft., respectively. The average depth of ponding (h_1) for this event was zero. The average depth of water in the stone (h_2) was 0.143 ft. (about 1/3 the elevation of the underdrain invert). The depth of the filter bed (d_f) was 2 ft.

The time over which the infiltration occurred was observed and can be estimated from Figure 22. The term $F_{1H}\ (t_Q)$ represents the lateral infiltration from the BSM to the native soils. The time for lateral infiltration through the BSM is estimated by the duration of the runoff (t_Q). The duration of the runoff for this example was 0.9 hours. The duration over which the stone layer is ponded and infiltrates through the terms $F_{2H}(t_E)$ and $F_{2V}(t_E)$ is represented by the duration of the event. The event duration (t_E) for this example was 87.6 hours (not entirely shown in Figure 22).

The final group of variables needed for the infiltration functions are characteristics of the native soils. The remaining variables are matric potential, change in soil moisture, and saturated hydraulic conductivity in both the vertical and horizontal directions. Some degree of in situ sampling is required for estimation of these characteristics. At a minimum, a representative PSD of the native soils outside each of the bioretention layers is required. If direct measurements of these parameters cannot be obtained, they may be estimated based on soil classification from the PSD. However, direct measurements are preferred to estimations. For the HSBS, three boreholes were dug to the depth of the

bioretention excavation. Soil samples were collected to create a PSD using the dry sieve and hydrometer analyses, and the saturated hydraulic conductivity was measured at various head depths using the Guelph permeameter as described in Section 3.7. Refer to that section for soil textures in the native soil profiles and methods for estimating the lateral and horizontal hydraulic conductivities. Because the boreholes had a small radius, the matric potential could not be directly measured with a soil tensiometer. Therefore, matric potentials were estimated for each soil texture based on tables from *Estimation of Infiltration Rate in the Vadose Zone: Application of Selected Mathematical Models, Volume II* (Williams, Ouyang, Chen, & Ravi, 1998), Morris and Johnson (1967), and Todd and Mays (Groundwater Hydrology, 3rd ed., 2005). These tables may also be used to estimate the saturated hydraulic conductivity and change in soil moisture based on the soil texture from PSD's if direct measurements are not possible.

The estimated infiltration terms may be calculated with the input values described. This analysis was performed for the events from HSBS using the same method presented here with the statistics from each storm. The results are shown in Figure 35 along with the same bottom-only infiltration from Figure 30 for comparison. Note that 27 events were analyzed as the remaining events with very low rainfall and runoff yielded estimated infiltration near zero or slightly negative. This was most likely due to the very small discharge depths near the threshold of measurement and not because of actual negative infiltration into the system from the native soils; there was no evidence of this in the TDR or well data. The median error for the model estimation was -8%. The RMSE for the bottom-only estimation and the proposed model were 3210 cu. ft. and 2650 cu. ft., respectively. The nonparametric Kendall Tau correlation coefficient between the

observed infiltration and event rainfall was 0.36; see Figure 55 in Appendix A.4 for details, along with the correlation between the observed infiltration and other calculated event parameters. During low infiltration events, the model overestimated infiltration; while it underestimated in high infiltration events. This roughly corresponded to the rainfall depth although there was low statistical correlation between rainfall and infiltration.

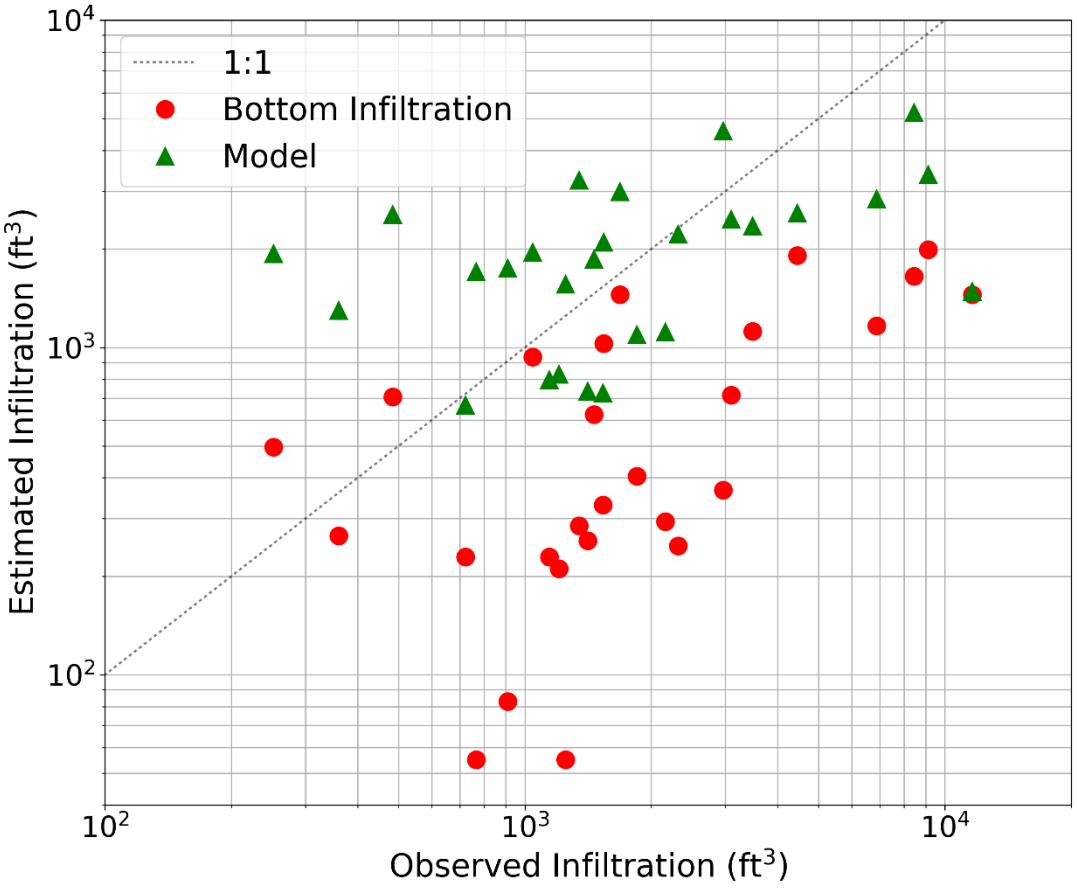

Figure 35: Total observed infiltration and the estimated infiltration using only the vertical component in the bottom of the filter (red circles) and the developed model (green triangles).

The three storms with infiltration below 500 cu. ft. observed infiltration were greatly overestimated using the model. This most likely occurred due to conflicts between the

model assumptions and the physical system behavior. The model assumed saturated conditions with uniform infiltration for the perimeter of the filter. However, as discussed in Section 3.9, the third and sometimes second treatment cell often do not reach saturation during very small events. The unique tiered treatment cells for the HSBS create conditions where the model assumptions may be incorrect for small events. The model assumed the entire perimeter of the BSM (all three cells) were saturated. This error may not be produced for level systems that are not tiered as the surface water would be evenly distributed and percolate into the BSM uniformly.

On average for the application of the model as shown for the events in Figure 35, the portion of each term in the governing equation was calculated and summarized in Table 8. The percentages are shown as the percentage of the total inflow or outflow, respectively. The total inflow and outflow each equal 100%.

Table 8: Median percentages of total inflows and outflows modeled for HSBS events.

	Percent of Inflow	Percent of Outflow
V_{in}	98%	
$P\ A_f$	2%	
V_{bypass}		63.5%
$ET\ A_f$		0.7%
$F_{1H}(t)\ A_{1H}$		13.2%
$F_{2H}(t)\ A_{2H}$		0.1%
$F_{2V}(t) A_{2V}$		21.2%
$\mathrm{d}S$		1.5%

A similar approach was used to employ the model in design, however, several variables such as the durations and water depths needed a generalized value instead of a value specific to one storm event. The watershed and soil characteristics remained the same as the previous approach. For design purposes, the volume in may be estimated

using the WQV using Equations (1) and (2). The design precipitation for a new design will be 1 inch in New Hampshire, however, the treatment storm for a retrofit system will be an unknown variable. As previously stated, the *P-ET* term was negligible for the HSBS. The V_{bypass} is zero as the design event should be treated by the bioretention and not overflow.

Several variables in the infiltration functions need to be defined. The length and area of the filter are unknown variables as discussed in Section 4.5. The mean water depths on the ponded surface (h_1) and in the stone layer (h_2) are estimated by 1/3 the maximum depth of ponding and the 1/3 of the elevation of the underdrain to represent the mean elevations during the event. These depths were estimated to be 1/3 the total height because they were assumed to start and end at zero and reach their respective maximum height during the event. As these are design variables, h_1 and h_2 are easily estimated.

The other terms that must be defined are the times. The median duration of the event may be estimated using a time series of rainfall data. The median event duration is calculated as the length of time from the start of the storm event to the start of the following storm. For the HSBS, the median duration of all events (t_E) was about 72 hours. The median duration of the runoff (t_Q) was calculated at 6.78 hours. To estimate the duration of runoff without direct measurement, a watershed modeling tool such as EPA SWMM or HEC-HMS may be used to route the design storm through the watershed and create a runoff hydrograph. The duration of the runoff hydrograph would be (t_Q).

The model was run for new and retrofit design approaches using the input values in Table 9 for the measured and estimated values for HSBS.

Table 9: Model input parameters for HSBS for new and retrofit design approaches.

Parameter	Variable	Other	BSM	Native 1	Native 2
Event duration (hr.)	t_E	72			
Runoff duration (hr.)	t_Q	6.78			
Watershed area (ac)	A_w	21.9			
Impervious cover	I	0.377			
Maximum depth of ponding (ft.)	h_{max}	0.405			
Pipe invert (ft.)	h_{pipe}	0.500			
1/3 Maximum depth of ponding (ft.)	h_1	0.135			
1/3 Pipe invert (ft.)	h_2	0.1667			
Depth of BSM (ft.)	d_f		2		
Porosity of stone	η_{stone}	0.522			
Soil Suction Head (positive) (ft.)	ψ		0.272	0.472	1.736
Saturated hydraulic conductivity: vertical (ft./hr.)	$K_{s\,V}$		5.28E-01		8.74E-02
Saturated hydraulic conductivity: horizontal (ft./hr.)	$K_{s\,H}$			1.38E-01	3.02E-03
Initial VWC	θ_i		0.204	0.1080	0.401
Saturated VWC	θ_s		0.448	0.443	0.435
Surface P and ET (ft.)	P-ET	~0			
Bioretention area (sq. ft.) (retrofit only)	A_f	2100			
Precipitation (in.) (new only)	P	1			

The solutions for the new and retrofit designs using the proposed model for HSBS are shown in Figures 36 and 37. The general solution curves are shown, but the points for

the HSBS are highlighted in Figure 37 for the built system dimensions. For comparison, the current static design would yield a new filter surface area of about 12,000 sq. ft.

Dynamically designing the HSBS as a new system using the climatic, watershed, and soils parameters from the HSBS would yield a system on the order of 4100 sq. ft. with a width two times the current built width; it would able to treat the 1-inch design storm. The retrofit model solution using the HSBS parameters and system dimensions yields a design storm of 0.52 in., which is just below the observed median rainfall for all events without bypass.

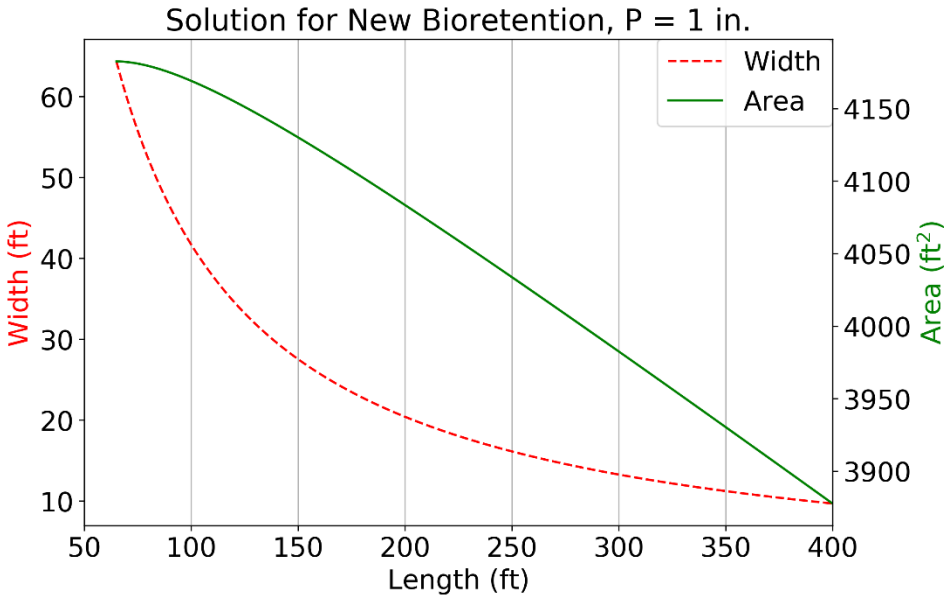

Figure 36: Model solution curves for a new design using HSBS parameters.

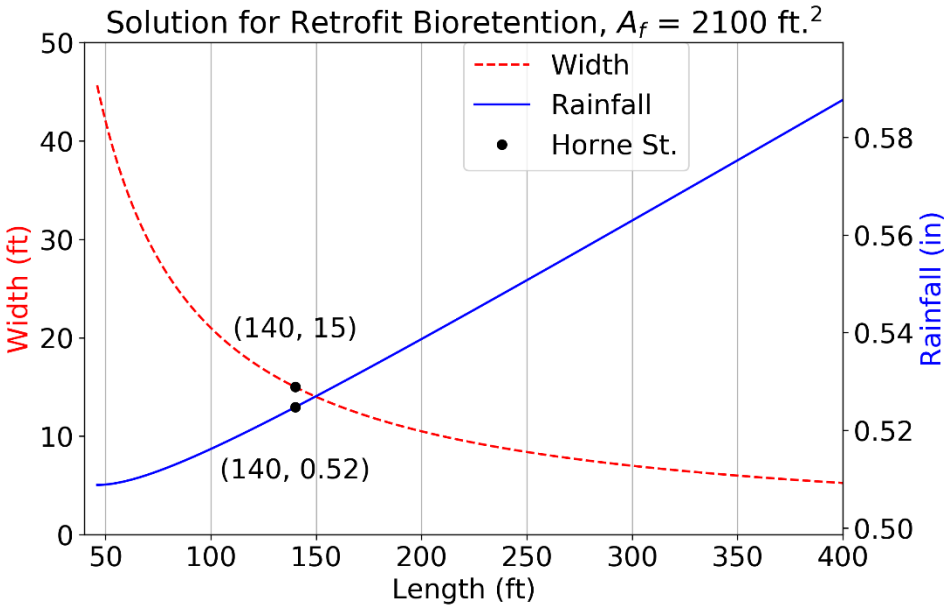

Figure 37: Model solution curves for a retrofit design using HSBS parameters.

The summary of event ponding and rainfall for events that do and do not have high-flow bypass with the current and model design rainfalls is shown in Figure 38. This is a copy of Figure 29 with the addition of the model treatment rainfall.

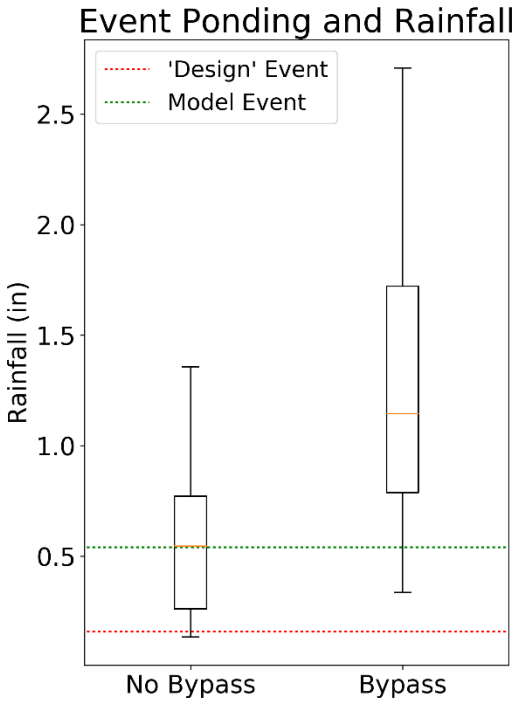

Figure 38: HSBS events without high-flow bypass and events with bypass compared to current design and model treatment rainfall.

4.7 Discussion

While the model was derived using the integration over the whole event rather than a dynamic time-step, the results comparing the observed and estimated infiltrated volumes show that the model greatly improved the estimation of total infiltrated water volume. Figure 35 shows the estimated volume of infiltration for all events if only considering bottom infiltration as is often assumed in LID systems. The mean error for such estimation compared to observed total infiltration was -79%. The mean error for the proposed model was -8%. While there were individual storms that were over- or under-estimated, the mean was greatly improved over the bottom-only estimation, which were almost all underestimated. The variance in performance for individual storms may be attributed to

the distribution and duration of rainfall (therefore, runoff) during the event. The model assumes a uniform, saturated wetting front which would not be the case if the runoff was not consistent. Despite the individual variance, the low mean indicates the model performs well on average, with the most accuracy with mid-ranged infiltration events. The model tends to overestimate the events with low infiltration. One explanation may be due to HSBS having three separate tiered treatment cells. The treatment cells fill from cells nearest the inlet to the outlet. Generally, during small events and periods of low runoff, only the first and maybe second cells are saturated; and the third cell may not receive surface runoff over the berm from cell two. This means lateral infiltration may primarily occur in cells 1-2. The model, however, assumes uniform lateral infiltration around the perimeter of the filter. This would overestimate the infiltration in the BSM. This overestimation error would be reduced in a system that was horizontal without a graded or tiered surface.

Figure 36 describes the solution curves for the HSBS if it were designed as a new system. Assuming the length of 140 ft. remained the constraint for construction, the design event of 1 inch would be treated by a 30 ft. wide system compared to the current built 15 ft. width. The design area would be about 4,200 sq. ft., which is about one third the size of the current static size for a 1 inch. While the model yielded a much smaller area for a new design, this result did not include the Factor of Safety and will not be compared further as the HSBS is a retrofit system.

The solution for the retrofit design approach for HSBS is shown in Figure 37. The exact solution for the HSBS is shown by points using the dimensions of the HSBS. The design event was estimated at 0.52 inches. That is 3.25 times larger (225%) than the

current design precipitation of 0.16 inches which does not consider any infiltration or storage.

Figure 38 shows the great improvement of the model over the current design to include more events that do not have bypass and are fully treated by the bioretention system. The Weibull plotting position was used to estimate the unbiased cumulative distribution functions for the HSBS data to compare to the two design events. Table 10 shows the summary of non-exceedance probabilities for the current design and the proposed model rainfalls compared to the HSBS event data.

Table 10: Unbiased non-exceedance probabilities for the HSBS storms compared to the current design and model retrofit rainfalls.

	Non-bypass	Bypass
Static Design	5.4%	2.8%
Model	49.3%	9.7%

Great improvement is seen in the 44% increase from the design to the model non-bypass events. This indicates that the proposed model more accurately describes the observed performance of the HSBS, including 44% more of the fully treated storms that did not have any bypass. While 6.9% more events that did have some bypass were also included in the model, that will be unavoidable in any model because of the overlap of the box and whiskers. The large events that did bypass were conveyed through the high-flow bypass without harming the system and did not affect the performance of treatment during storms the size of the “design” event or smaller. It should be noted that “bypass” events do not imply that they were completely untreated. Only the portion of the runoff that entered the high-flow bypass left the system untreated.

CHAPTER 6. CONCLUSION

6.1 Summary and Conclusion

Stormwater runoff on suburban and urban watersheds carry with it many pollutants from various non-point sources as well as increased water volumes to our receiving streams, rivers, and bays. Increased population density and urbanization is causing increased nutrient, pollutant, and volume loads in watersheds.

Aging and outdated conventional infrastructure should be replaced with stormwater treatment in mind. LID systems such as bioretention filters perform well in this treatment. Bioretention filters are designed with a layer of engineered soil mixture often planted with native vegetation or grasses and a layer of gravel or stone with an optional underdrain near the bottom. The BSM performs well at removing nutrient loads and filtering gross solids through mechanical filtration, plant root uptake, and microbial metabolization. Bioretention filters perform well at removing petroleum-based pollutants, TSS, hydrocarbons, and heavy metals (UNHSC, 2012a), (UNHSC, 2016a).

Guidelines suggest the contributing watershed for treatment for one bioretention should be between 0.25 to 1 acre (USEPA, 1999). For new design, the current design standard developed by PGDER for the filter area uses a static design sizing to hold the WQV. The filter area is estimated by the time it takes the Water Quality Treatment Volume to filter through the BSM in a set drain time, usually 1 to 4 days. This design ignores all characteristics of the surrounding soils and does not consider infiltration or

storage in the bioretention. The common retrofit design is also a static design which holds the WQV in the pore space of the filter and on the ponding surface.

There have been other models developed in attempts to size the filters dynamically with various stages of ponding and infiltration. One such model developed by Akan (2013), also only considers vertical infiltration through the BSM layer. However, it is a dynamic model with four possible stages of filling and draining. This could be a useful preliminary design aid as noted by the author.

A computational model was developed by Palhegyi (2010) that included ET and simulated the water balance for vertical distribution in the soil layers. The soil moisture can be depleted by ET or by percolation into native soils. His conclusion was that systems built for watersheds with 100% impervious cover should be sized to treat a runoff volume from 2 to 4 inches of precipitation; watersheds with around 20% to 30% IC should be sized for the 1-inch precipitation. While the model performed well against several built systems, the author noted that the results were specific to the areas where the study was conducted.

Other dynamic models such as EPA SWMM can route an inflow hydrograph through green infrastructure, however, these models assume that horizontal flow is negligible relative to vertical seepage. While the dynamic models more accurately describe the inflow hydrograph, ignoring lateral infiltration may underestimate the total infiltrated volumes.

As the current design standard using static design and vertical infiltration through the BSM overestimates the filter area, a new design approach including horizontal flow and time-varying rainfall is needed. The model developed here addresses the first issue

to include anisotropy and horizontal flow, but it is still a pseudo-static design as the governing equation was integrated over the event duration.

The model developed in this study was derived from a volume balance for a control volume around the entire bioretention system rather than the BSM. The volume balance accounted for inflow runoff, precipitation, evapotranspiration, and vertical and horizontal seepage into the native soils. The inflow runoff is equal to the WQV for the design precipitation.

The vertical and horizontal seepage terms and the volume balance were developed in a similar fashion as the original Green and Ampt equation. The vertical term takes on the same form as the Green and Ampt equation with the inclusion of a term for constant ponding. While there is not constant ponding during an event, this allows for more control in the design process as the parameter may be manipulated to represent various ponded situations. The implicit, vertical, cumulative infiltration function under constant head was derived to calculate infiltration in the bottom of the filter.

The horizontal component was derived using a similar infiltration rate to the horizontal term except the gravimetric term L in the numerator was removed. The explicit, horizontal, cumulative infiltration function under constant head was derived for the horizontal infiltration component of the governing equation.

With the calculation of the change in storage of water in the BSM and stone layers and the terms mentioned above, the complete water balance was calculated. Because there was more than one dependent variable in the volume balance, the solution had the form of a curve rather for design applications.

The form of the volume balance makes it easy and efficient to find solutions for either a new or retrofit design. For new designs, the precipitation is a constant set by standard design (1 inch in NH), and the filter area, length, and width are calculated in the solution curves. For retrofit designs, the maximum possible filter area is a constant, and the filter length, width, and design precipitation are calculated. Examples of the solution curves can be seen in Figures 36 and 37. However, this study compared the model to a retrofit study system and the new design approach needs further study.

The bioretention system on Horne St., Dover, NH treats the runoff from a suburban watershed of 21.9 acres with 38% impervious cover. The time of concentration is 16.5 minutes. The retrofit system was sized to treat a 0.16-inch rainfall. Analysis of forty-five storms with one-minute logging intervals showed that the system outperformed the design event and is oversized by the current standard. The mean peak flow reduction was 62% with a standard deviation of 25%. The mean volume reduction was 35% with a standard deviation of 37%. Rainfall events over 800% of the current retrofit treatment rainfall occurred without ponding (or bypass) on the surface. However, 90% of events that had any high-flow bypass were over 330% the current design treatment rainfall. This illustrates that the built system is oversized compared to the rainfall it was designed to treat. Applying the model developed in this study yielded a larger dynamic design event of 0.52 inches. The model design event included 49% of the observed events that did not have high-flow bypass while excluding 90% of observed events that did have high-flow bypass. This is an improvement of 44% inclusion of observed non-bypass events over the current design.

Because the current design standard requires few parameters and is only one equation, it can quickly be calculated and compared to the model developed in this study. Additionally, models such as that developed by Akan (2013) can be used as a preliminary design aid. However, Akan's preliminary design process may not be used for the site study as the lowest possible treatment rainfall for a valid solution is 0.06 inches and peak runoff must be above 1.5 cfs (observed median runoff was 0.9 cfs). Having several models that give a solution for a bioretention area will equip the designer to better evaluate which parameters dominate design. The final design may be changed accordingly at the discretion of the engineer. For example, if the site is large enough and peak flow reduction is the design priority, the current static sizing may outperform the other models as it tends to overestimate the filter area. However, static sizing is unable to accurately predict real-time performance.

Designing a "new" system with the model results in a smaller filter area which thereby reduces the cost of construction, materials, and maintenance. The HSBS was originally designed with a filter area of 12,000 sq. ft. to manage the 1-inch storm. The model developed here would suggest a filter of 4140 sq. ft. would equally treat the 1-inch design event. A filter size reduction of 67% would reduce the cost of this one system alone. However, it is often desirable to have a conservative design for new construction, and the analysis of model results in this study focused on retrofit application. In a retrofit application where size constraints dictate design, the model generates a more accurate precipitation depth and representation of the bioretention performance by the inclusion of the horizontal and vertical infiltration into the native soils over the duration of the storm. For the Horne St. study site, the model's design rainfall

was 3.25 times larger than the current design rainfall and very similar to the median observed rainfall for all events that were fully treated without any bypass. This has significance in credits for volume and pollution load reduction.

6.2 Future Work

The assumption that rainfall events follow SCS 24 hr. rainfall distributions instead of the highly time-variable events leads to simplified time series models. The use of dynamic models based on time-varying rainfall from historic or simulated rainfall should reduce much of the error from the assumed simplified rainfall models and increase the ability to run the model thousands of times for more statistically accurate analyses. The current static sizing design should be replaced because parameters such as peak flows, peak ponding depths, etc. do not give any indication as to the period of time over which they occur. Using a dynamic model may correct the system dimensions according to the time-varying parameters.

In addition to time-varying dynamic models, a more accurate yet more time and parameter consumptive model would consider flow in the unsaturated soils. The simplifying assumption that soils during rainfall events are saturated may overestimate infiltration. However, as there are hysteresis effects and more soil parameters needed to create a soil wetting and drying curve, the effort in creating such a model may outweigh the overestimation in assuming saturated conditions.

The lateral infiltration model developed here was a useful estimation for an event volume infiltrated, however, the simplifying assumptions limit the accuracy of the model over time. As time increases, the horizontally infiltrated water would be affected by gravity

and start to move downward toward the vertically infiltrated mound. These effects were not considered in this model and should be explored further.

LIST OF REFERENCES

Akan, A. O. (2013). Preliminary Design Aid for Bioretention Filters. *Journal of Hydrologic Engineering, 18*(3), 318-323. doi:10.1061/(ACSE)HE.1943-5584.0000554

ASTM Int'l. (2004). *D6913-04: Standard Test Methods for Particle-Size Distribution (Gradation) of Soils Using Sieve Analysis.* West Conshohocken, PA: ASTM International.

ASTM Int'l. (2009). *D3385-09: Standard Test Method for Infiltration Rate of Soils in Field Using Double-Ring Infiltrometer.* West Conshohocken, PA: ASTM International.

ASTM Int'l. (2016). *D7928-16: Standard Test Method for Particle-Size Distribution (Gradation) of Fine-Grained Soils Using the Sedimentation (Hydrometer) Analysis.* West Conshohocken, PA: ASTM International.

Bouwer, H. (1966). Rapid Field Measurement of Air Entry Value and Hydraulic Conductivity of Soil as Significant Parameters in Flow System Analysis. *Water Resources Research, 2*(4), 729-738.

Bouwer, H., & Jackson, R. D. (1974). Determining Soil Properties. *Drainage for Agriculture, 17*, 611-672.

Campbell Scientific, Inc. (2011). *Operator's Manual: CR1000 Measurement and Control System.* Logan, UT.

Chu, S. T. (1978, June). Infiltration During an Unsteady Rain. *Water Resources Research, 14*(3), 461-466.

Claytor, R. A., & Schueler, T. R. (1996). *Design of Stormwater Filtering Systems.* Ellicott City, MD: The Center for Watershed Protection.

Comprehensive Environmental Inc. & NH DES. (2008). *New Hampshire Stormwater Manual, Volume 2: Post-Construction Best Management Practices Seleciton & Design.*

Dussailant, A. R., & Wu, C. H. (2004). Richards equation model of a rain garden. *Journal of Hydrologic Engineering, 9*(3), 219-225.

Ebrahimi, M., & Moradi, S. (2015). A Comparison Of Guelph Permeameter And Double Ring Infiltrometer Methods For Estimating The Saturated Hydraulic Conductivity

In Sandy Soils. *IJREAT International Journal of Research in Engineering & Advanced Technology, 3*(4), 218-222.

Elrick, D. E., Reynolds, W. D., & Tan, K. A. (1989). Hydraulic Conductivity Measurements in the Unsaturated Zone Using Improved Well Analysis. *Ground Water Monitoring and Remediation, 9*, 184-193.

Green, W., & Ampt, G. (1911). Studies on Soil Physics Part I - The Flow of air and Water Though Soils. *Journal of Agricultural Science, 4*, 1-24.

Gupta, R. K., Rudra, R. P., Dickinson, W. T., Patni, N. K., & Wall, G. J. (1993). Comparison of Saturated Hydraulic Conductivity Measured by Various Field Methods. *Trans. ASAE, 36*(1), 51-53.

Hillel, D. (1998). *Environmental Soil Physics.* San Diego, CA: Academic Press.

Huang, R. Q., & Wu, L. Z. (2012). Analytical solutions to 1-D horizontal and vertical water infiltration in saturated/unsaturated soils considering time-varying rainfall. *Computers and Geotechnics, 39*, 66-72.

Hydrologic Aspects of Nonpoint Pollution. (1995). In V. Novotny (Ed.), *Nonpoint Pollution and Urban Stormwater Management.* Lancaster: Technomic Pub. Co.

Lee, D. M., Reynolds, W. D., Elrick, D. E., & Clothier, B. E. (1985). A Comparison of Three Field Methods for Measuring Saturated Hydraulic Conductivity. *Canadian Journal of Soil Science, 65*, 563-573.

McCuen, R. H. (1941). *Hydrologic Analysis and Design - 3rd ed.* Upper Saddle River, NJ: Pearson Education, Inc.

Mishra, S., Parker, J. C., & Singhal, N. (1989). Estimation of Soil Hydraulic Properties and Their Uncertainty From Particle Size Distribution Data. *Journal of Hydrology, 108*, 1-18.

Mohanty, B. P., Kanwar, R. S., & Everts, C. J. (1994). Comparison of Saturated Hydraulic Conductivity Measurement Methods for a Glacial Till Soil. *Soil Science Society of America Journal, 58*, 672-677.

Morris, D. A., & Johnson, A. I. (1967). Summary of Hydrologic and Physical Properties of Rock and Soil Materials. *U.S. Geological Survey Water-Supply Paper 1839-D*.

National Research Council. (2008). *Urban Stormwater Management in the United States.* Washington, D.C.: The National Academies Press.

NOAA. (December 1982). *Technical Report NWS 34: Mean Monthly, Seasonal, and Annual Pan Evaporation for the United States.* Washington, D.C.: NOAA.

Palhegyi, G. E. (2010). Modeling and Sizing Bioretention Using Flow Duration Control. *Journal of Hydrologic Engineering, 15*(6), 417-425. doi:10.1061/(ASCE)HE.1943-5584.0000205

Philadelphia Water Department. (2015). *Stormwater Management Guidance Manual, Version 3.0.* Philadelphia, PA: Philadelphia Water Department.

Philip, J. R. (1992, August). Falling Head Ponded Infiltration. *Water Resources Research, 28*(8), 2147-2148.

Philip, J. R. (1993, July). Variable Head Ponded Infiltration Under Constant or Variable Rainfall. *Water Resources Research, 29*(7), 2155-2165.

Prince George's County Department of Environmental Resources (PGDER). (1993). *Design Manual for Use of Bioretention in Storm Water Management.* Landover, MD: Division of Environmental Management, Watershed Protection Branch.

Ravi, V., & Williams, J. R. (1998). *Estimation of Infiltration Rate in the Vadose Zone: Compilation of Simple Mathematical Models Volume I.* Ada, OK: U.S. EPA.

Reeve, R. C., & Kirkham, D. (1951). Soil Anisotropy and Some Field Methods for Measuring Permeability. *American Geophysical Union Transactions, 32*(4), 582-590.

Reynolds, W. D., & Elrick, D. E. (1986). A Method for Simultaneous In Situ Measurement in the Vadose Zone of Field Saturated Hydraulic Conductivity Sorptivity and the Conductivity Pressure Head Relationship. *Ground Water Monitoring and Remediation, 6*, 84-95.

Rossman, L. A. (2017). *Storm Water Management Model Reference Manual, Volume II - Hydraulics.* Cincinnati, OH: U.S. EPA.

Salvucci, G. D., & Entekhabi, D. (1994). Explicit Expressions for Green-Ampt (Delta function diffusivity) Infiltration Rate and Cumulative Storage. *Water Resources Research, 30*, 2661-2663.

Todd, D. K., & Mays, L. W. (2005). *Groundwater Hydrology, 3rd ed.* John Wiley & Sons, Inc.

UNHSC. (2005). *2005 Data Report.* Durham, NH: University of New Hampshire Stormwater Center.

UNHSC. (2009). *2009 Biannual Report.* Durham, NH: University of New Hampshire Stormwater Center.

UNHSC. (2012a). *2012 Biennial Report.* Durham, NH: University of New Hampshire Stormwater Center.

UNHSC. (2012b). *Quality Assurance Project Plan for: Rain Garden Capacity Demonstration 'Right Sizing Project'.* Durham, NH: University of New Hampshire Stormwater Center.

UNHSC. (2016a). *Breaking Through: 2016 Report.* Durham, NH: University of New Hampshire Stormwater Center.

UNHSC. (2016b). *Quality Assurance Project Plan for: Taking it to the Streets: Green Infrastructure for Sustainable Philadelphia Communities.* Durham, NH: University of New Hampshire Stormwater Center.

UNHSC. (2017a). *Bioretention Soil Specification.* Durham, NH: University of New Hampshire Stormwater Center.

UNHSC. (2017b). *Regular Inspection and Maintenance Guidance for Bioretention Systems / Tree Filters.* Durham, NH: University of New Hampshire Stormwater Center.

USDA NRCS. (1986). *Urban Hydrology for Small Watersheds: TR-55.* Washington, D.C.: USDA NRCS.

USDA NRCS. (2007). Chapter 7: Hydrologic Soil Groups. In *National Engineering Handbook Part 630: Hydrology.* USDA NRCS. Retrieved from https://directives.sc.egov.usda.gov/OpenNonWebContent.aspx?content=17757.wba

USDA NRCS. (2010). Chapter 15: Time of Concentration. In *National Engineering Handbook Part 630: Hydrology.* USDA NRCS. Retrieved from https://www.nrcs.usda.gov/wps/portal/nrcs/detailfull/national/water/manage/hydrology/?cid=stelprdb1043063

USDA SCS. (1987). *Soil Mechanics Level I: Module 3: USDA Textural Classification.* U.S. Department of Agriculture: Soil Conservation Service.

USEPA. (1999). *Storm Water Technology Fact Sheet - Bioretention.* Washington, D.C.: U.S. EPA.

Williams, J. R., Ouyang, Y., Chen, J.-S., & Ravi, V. (1998). *Estimation of Infiltration Rate in the Vadose Zone: Compilation of Simple Mathematical Models Volume II.* Ada, OK: U.S. EPA.

APPENDIX

A.1 Estimation of Time of Concentration and Lag

The Time of Concentration (T_c) was estimated using TR-55 velocity method and compared to observed hydrograph data for the HSBS. The path length from the hydraulically farthest point of the watershed to the outlet is 1854 feet. The average slope of the path is about 0.8%. Using Figure 15-4 from Chapter 15 of Part 630 in the National Engineering Handbook (USDA NRCS, 2010) for nearly all “Pavement and small upland gullies” yields an average velocity of about 1.8 fps.

The travel time over the path is simply the distance divided by velocity.

$$T_{c\,Velocity} = \frac{1854\ ft}{1.8\ fps}\left(\frac{1\ min}{60\ s}\right) = 17.2\ min$$

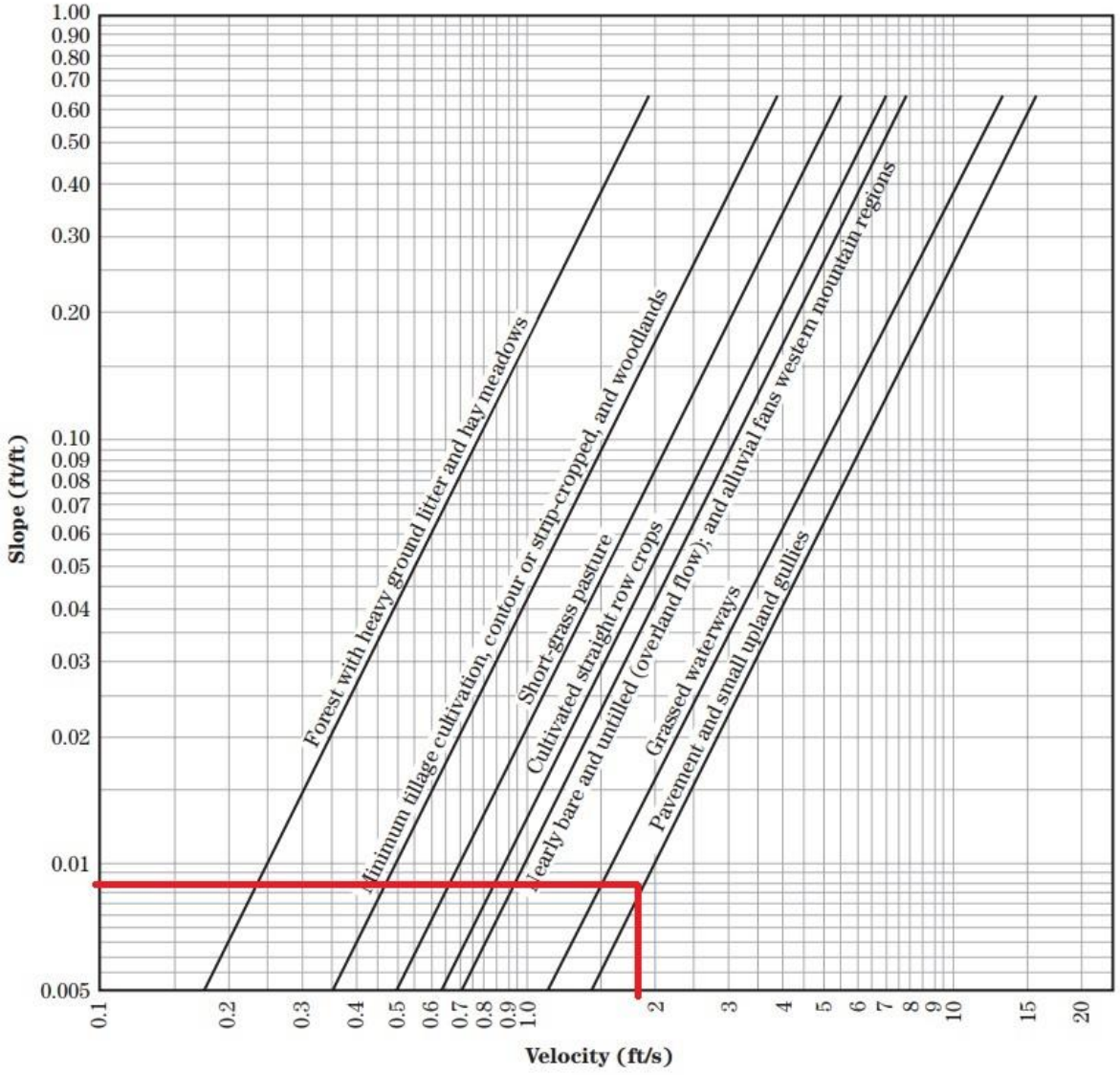

Figure 39: Average velocities and watershed slope for shallow concentrated flow (USDA NRCS, 2010).

The observed time of concentration for the HSBS was estimated using individual storm event hydrographs. T_c is the time from the end of excess rainfall to the point of inflection on the receding limb of the hydrograph (USDA NRCS, 2010) and shown in Figure 40. Note that the lag time here was calculated as from the time excess precipitation began instead of from the centroid as shown in Figure 40.

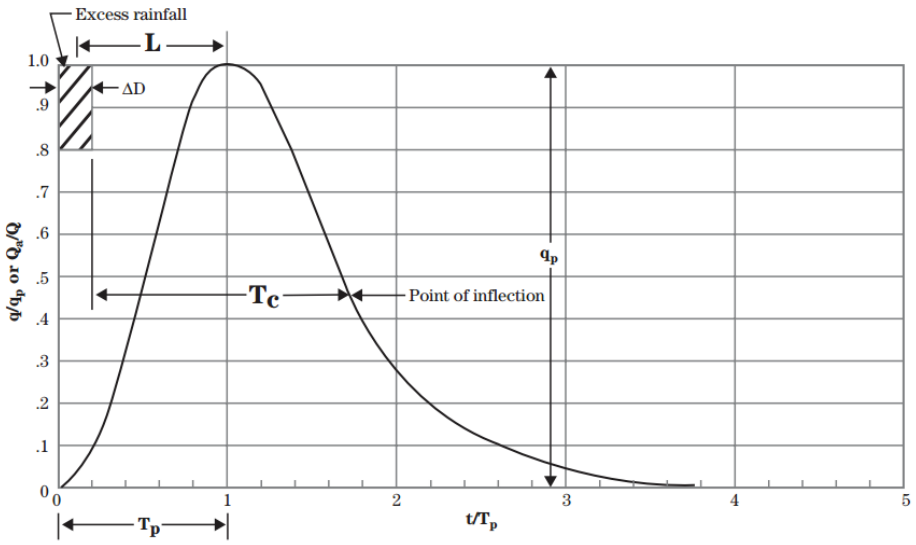

where:
L = Lag, h
T_c = time of concentration, h
T_p = time to peak, h
ΔD = duration of excess rainfall, h
t/T_p = dimensionless ratio of any time to time to peak
q = discharge rate at time t, ft^3/s
q_p = peak discharge rate at time T_p, ft^3/s
Q_a = runoff volume up to t, in
Q = total runoff volume, in

Figure 40: The relation of time of concentration (T_c) to the dimensionless unit hydrograph (USDA NRCS, 2010).

An example of the estimation of the T_c and lag using a storm for the HSBS is shown in Figure 41. This the same 0.17-inch event from Figure 22. The upper subplot shows the rainfall intensity and inflow hydrograph as in Figure 22 with the addition of the constant loss function using the iterative phi-index method (McCuen, 1941). The bottom subplot shows the second derivative of the inflow hydrograph using the central difference approximation.

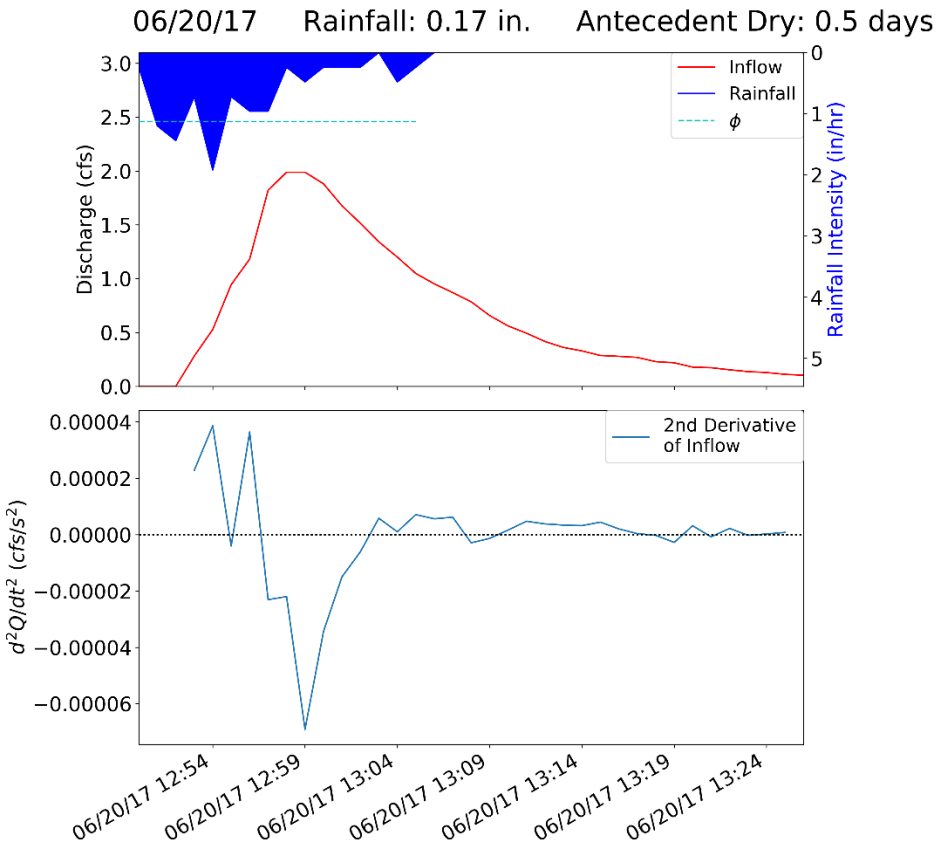

Figure 41: 0.17-inch storm for HSBS with the hyetograph, inflow hydrograph, and phi-index of 1.132 in./hr. in the upper plot. The lower plot shows the second derivative of the inflow hydrograph using the central difference approximation.

The iterative phi-index method was used to estimate the loss function as it was simpler and faster than other infiltration-capacity curve methods. The initial phi-index estimation for this storm was 0.610 in./hr., and the final iteration yielded 1.132 in./hr. Rainfall intensities greater than the phi-index were considered excess rainfall. The excess rainfall began about 12:51 and ended about 12:55. The second derivative of the inflow hydrograph was used to find the time where the peak discharge and the inflection point on the receding limb of the inflow hydrograph occurred. The peak occurs at the minimum value, and the inflection point occurs when the second derivative equals zero. For the

example in Figure 41, the peak discharge occurred at 12:59, and the inflection point occurred at 13:03. For this storm, the observed T_c and lag were both 8 minutes. The summary of select events is shown in Table 11. For all observed HSBS events, the mean lag was 9 minutes; the mean T_c was 16.5 minutes.

Table 11: Estimated lag and time of concentration for select HSBS events.

Event Start	Lag (min.)	Tc (min.)	Event Start	Lag (min.)	Tc (min.)
8/22/16 0:05	2	8.5	11/29/16 10:11	9	25.5
9/11/16 10:16	7	14.5		11	
10/1/16 7:11	11	19.5		12	
	6	13.5		14	
10/9/16 3:34	10	19.5		12	
	12	17.5		8	15.5
	8	16.5	11/30/16 13:38	5	9.5
	10	21.5		5	16.5
10/21/16 19:07	3	10.5	4/6/17 10:40	6	12.5
	14	15.5		12	
	8	13.5		6	18.5
10/27/16 14:05	10	18.5	4/12/17 14:10	11	
	14	28.5		13	18.5
	13	18.5	4/21/17 3:46	8	16.5
11/3/16 6:12	11		4/25/17 6:57	5	13.5
	7	17.5		6	12.5
	6	16.5		4	11.5
11/15/16 16:30	8	19.5	5/1/17 18:04	6	12.5
	10	18.5		7	14.5
11/20/16 1:11	14	22.5		13	
11/24/16 22:30	11	22.5		8	17.5
			6/20/17 12:48	8	8

A.2 PSD Data

The collected data from the PSD in Figure 19 is shown here for one representative borehole located in the 73 ft. from the HSBS inlet and 2 ft. West of the bioretention edge in the native soils. Soil samples were collected as the soil texture was observed to change while digging the borehole. The samples were gradated and analyzed using the ASTM Method D7928-16 using a hydrometer analysis. The samples were then processed according to ASTM D6913-04 using a dry sieve analysis. The PSD data for the two analyses were combined to form one PSD for each sample as shown in Figure 19. The BSM sample processed by UNHSC staff omitted the hydrometer analysis as the engineered soil had a sand texture and a sieve analysis was sufficient. Table 12 shows the data measured for the BSM sieve analysis.

Table 12: Sieve analysis of the BSM sample at HSBS.

Analyst Name	Tim Puls, Rosie Read		
Test Date	10/23/2013		
BMP	Horne St., Dover, NH		
Sample Description	BSM, 12 in. depth		
Sample mass (g)	889.8		
ASTM Method	D422-63		
US sieve number	Sieve opening (mm)	Mass retained (g)	Mass Percent Finer
4	4.750	89.3	90.0%
10	2.000	86.7	80.2%
20	0.850	166.7	61.5%
40	0.425	235.1	35.1%
60	0.250	189.0	13.8%
100	0.150	55.3	7.6%
200	0.075	4.5	7.1%
Pan	-	63.2	0.0%
	Total mass (g)	889.8	

Tables 13 to 20 show the alternating hydrometer then sieve analyses for the four sample depths in the borehole.

Table 13: Hydrometer analysis of the sidewall borehole at HSBS, 73 ft., 0-18 in. depth.

Analyst Name	Daniel Macadam, Ethan Ely			Moist mass of sample (g)		60.00
Test Date	3/8/2017			Mass of dispersant M_{disp} (g)		5.00
BMP	Horne St., Dover, NH			Cylinder Diameter D_C (cm)		6.2
Sample Description	Native sidewall, 0-18 in.			Meniscus Correction C_m		0.001
ASTM Method	D7928-16			Volume suspension in cylinder V_{sp} (cm^3)		1000.0
				Mass of soil plus dispersant M_{dd} (g)		90.70
				Mass of soil M_d (g)		85.70
				Specific Gravity of soil G_s		2.395
Hydrometer Analysis						
Elapsed Time	Offset	Hydrometer Reading	Temp.	Effective Depth	Particle Size	Mass Percent Finer
t (min)	$r_{d,m}$	r_m	T (°C)	H_m (cm)	D_m (mm)	N_m (%)
1	1.00000	1.00850	21.87	16.29	0.0598	16.8%
2	1.00000	1.00750	21.87	16.52	0.0426	14.8%
5	1.00000	1.00700	21.90	16.64	0.0270	13.9%
15	1.00000	1.00600	21.98	16.87	0.0157	11.9%
30	1.00000	1.00500	22.00	17.10	0.0112	9.9%
60	1.00000	1.00500	22.00	17.10	0.0079	9.9%
240	1.00000	1.00425	22.00	17.28	0.0040	8.4%
1440	1.00000	1.00450	20.50	17.22	0.0016	8.9%

Table 14: Sieve analysis of the sidewall borehole at HSBS, 73 ft., 0-18 in. depth

Analyst Name	Daniel Macadam		
Test Date	3/8/2017		
BMP	Horne St., Dover, NH		
Sample Description	Native sidewall, 0-18 in.		
Sample mass (g)	85.70		
ASTM Method	D6913-04		
US sieve number	Sieve Opening (mm)	Mass retained (g)	Mass Percent Finer
10	2.000	0.6	99.3%
20	0.833	1.3	97.8%
40	0.425	5.4	91.5%
60	0.250	11.5	78.1%
100	0.150	10.1	66.3%
200	0.075	9.6	55.1%
Pan	-	47.2	0.0%
	Total mass (g)	85.7	

Table 15: Hydrometer analysis of the sidewall borehole at HSBS, 73 ft., 18-26 in. depth.

Analyst Name	Daniel Macadam, Ethan Ely		Moist mass of sample (g)			60.00
Test Date	3/8/2017		Mass of dispersant M_{disp} (g)			5.00
BMP	Horne St., Dover, NH		Cylinder Diameter D_C (cm)			6.2
Sample Description	Native sidewall, 18-26 in.		Meniscus Correction C_m			0.001
ASTM Method	D7928-16		Volume suspension in cylinder V_{sp} (cm^3)			1000.0
			Mass of soil plus dispersant M_{dd} (g)			59.00
			Mass of soil M_d (g)			54.00
			Specific Gravity of soil G_s			2.426
Hydrometer Analysis						
Elapsed Time	Offset	Hydrometer Reading	Temp.	Effective Depth	Particle Size	Mass Percent Finer
t (min)	$r_{d,m}$	r_m	T (°C)	H_m (cm)	D_m (mm)	N_m (%)
1	1.00000	1.01300	21.93	15.23	0.0572	40.5%
2	1.00000	1.01150	21.94	15.58	0.0409	35.8%
5	1.00000	1.01050	21.96	15.82	0.0261	32.7%
15	1.00000	1.00925	22.00	16.11	0.0152	28.8%
30	1.00000	1.00850	22.00	16.29	0.0108	26.5%
60	1.00000	1.00750	22.00	16.52	0.0077	23.4%
240	1.00000	1.00650	22.00	16.75	0.0039	20.2%
1440	1.00000	1.00575	20.50	16.93	0.0016	17.9%

Table 16: Sieve analysis of the sidewall borehole at HSBS, 73 ft., 18-26 in. depth

Analyst Name	Daniel Macadam		
Test Date	3/8/2017		
BMP	Horne St., Dover, NH		
Sample Description	Native sidewall, 18-26 in.		
Sample mass (g)	54.00		
ASTM Method	D6913-04		
US sieve number	Sieve Opening (mm)	Mass retained (g)	Mass Percent Finer
10	2.000	0.1	99.8%
20	0.833	0.2	99.4%
40	0.425	1.0	97.6%
60	0.250	2.6	92.9%
100	0.150	4.9	83.8%
200	0.075	11.3	62.9%
Pan	-	33.9	0.0%
	Total mass (g)	54.0	

Table 17: Hydrometer analysis of the sidewall borehole at HSBS, 73 ft., 26-28 in. depth.

Analyst Name	Daniel Macadam, Ethan Ely		Moist mass of sample (g)			60.00
Test Date	3/8/2017		Mass of dispersant M_{disp} (g)			5.00
BMP	Horne St., Dover, NH		Cylinder Diameter D_C (cm)			6.2
Sample Description	Native sidewall, 26-28 in.		Meniscus Correction C_m			0.001
ASTM Method	D7928-16		Volume suspension in cylinder V_{sp} (cm^3)			1000.0
			Mass of soil plus dispersant M_{dd} (g)			55.80
			Mass of soil M_d (g)			50.80
			Specific Gravity of soil G_s			2.509
Hydrometer Analysis						
Elapsed Time	Offset	Hydrometer Reading	Temp.	Effective Depth	Particle Size	Mass Percent Finer
t (min)	$r_{d,m}$	r_m	T (°C)	H_m (cm)	D_m (mm)	N_m (%)
1	1.00000	1.02000	21.99	13.59	0.0526	64.7%
2	1.00000	1.01850	22.00	13.95	0.0376	59.8%
5	1.00000	1.01750	22.00	14.18	0.0240	56.6%
15	1.00000	1.01600	22.00	14.53	0.0140	51.8%
30	1.00000	1.01450	22.00	14.88	0.0100	46.9%
60	1.00000	1.01425	22.00	14.94	0.0071	46.1%
240	1.00000	1.01175	22.00	15.53	0.0036	38.0%
1440	1.00000	1.00925	20.50	16.11	0.0015	29.9%

Table 18: Sieve analysis of the sidewall borehole at HSBS, 73 ft., 26-28 in. depth

Analyst Name	Daniel Macadam		
Test Date	3/8/2017		
BMP	Horne St., Dover, NH		
Sample Description	Native sidewall, 26-28 in.		
Sample mass (g)	50.80		
ASTM Method	D6913-04		
US sieve number	Sieve Opening (mm)	Mass retained (g)	Mass Percent Finer
10	2.000	0.0	100.0%
20	0.833	0.1	99.8%
25	0.701	0.1	99.6%
40	0.425	0.5	98.6%
50	0.300	0.9	96.9%
60	0.250	0.6	95.7%
80	0.180	1.7	92.3%
100	0.150	2.2	88.0%
200	0.075	10.8	66.7%
Pan	-	33.9	0.0%
	Total mass (g)	50.8	

Table 19 Hydrometer analysis of the sidewall borehole at HSBS, 73 ft., 28-48 in. depth.

Analyst Name	Daniel Macadam, Ethan Ely			Moist mass of sample (g)		60.00
Test Date	3/8/2017			Mass of dispersant M_{disp} (g)		5.00
BMP	Horne St., Dover, NH			Cylinder Diameter D_C (cm)		6.2
Sample Description	Native sidewall, 28-48 in.			Meniscus Correction C_m		0.001
ASTM Method	D7928-16			Volume suspension in cylinder V_{sp} (cm^3)		1000.0
				Mass of soil plus dispersant M_{dd} (g)		56.30
				Mass of soil M_d (g)		51.30
				Specific Gravity of soil G_s		2.595
Hydrometer Analysis						
Elapsed Time	Offset	Hydrometer Reading	Temp.	Effective Depth	Particle Size	Mass Percent Finer
t (min)	$r_{d,m}$	r_m	T (°C)	H_m (cm)	D_m (mm)	N_m (%)
1	1.00000	1.03150	22.00	10.90	0.0458	98.7%
2	1.00000	1.03000	22.00	11.25	0.0329	94.0%
5	1.00000	1.02800	22.00	11.72	0.0212	87.8%
15	1.00000	1.02450	22.00	12.54	0.0127	76.8%
30	1.00000	1.02250	22.00	13.01	0.0091	70.5%
60	1.00000	1.02050	22.00	13.48	0.0066	64.2%
240	1.00000	1.01650	22.00	14.41	0.0034	51.7%
1440	1.00000	1.01300	20.50	15.23	0.0014	40.7%

Table 20: Sieve analysis of the sidewall borehole at HSBS, 73 ft., 28-48 in. depth

Analyst Name	Daniel Macadam		
Test Date	3/8/2017		
BMP	Horne St., Dover, NH		
Sample Description	Native sidewall, 28-48 in.		
Sample mass (g)	51.30		
ASTM Method	D6913-04		
US sieve number	Sieve Opening (mm)	Mass retained (g)	Mass Percent Finer
10	2.000	0.0	100.0%
20	0.833	0.1	99.8%
25	0.701	0.1	99.6%
40	0.425	0.2	99.2%
50	0.300	0.3	98.6%
60	0.250	0.2	98.2%
80	0.180	0.2	97.9%
100	0.150	0.3	97.3%
200	0.075	1.0	95.3%
Pan	-	48.9	0.0%
	Total mass (g)	51.3	

A.3 Calculation of Water Volume in the Stone Layer

The calculation of the volume of water in the stone layer as measured by the pressure transducers P40 and P41 shown in Figure 10 is shown here. The level of water was assumed to be level except between the connection from P40 to P41, where it was assumed to be linear between the two measurements. Generally, Figure 42 describes the ponded levels between P40 and P41. The vertical axis is exaggerated. The system was built with a 1% grade (*S*).

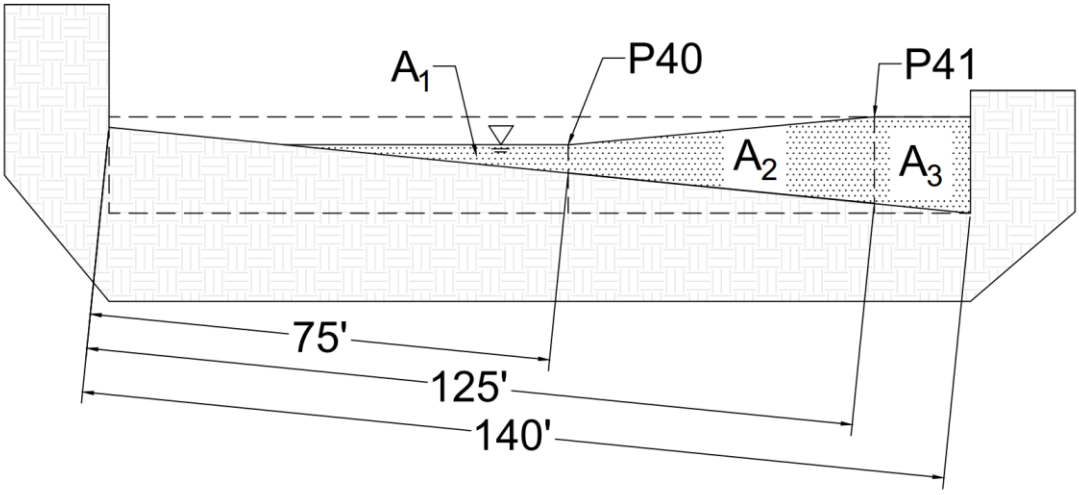

Figure 42: Profile sketch of the water levels in the stone layer with pressure transducers P40 and P41.

Figure 42 shows the three profile areas of water in the stone layer as A_1-A_3. Where the solid lines depict a physical boundary such as the bottom of excavation; dashed lines are geometric reference lines, and the shaded areas are stored water. Generally, the sum of the three areas gives the total profile area of water. To calculate the volume of water in storage in the stone, the total area (A_T) is multiplied by the width of the system (w) and the porosity of the stone (η).

$$V_w = A_T\, w\, \eta = (A_1 + A_2 + A_3)\, w\, \eta \tag{18}$$

Because the lengths of 75 ft., 125 ft. and 140 ft. lie on the hypotenuse (*c*) of a triangle, the general relationship between the base (*b*), surface slope (*S*), and hypotenuse is shown in Figure 43.

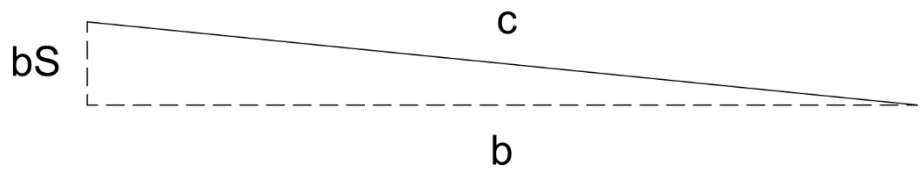

Figure 43: General trigonometric relationship between the base (b), surface slope (S), and hypotenuse (c).

Note the values of *b*, *bS*, and *c* are general and may be unique according to the geometry for A_1, A_2, or A_3. Generally, for the geometry of the system, each hypotenuse is known and the base is not. Equation (19) gives the general relationship between the hypotenuse, system slope, and the base.

$$b = \left(\frac{c^2}{1 + S^2}\right)^{1/2} \tag{19}$$

Calculation of A_1

There are two possible scenarios for the geometry of A_1. For case 1, the elevation of the water in P40 is greater than the *bS* shown in Figure 44 and the water contacts the sidewall (near the inlet) on the left as seen from this perspective. If case 1 is not true, case 2 is all other elevations of P40 where the water level does not contact the left sidewall. The definitions of *b* are unique to Figures 44 and 45.

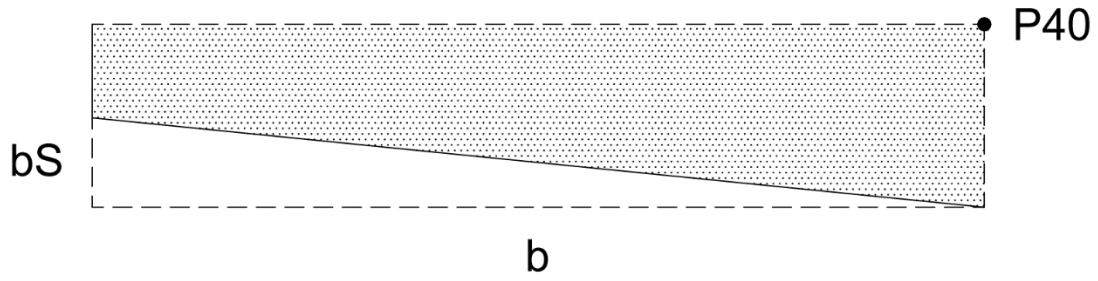

Figure 44: Definition sketch for A_1 case 1 where P40 is greater than bS.

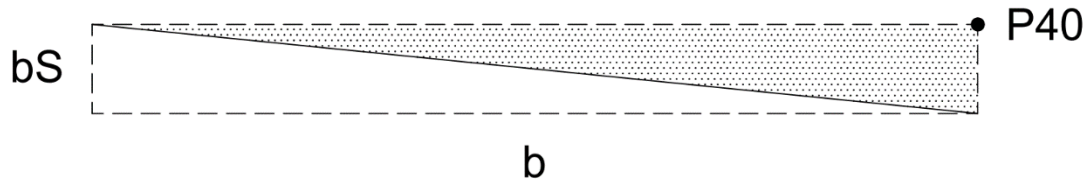

Figure 45: Definition sketch for A_1 case 2 where case 1 does not apply.

For case 1:

$$A_1 = P40 - \frac{1}{2}b^2S \quad , \quad P40 > bS$$

Where

$$b = \left(\frac{75^2}{1 + 0.01^2}\right)^{1/2}$$

For case 2:

$$A_1 = \frac{1}{2}(P40)^2S \quad , \quad P \leq bS$$

Calculation of A_2

The calculation for A_2 has three possible cases. Either P40 is greater than P41 or the opposite is true, or they are equal. The first two cases are shown in Figures 46 and 47. In both cases, *b* and *bS* are equal.

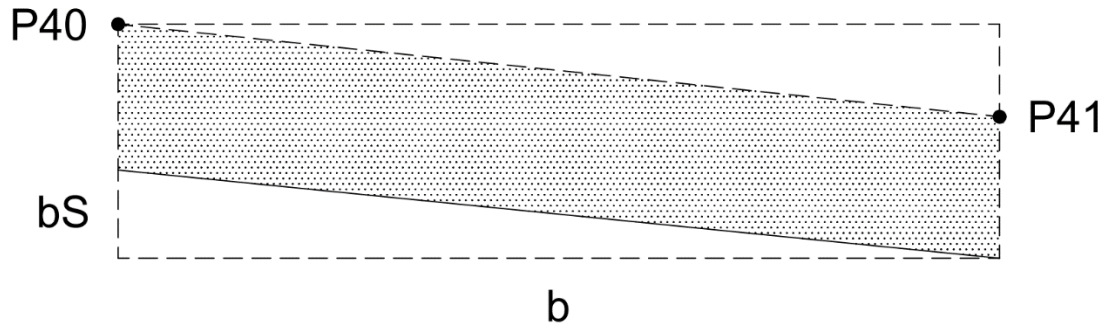

Figure 46: Definition sketch for A_2 case 1 where P40 is greater than P41.

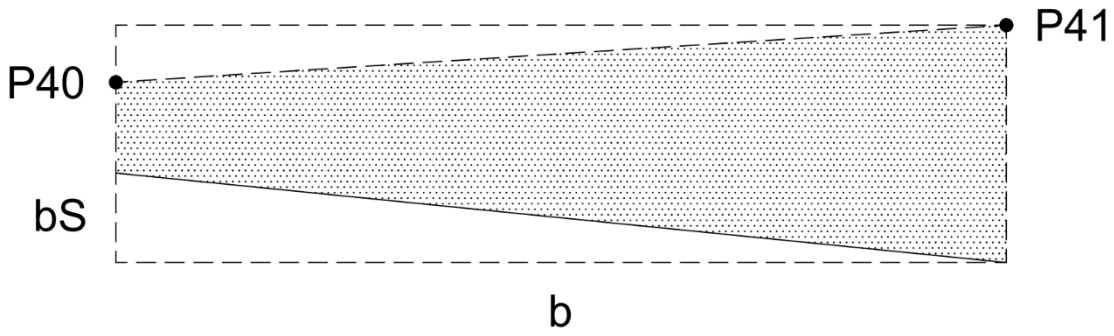

Figure 47: Definition sketch for A_2 case 2 where P40 is less than P41.

The general equation for calculating A_2 is the same for all cases. Let the variable *z* describe the maximum height of the dashed rectangle in either case.

$$z = \max(P40 + bS, P41)$$

$$A_2 = bz - \frac{1}{2}b^2S - \frac{1}{2}\ b\ \left|P40 - P41\right|$$

Where

$$b = \left(\frac{(125-75)^2}{1+0.01^2}\right)^{1/2}$$

Calculation of *A₃*

The area *A₃* only has one case because the elevation of P41 is always greater than the ride sidewall because of the gradation of the excavation. The sketch is shown in Figure 48.

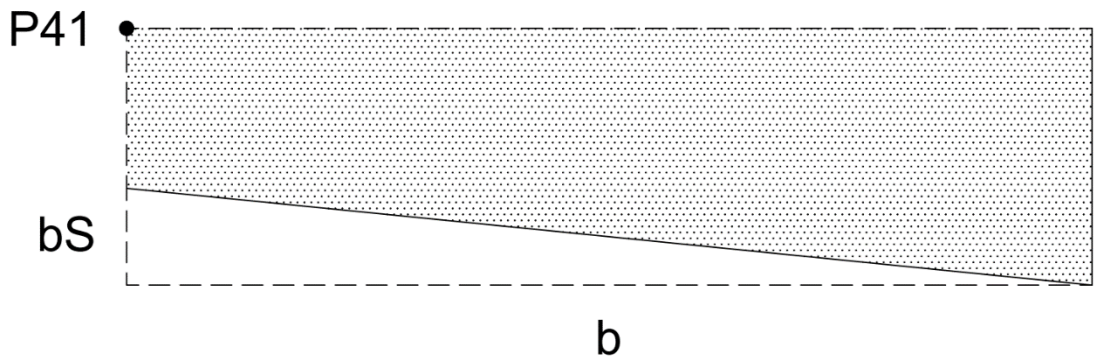

Figure 48: Definition sketch for A_3.

$$A_3 = b(bS + P41) - \frac{1}{2}b^2S$$

Where

$$b = \left(\frac{(140-125)^2}{1+0.01^2}\right)^{1/2}$$

A.4 Additional HSBS Results

Figure 49 shows the level of saturation for all TDR's calculated for the extent of all events in the HSBS.

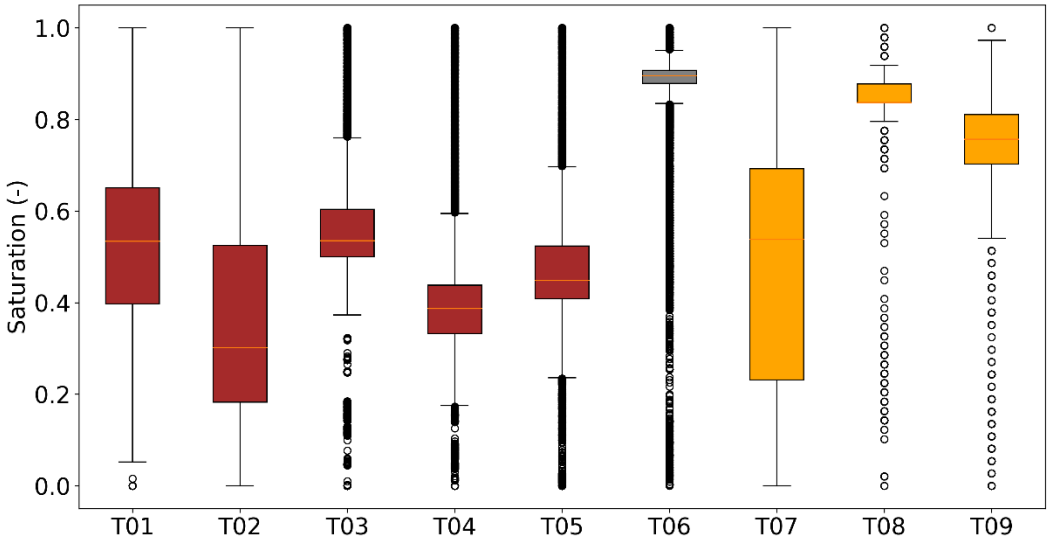

Figure 49: Saturation in all TDR's in the HSBS for the duration of events.

Figure 50 shows the level of saturation for all TDR's calculated during periods when runoff occurred in the system.

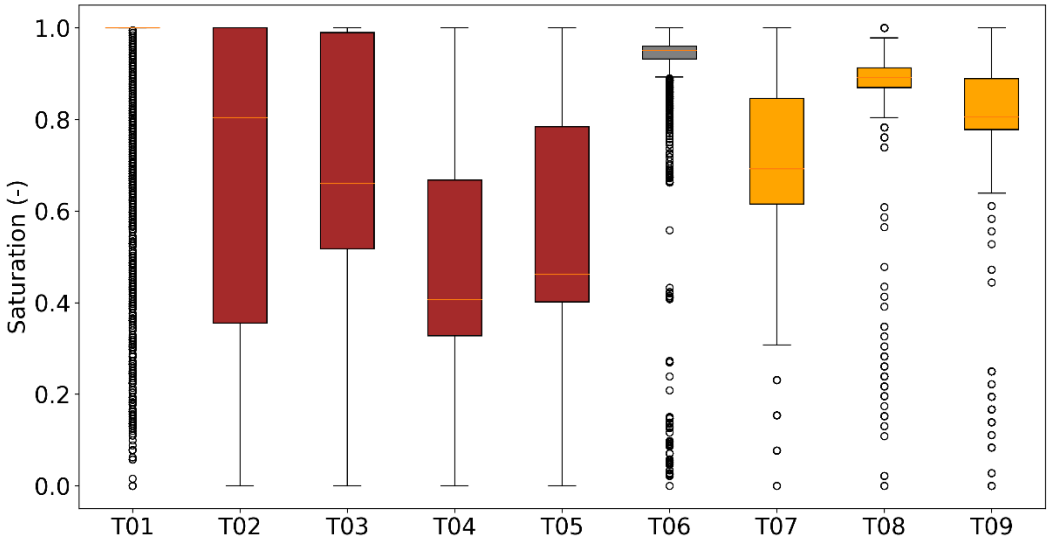

Figure 50: Saturation in all TDR's in the HSBS for the duration of runoff during events

Figure 51 shows the total event rainfall and the calculated peak flow reduction for each event. Figure 52 is similar but shows the event rainfall and the calculated volume reduction from the influent to effluent.

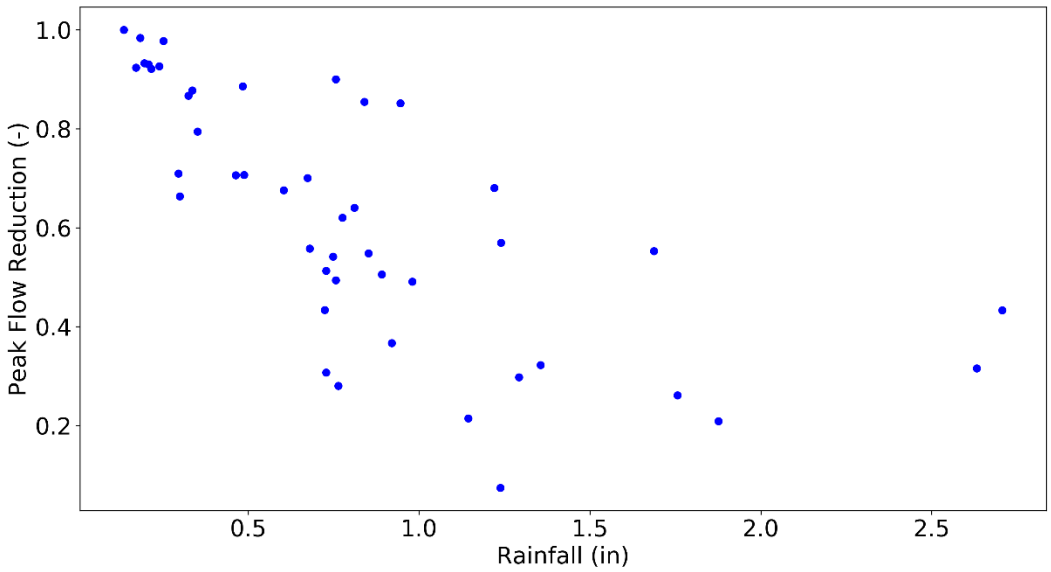

Figure 51: Event rainfall and the peak flow reduction.

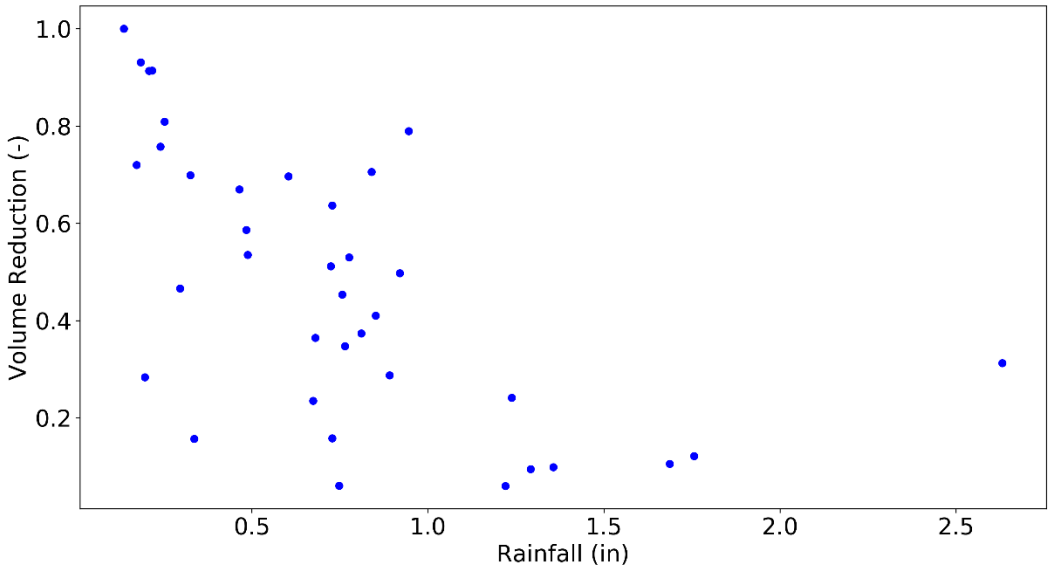

Figure 52: Event rainfall and the volume reduction from influent to effluent.

Additional summary statistics for all events with complete datasets and one-minute logging intervals are shown in Table 21.

Table 21: Summary statistics for HSBS events with one-minute logging intervals.

	Count	Mean	Standard Deviation	Minimum	25%	50%	75%	Maximum
Rainfall (in.)	45	0.82	0.60	0.14	0.34	0.75	0.98	2.71
Effective Rainfall (in.)	45	0.070	0.060	0.002	0.024	0.060	0.091	0.321
Antecedent (day)	45	3.3	3.0	0.3	0.8	2.6	4.0	11.2
Rainfall Duration (hr.)	45	9.6	6.7	0.3	3.8	9.5	14.1	24.0
Runoff Duration (hr.)	45	8.5	6.9	0.6	2.7	6.8	14.7	21.8
Event Duration (hr.)	45	81	65	11	32	72	105	276
Volume Influent (cu. ft.)	45	5615	4815	132	1941	4745	7211	25539
Volume Effluent (cu. ft.)	45	4182	4058	28	1015	3034	5786	18304
Storage BSM (cu. ft.)	45	70	127	-199	4	63	141	342
Storage Stone (cu. ft.)	45	18	69	-205	-7	9	40	209
Peak Inflow (cfs)	45	1.37	1.06	0.10	0.60	0.90	2.10	3.80
Peak Outflow (cfs)	45	0.56	0.60	0.00	0.10	0.40	0.70	2.60
Peak Ponding (ft.)	45	0.27	0.34	0.00	0.00	0.00	0.59	0.98
Peak Rainfall Intensity (in./hr.)	45	1.32	1.25	0.14	0.48	0.96	1.68	5.46
Peak Flow Reduction (%)	45	62%	25%	7%	43%	64%	87%	100%
Volume Reduction (%)	45	35%	37%	0%	10%	36%	67%	100%
Volume Reduction (cu. ft.)	45	1629	2623	0	309	1193	2278	12053
Non-bypass Events (in Rainfall)	30	0.59	0.35	0.14	0.26	0.55	0.77	1.36
Bypass Events (in Rainfall)	15	1.29	0.71	0.34	0.26	1.14	0.77	2.71

All temperatures recorded for the TDR and PT instruments since installation are shown in Figure 53.

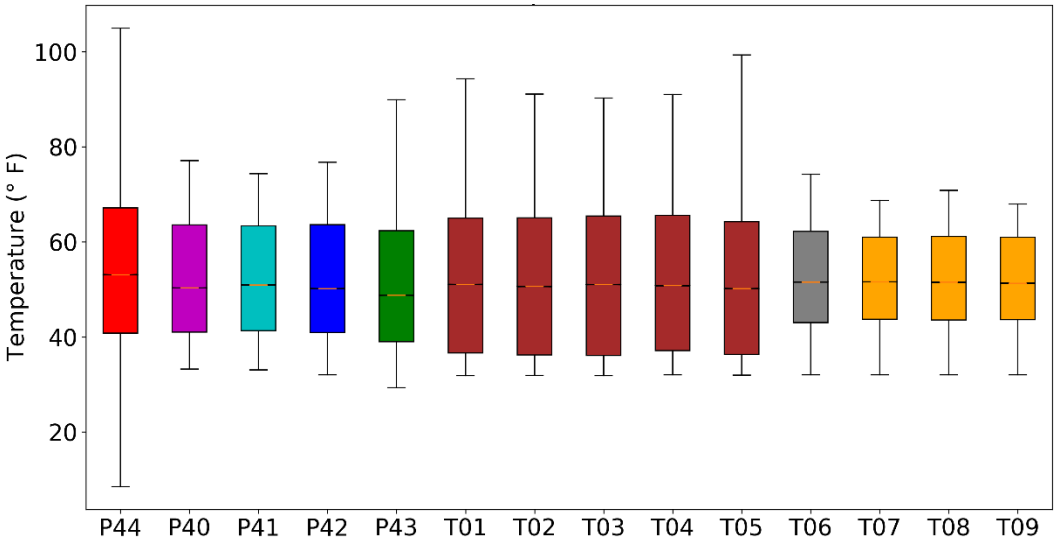

Figure 53: HSBS temperatures for all pressure transducers and time domain reflectometers.

Figure 54 shows the relationship between peak influent and peak effluent for all one-minute events.

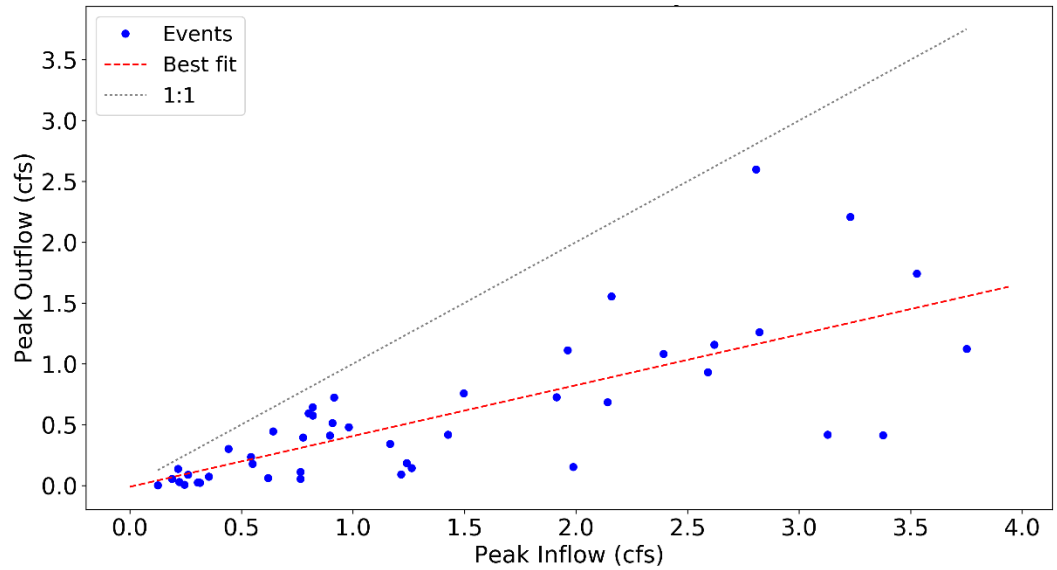

Figure 54: Peak effluent vs peak influent for all events with one-minute logging intervals.

The nonparametric Kendall Tau correlation coefficient was calculated for between all calculated parameters of the events at 1-minute logging intervals. The heatmap of the Tau values is shown in Figure 55. Note that the green diagonal represents the autocorrelation values of 1.

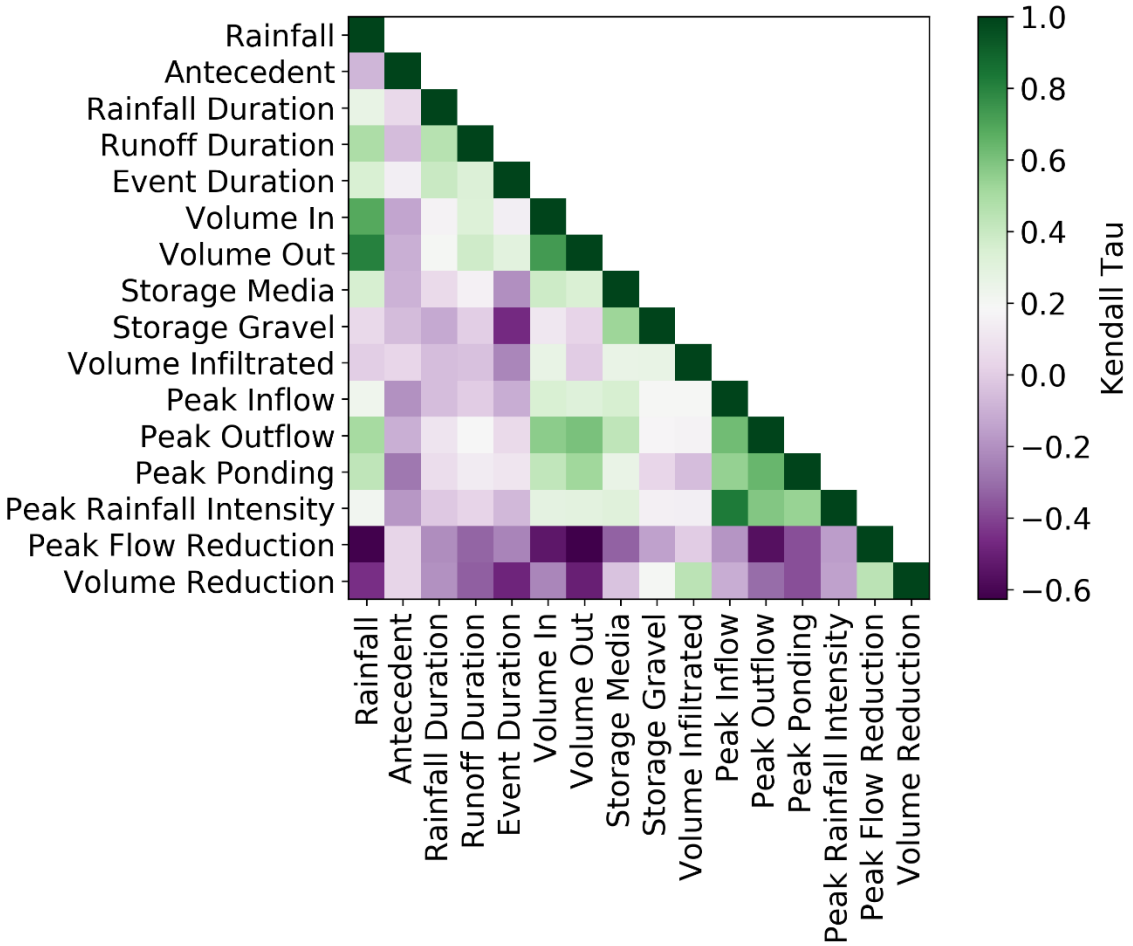

Figure 55: Nonparametric Kendall Tau correlation coefficients for 45 events with 1-minute logging intervals.

The cumulative probability distribution using an unbiased Weibull plotting position for 195 recorded rainfall events is shown in Figure 56. This includes all events that are not during winter months where the rain gage may have frozen.

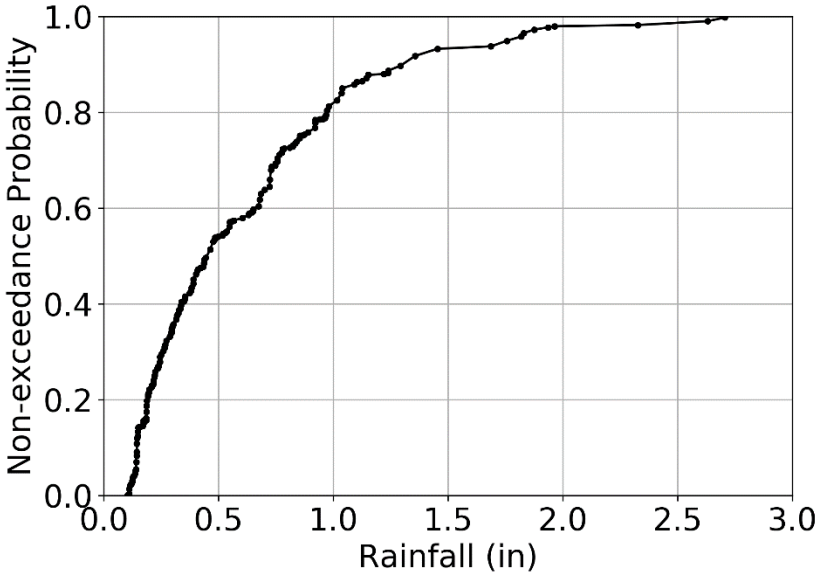

Figure 56: Cumulative non-exceedance probability for 195 rainfall events using the unbiased Weibull plotting position.

A.5 Model Derivation

The full derivations of the cumulative infiltration functions are shown in this appendix. The horizontal and vertical cumulative infiltration functions will be derived and shown step by step starting from the infiltration rates in Equations (8) and (9).

The vertical component will be derived first as it is perhaps most familiar as it very nearly resembles the Green and Ampt model with the addition of the ponded term (*h*). The derivation is shown for a general vertical infiltration and not specific to any bioretention layer. Equations (9) and (10) are the starting point.

$$f_V = K_V\left(\frac{h + L_V + \Psi}{L_V}\right) \quad , \quad F_V = L_V\,\Delta\theta$$

Substituting the $L_V = F_V/\Delta\theta$ into the infiltration rate and some algebra yields:

$$f_V = K_V\left(\frac{(h + \Psi)\Delta\theta + F_V}{F_V}\right)$$

Using the general relationship between the infiltration rate and the cumulative infiltration given by Equation (11), they may be set equal and integrated using separation of variables.

$$f_V = K_V\left(\frac{(h + \Psi)\Delta\theta + F_V}{F_V}\right) = \frac{dF_V}{dt}$$

$$\left(\frac{F_V}{(h + \Psi)\Delta\theta + F_V}\right) dF_V = K_V\ dt$$

$$\left(\frac{(h + \Psi)\Delta\theta + F_V}{(h + \Psi)\Delta\theta + F_V} - \frac{(h + \Psi)\Delta\theta}{(h + \Psi)\Delta\theta + F_V}\right) dF_V = K_V\ dt$$

$$\int_0^{F_V(t)} \left(1 - \frac{(h + \Psi)\Delta\theta}{(h + \Psi)\Delta\theta + F_V}\right) dF_V = \int_0^t K_V\ dt$$

Note that $\int \frac{a}{a+x} dx = a \ln(|x + a|)$.

Let $a = (h + \Psi)\Delta\theta$.

$$\int_0^{F_V(t)} 1 \; dF_V - \int_0^{F_V(t)} \left(\frac{a}{a + F_V}\right) dF_V = \int_0^t K_V \; dt$$

$$F_V\Big|_0^{F_V(t)} - \; a \ln(|F_V + a|)\Big|_0^{F_V(t)} = \; K\, t\Big|_0^t$$

$$F_V(t) - a[\ln(|F_V(t) + a|) - \ln(|F_V(t) + a|)] = K\, t$$

$$F_V(t) - a \ln\left(\left|\frac{F_V(t) + a}{a}\right|\right) = K\, t$$

$$F_V(t) - a \ln\left(\left|1 + \frac{F_V(t)}{a}\right|\right) = K\, t$$

Substituting the *a* relationship back in yields the general, implicit solution for the vertical cumulative infiltration function as in Equation (13):

$$F_V(t) - (h + \Psi)\Delta\theta \ln\left(\left|1 + \frac{F_V(t)}{(h + \Psi)\Delta\theta}\right|\right) = K\, t$$

The horizontal cumulative infiltration function will be derived from the general horizontal infiltration rate given by Equation (8).

$$f_H = K_H \left(\frac{h + \Psi}{L_H/2}\right) \;\; , \;\; F_H = L_H \, \Delta\theta$$

Substituting the $L_H = F_H/\Delta\theta$ into the infiltration rate and some algebra yields:

$$f_H = K_H \left(\frac{2 \, (h + \Psi) \, \Delta\theta}{F_H}\right)$$

Using the general relationship between the infiltration rate and the cumulative infiltration given by Equation (11), they may be set equal and integrated using separation of variables.

$$f_H = K_H \left(\frac{2(h + \Psi)\, \Delta\theta}{F_H} \right) = \frac{dF_H}{dt}$$

$$\left(\frac{F_H}{2(h + \Psi)\, \Delta\theta} \right) dF_H = K_H \; dt$$

Let $a = 2(h + \Psi)\, \Delta\theta$.

$$\int_0^{F_H(t)} \frac{F_H}{a} \, dF_H = \int_0^t K_H \; dt$$

$$\frac{F_H^2(t)}{2a} = K_H \, t$$

Solving for $F_H(t)$ and substituting the relationship for *a* yields the explicit solution for the horizontal cumulative infiltration function in Equation (12):

$$F_H(t) = [4(h + \Psi)\, \Delta\theta \; K_H \, t]^{1/2}$$